Hepatic ceramide synthesis links systemic inflammation to organelle dysfunction in cancer

Ying Liu[1, #, *], Ting Miao[1, #], Alice Wang[2], Ezequiel Dantas[3], Ah-Ram Kim[1], Zhongjie Zhang[1], Xiaomei Sun[1], Richard Binari[1], John M. Asara[4, 5], Yanhui Hu[1], Marcus D. Goncalves[3], Tobias Janowitz[2,6], Norbert Perrimon[1, 7, *]

[1] Department of Genetics, Blavatnik Institute, Harvard Medical School, Boston, MA 02115, USA

[2] Cold Spring Harbor Laboratory, Cold Spring Harbor, New York, NY 11724 USA

[3] Department of Medicine, New York University Grossman School of Medicine, New York, NY 10016, USA

[4] Department of Medicine, Harvard Medical School, Boston, MA, USA

[5] Division of Signal Transduction, Beth Israel Deaconess Medical Center, Boston

[6] Northwell Health Cancer Institute, Northwell Health, New Hyde Park, New York, NY 11042 USA

[7] Howard Hughes Medical Institute, Boston, MA, USA

[#] Authors contribute equally

*Correspondence:

Ying Liu: ying_liu@hms.harvard.edu

Norbert Perrimon: perrimon@genetics.med.harvard.edu

Abstract

Paraneoplastic syndromes arise when tumor-derived cytokines reprogram distant organs. Although mediators such as Interleukin-6 have been implicated, how these signals impair host organ function remains incompletely defined. Here, we identify a cytokine-lipid axis that drives hepatic autophagy dysfunction. Specifically, in *Drosophila*, the gut tumor-derived interleukin-like cytokine Upd3 induces the expression of the triglyceride lipase *CG5966*, which we named "*cancer-associated lipid mobilizer* (*calm*)", and the ceramide synthase *schlank* in the fat body. This upregulation rewires fat body lipid metabolism, resulting in an autophagic-flux blockade. Genetic reduction of either *CG5966* or *schlank* restores organelle homeostasis and mitigates paraneoplastic phenotypes. This mechanism is conserved in mammals: in mice, IL-6 upregulates the lipoprotein lipase *Lpl* and ceramide synthases which in turn trigger a hepatic autophagy-flux blockade; in humans, hepatic *LPL* and ceramide synthases expression correlates with poorer survival in hepatocellular carcinoma. Our findings position hepatic lipid metabolism rewiring, especially ceramide synthesis as a critical, conserved node coupling systemic inflammation to organelle dysfunction, and suggest this pathway as a possible therapeutic entry point for cancer-associated liver disorders.

Introduction

Paraneoplastic syndromes are systemic disorders in cancer patients caused by tumor-derived factors that disrupt distant organs (Pelosof and Gerber, 2010). Among these factors, cytokines, particularly interleukin-6 (IL-6), are prominent paraneoplastic factors that drive diverse clinical manifestations (Ferrer et al., 2023; Flint et al., 2016; Pelosof and Gerber, 2010; Wu et al., 2017). IL-6 engages the JAK/STAT signaling cascade in distant tissues, leading to transcriptional reprogramming that drives systemic inflammation, enhanced thrombopoiesis, and cachectic wasting (Ding et al., 2021; Liu et al., 2025; Stone et al., 2012). One of the primary target tissues of IL-6 in paraneoplastic syndrome is the liver, a central hub of systemic metabolic regulation (Fearon et al., 2012; Liu et al., 2025). In response to chronic IL-6-driven inflammatory cues , the liver enhances gluconeogenesis while promoting adipose lipolysis and skeletal muscle proteolysis, metabolic adaptations that collectively culminate in cancer cachexia. (Ding et al., 2021; Liu et al., 2025). Within hepatocytes, basal autophagy is essential for proteostasis and organelle quality control (Qian et al., 2021). Consistent with this, genetic ablation of core autophagy genes leads to the accumulation of ubiquitinated proteins and p62/SQSTM1-positive inclusions, oxidative stress, hepatomegaly, and hepatic steatosis, underscoring the role of autophagy in maintaining liver function (Komatsu et al., 2007, 2005; Ni et al., 2014). However, whether tumor-derived signals impair hepatic autophagy in a way that contributes to paraneoplastic syndromes remains unknown.

Autophagy is a dynamic membrane-trafficking process that is intrinsically linked to lipid metabolism, making it a highly lipid-demanding pathway. Autophagosome formation begins with the nucleation of an isolation membrane (phagophore), followed by elongation around cytosolic cargo and sealing into a mature vesicle (Ryter et al., 2013; Ueno and Komatsu, 2017). Phospholipids furnish the structural material for phagophore nucleation, membrane elongation, and remodeling during autophagosome biogenesis (Harayama and Riezman, 2018; Rowland et al., 2023). The supply of phospholipids, synthesized from fatty acyl-CoA and glycerol-3-phosphate, sets a key rate constraint; fatty acyl-CoAs are derived

from *de novo* lipogenesis or liberated via lipolysis, directly linking autophagic dynamics to cellular lipid metabolism (Harayama and Riezman, 2018; Rowland et al., 2023). Consistently, long-chain acyl-CoA synthetases (ACSLs), which channel fatty acids into *de novo* phospholipid synthesis, relocalize to nascent phagophores to boost local lipid production required for membrane expansion (Dong et al., 2018; Schütter and Graef, 2020). Autophagosome expansion also requires the lipidation and membrane association of ubiquitin-like protein Atg8/LC3: increasing Atg8 enlarges autophagosomes through enhanced elongation and cargo capture, whereas reducing it yields smaller vesicles (Weidberg et al., 2011; Xie et al., 2008). Thus, in metabolically stressed liver, tumor-induced shifts in lipid supply and/or Atg8 abundance are poised to modulate autophagosome number and size, with direct consequences for autophagic capacity (Rowland et al., 2023; Schütter and Graef, 2020; Ueno and Komatsu, 2017).

Dysregulated sphingolipid metabolism exemplifies how lipid imbalances can disrupt autophagy. Ceramides, synthesized *de novo* from serine and palmitoyl-CoA by a family of ceramide synthases (CerS1–6), accumulate in metabolic diseases and some cancers (Hannun and Obeid, 2018; Mullen et al., 2012). While modest increases in ceramide can induce protective autophagy (Taniguchi et al., 2012), chronic or excessive ceramide accumulation impairs autophagic flux, often by compromising lysosomal integrity (Gabandé-Rodríguez et al., 2014; Liu et al., 2016). Mechanistically, sustained ceramide accumulation destabilizes lysosomes, leading to defective hydrolase maturation and leakage of cathepsins into the cytosol, thereby blocking the final stages of autophagic degradation (Gabandé-Rodríguez et al., 2014; Liu et al., 2016; Turk et al., 2001). These findings raise the possibility that tumor-driven perturbation in lipid flux, particularly the buildup of ceramides, could blunt hepatic autophagy and thereby contribute to hepatic impairment and broader systemic dysfunction.

98 *Drosophila melanogaster* offers a powerful genetic system for dissecting such cross-organ
99 interactions. Multiple fly tumor models exhibit paraneoplastic-like phenotypes, enabling
100 systematic analysis of underlying tumor-host signaling (Bilder et al., 2021; Cheng et al.,
101 2025; Liu et al., 2022). In the Yorkie (Yki) model, gut tumors induced by overexpressing an
102 active form of the oncoprotein Yki, the fly homolog of YAP (*esg>yki*^{act}; referred to as Yki
103 flies), elicit systemic effects reminiscent of human paraneoplastic syndromes (Kwon et al.,
104 2015). Yki-driven tumors secrete circulating factors, including PDGF- and VEGF-related
105 factor 1 (Pvf1) and the IL-6-like cytokine Unpaired 3 (Upd3), which act on distant tissues
106 like muscle and fat body to induce wasting (Ding et al., 2021; Liu et al., 2025; Song et al.,
107 2019). The genetic and physiological tractability of the fly fat body, an organ analogous to
108 the vertebrate liver and adipose tissue, makes it an ideal model to investigate how tumor-
109 derived cytokines reshape hepatic lipid metabolism and autophagy to drive paraneoplastic
110 pathology (Liu et al., 2025). Here, guided by a cross-organ gene expression analysis of
111 paraneoplastic progression, we demonstrate that tumor-derived Upd3 activates JAK-STAT
112 signaling to upregulate the lipase *CG5966* and the ceramide synthase *schlank* in the fat
113 body, disrupting lipid homeostasis and triggering severe autophagy dysfunction.
114 Importantly, this pathogenic axis is conserved in mammals, as IL-6 drives expression of
115 lipoprotein lipase (*LPL*) and ceramide synthases in mouse models. Further, elevated *LPL*
116 and *CERS5/6* expression are significantly associated with reduced survival in
117 hepatocellular carcinoma. Together, these findings suggest that hepatic lipid metabolism,
118 namely ceramide synthesis may be a therapeutic target for cancer-associated hepatic
119 dysfunction.

120

121 **Results**

122 **Identification of CG5966 as a paraneoplastic factor**

123 In cancer patients, the timing of paraneoplastic syndrome onset frequently diverges from
124 tumor growth (Pelosof and Gerber, 2010). Similarly, in the Yki gut-tumor model, peripheral
125 organ dysfunction (renal failure, muscle degeneration, ovary atrophy) emerges with a delay,

robust by day 8 following tumor maturation at day 5 (Kwon et al., 2015; Liu et al., 2025; Song et al., 2019; Xu et al., 2024). To distinguish the effects of tumor burden from tumor-driven systemic signals, we leveraged our full-body single-nucleus transcriptomic data generated previously (Liu et al., 2025), which profiles gene expression dynamics of both gut tumors and host organs at days 5 and 8. We integrated, across cell clusters, both effect size (fold-change) and statistical significance to compute a progression association index for each gene (Fig. 1a). Genes whose differential expression increased from day 5 to day 8 (positive index) were classified as progression-associated and thus prioritized as candidates contributing to paraneoplastic syndrome progression (Fig. 1a). Among cell clusters, enterocytes (ECs) exhibited the largest share of genes associated with progression, consistent with continued differentiation of tumor intestinal stem cells (ISCs) into ECs, followed by follicle cells and indirect flight muscle, reflecting ovarian atrophy and muscle decline, respectively (Fig. S1a) (Liu et al., 2025). Notably, while fat body cell proportions remained relatively stable at both day 5 and day 8 (Liu et al., 2025), it exhibited a higher fraction of progression-associated genes compared with other tissues (Fig. S1a). Top genes identified by the progression association index, including *CG14275, Pepck1, IM2, CG5966,* and *ScsβA*, were predominantly upregulated in the fat body (Fig. 1a; FigS1b-f). Of these, we previously implicated *Pepck1* and *ScsβA* as causal mediators of hepatic gluconeogenic dysregulation and cachectic progression (Liu et al., 2025). Together, these analyses identify the fat body, a fly tissue with many liver-like functions, as a central driver of paraneoplastic progression.

Among the genes with the highest progression association index score, *CG5966* is an unannotated gene (Fig. 1a). To test whether its induction contributes to pathogenesis rather than simply reflecting end-stage dysfunction, we combined esg-LexA/LexAop to activate Yki in ISCs (*esg-LexA, LexAop-Yki*^{act}) with Lpp-Gal4/UAS to knockdown *CG5966* specifically in the fat body (*Lpp-Gal4, UAS-CG5966-RNAi*). Fat-body *CG5966* depletion did not alter GFP-labelled gut tumor size nor phospho-Histone 3 (pH3) signal, a cell mitoses marker, indicating no effect on tumor burden or proliferation (Fig. 1b-d). In contrast, *CG5966*

knockdown significantly reduced bloating, a hallmark of paraneoplastic phenotype in Yki flies (Kwon et al., 2015; Liu et al., 2025), as evidence by reduced abdomen-to-head (A/H) ratio and total body fluid, suggesting an attenuation of paraneoplastic progression (Fig. 1b, e-g). Consistent with rescue of systemic deterioration, climbing ability improved and lifespan was extended in Yki flies upon fat-body *CG5966* knockdown (Fig. 1h, i). Collectively, these data establish *CG5966* as a fat-body-expressed contributor to paraneoplastic pathology in the Yki model.

CG5966 targets a subset of triglycerides and reroutes fatty acids into phospholipids

We next investigated the pathogenic mechanism of CG5966. FlyBase annotates *CG5966* as a putative triglyceride (TG) lipase. As it associates with cancer and is a lipase, we named *CG5966* as *Cancer-Associated Lipid Mobilizer* (*calm*). Sequence alignment with classical human lipases revealed the signature motif G-x-S-x-G in CG5966, as well as the conserved catalytic triad residues (Ser199-Asp227-His312) required for lipid hydrolysis (Fig. S2a). Complementing this, 3D structural modeling using AlphaFold revealed the closest similarity to human pancreatic lipase (PNLIP) and lipoprotein lipase (LPL) (Fig. 2a, b), supporting a close functional relationship between CG5966 and these lipases. Because Yki flies show reduced TG levels (Kwon et al., 2015), we initially hypothesized that upregulated CG5966 simply drives bulk TG hydrolysis to deplete energy stores. However, fat-body-specific *CG5966* knockdown in Yki flies did not restore total TG levels in the abdomen carcass mainly containing fat body tissue (Fig. S2b), suggesting its selective role in TG hydrolysis. To test substrate preference of CG5966 independent of tumors, we profiled lipids in abdomen in wild-type flies with or without fat-body *CG5966* overexpression (Fig. S2c). Consistent with the observations in Yki flies, total TG abundance remained unchanged upon *CG5966* overexpression (Fig. 2c). By contrast, species-resolved lipidomics revealed selective depletion of TGs bearing 16:0, 16:1, 18:0, or 18:1 acyl chain upon *CG5966* overexpression (Fig. 2d-g; S2d), suggesting that CG5966 preferentially acts on specific molecular TGs. To further assess the lipase activity of CG5966, we performed molecular docking using TG (16:0/18:1/18:1), one abundant TG species in both fly and

184 mammals that was significantly depleted upon *CG5966* overexpression. The Boltz-2
185 docking model positioned the ester bond of the TG substrate in close proximity to the
186 catalytic triad, with a predicted binding free energy of -8.2 kcal/mol, indicating a highly
187 efficient substrate recognition (Fig. 2h) (Mirdita et al., 2022; Passaro et al., 2025).
188 Altogether, our data suggest CG5966 preferentially targets TG containing C16 and C18 acyl
189 chains.

190

191 As the induction of *CG5966* may not be the leading reason of storage lipid depletion in our
192 tumor model, we investigated the possible physiological consequences of CG5966-
193 mediated C16/18 TG liberation. Lipidomic profiling revealed that phospholipids bearing the
194 same acyl chains were enriched upon *CG5966* overexpression: C18:1 increased in
195 Phosphatidylethanolamine (PE), Phosphatidylcholine (PC), Phosphatidylinositol (PI), and
196 Phosphatidylglycerol (PG) (Fig. 2d; Fig. S2e), C18:0 increased in PI (Fig. 2e; Fig. S2f), and
197 C16:1/C16:0 increased in PE/PC/PG (Fig. 2f,g; Fig. S2g,h). As most phospholipids contain
198 C16 and C18 acyl chains (Skotland and Sandvig, 2019), these compositional shifts were
199 companied by increases in total PC, PG, and PI pools (Fig. S2i-k). These data suggest that
200 C16/C18 fatty acyl-CoAs liberated from CG5966-mediated TG depletion are subsequently
201 utilized for phospholipid synthesis. Given that phospholipids are major membrane building
202 blocks (Harayama and Riezman, 2018), we hypothesized that CG5966 play a role in
203 supplying membrane-lipid precursors. If so, it would interact with membrane-lipid
204 biogenesis regulators or enzymes. To test this, we used AlphaFold-Multimer (AFM) to
205 screen putative CG5966 protein-protein interfaces with markers of specific compartments
206 (lysosome, ER, Golgi, plasma membrane) and lipid-metabolic enzymes (Fig. S2l) (Evans et
207 al., 2021). We modeled 3,686 proteins (five AF-M models each; 18,430 total predictions)
208 and, using integrated Local Interaction Score (iLIS) (Kim et al., 2024), retained 248 high-
209 confidence interfaces (1.35%), corresponding to 158 candidate interactors (Fig. 2i; Fig.
210 S2l). Clustering of these candidates by interacting sites yielded 13 groups (Fig. 2j). The
211 most enriched group (Cluster 1) contains membrane-lipid biogenesis regulators, and the
212 second enriched group (cluster 8) includes factors acting at multiple steps of autophagy

213 (Fig. 2j, k). We further checked the interacting interfaces by these top two cluster of
214 proteins, autophagy factors interact CG5966 at out surface, whereas the membrane-lipid
215 biogenesis regulators interact closely to the catalytic triad residues (Ser199-Asp227-
216 His312), suggesting a coordinated procession of lipid (Fig. 2i). Top-scoring partners in the
217 membrane-biogenesis cluster included PGAP5, PIG-H, GPAA1/GAA1 (GPI-anchor
218 synthesis/remodeling) (Kinoshita et al., 2006; Kinoshita, 2020; Tiede et al., 2000), and
219 glycosyltransferases (e.g., α4GT2) implicated in ER/Golgi membrane maturation (Fig. 2k)
220 (Hamel et al., 2010). From the autophagy enriched cluster 8, we recovered autophagy-
221 trafficking factors involved in multiple steps of autophagy process, including Atg12
222 (ubiquitin-like conjugation system required for autophagosome formation) (Mulakkal et al.,
223 2014), Rab26/27/40 (small GTPases coordinating vesicle dynamics) (Gillingham et al.,
224 2014), CG5367 (Cathepsin L4), and GILT1 (a lysosomal thiol-reductase linked to
225 autolysosome function) (Kongton et al., 2014) (Fig. 2k, m-p). Based on these predictions,
226 we investigated whether CG5966 mediated TG hydrolysis regulates autophagy in the fat
227 body. We assayed autophagy *in vivo* with CYTO-ID® Autophagy Detection Reagent that
228 stains autophagic vesicles (pre-autophagosomes, autophagosomes, and autolysosomes).
229 Indeed, fat-body *CG5966* overexpression increased the number of autophagic vesicles,
230 while vesicle sizes were unchanged (Fig. 2q-s). This is consistent with previous report that
231 autophagosome formation depends on the membrane delivery, while size scaling requires
232 other regulators such as ubiquitin-like protein Atg8/LC3 (Weidberg et al., 2011; Xie et al.,
233 2008). Altogether, our results suggest that CG5966 preferentially liberates C16/C18 acyl
234 chains from TG, thereby fueling phospholipid synthesis, expanding membrane lipid supply,
235 and promoting autophagosome formation.

236

237 **CG5966 promotes autophagosome formation in Yki flies**

238 We next asked whether CG5966 modulates autophagy in the Yki model. Fat-body staining
239 in Yki flies revealed a robust increase in number of autophagic vesicles, mirroring the effect
240 of *CG5966* overexpression in wild-type animals, with an additional enlargement of vesicle
241 sizes unique to the Yki background (Fig. 3a-c). Both phenotypes (increased vesicle

numbers and sizes) were suppressed by fat-body-specific *CG5966* depletion (Fig. 3a-c). These observations suggest a *CG5966*-mediated upregulation of autophagosome formation in Yki flies. Elevated autophagosome formation typically reflects enhanced initiation of the autophagy process (Fig. S3a-d). Supporting this, expression of the autophagy-initiating kinase *Atg1* and *Atg17* was elevated in the fat body of Yki flies at day 8 (Fig. S3a-c). To directly test whether autophagy initiation was promoted in Yki flies, we depleted *Atg1* specifically in the fat body of Yki flies. As expected, *Atg1* knockdown blunted autophagic-vesicle staining, restoring vesicle numbers and sizes to normal levels (Fig. 3d-f). This result confirms enhanced autophagy initiation in Yki flies. We then examined whether this activated autophagy initiation contributes to paraneoplastic syndrome. Indeed, fat-body-specific *Atg1* depletion did not alter tumor burden or proliferation (Fig. 3g-i) but significantly reduced bloating and total body fluid (Fig. 3g, j, k) and improved climbing ability (Fig. 3l). Together, these data demonstrate that activation of autophagy initiation contributes to the paraneoplastic syndrome in *Yki* flies, likely mediated by *CG5966* through promoting autophagosome formation. Notably, although not observed in *CG5966*-overexpressing wild-type flies (Fig. 2q, s), autophagic vesicle enlargement was evident in *Yki* flies and was rescued by either *CG5966* or *Atg1* knockdown (Fig. 3a, c, d, f). This discrepancy suggests that in the tumor context, autophagy perturbation extend beyond initiation, implicating additional mediators besides CG5966 in the dysregulation of autophagy in Yki flies.

Autophagic flux is blocked in Yki flies

We therefore examined classical markers of autophagic flux to clarify the dysregulation in Yki flies. Consistent with the increased number of autophagic vesicles, immunoblotting showed elevated levels of Atg8-II (LC3-II) (Fig. S4a), the lipidated, membrane-bound form of Atg8 associated with autophagosomes (Xie et al., 2008). Because accumulation of Atg8-II can reflect enhanced autophagosome biogenesis and/or flux blockade at autophagosome-lysosome fusion or lysosomal degradation steps, we next assessed autophagic flux and lysosomal function. The anti-p62/Ref(2)P antibody, a negative indicator

271 of autophagic flux, did not yield reliable detection in the adult fat body, so we evaluated
272 cathepsin L (CtsL) maturation as a readout of lysosomal proteolytic activity. CtsL is
273 synthesized as a pro-enzyme that undergoes proteolytic processing into its mature
274 lysosomal form (Turk et al., 2001). Notably, Yki flies displayed elevated levels of pro-CtsL
275 (Fig. 4a), indicating insufficient lysosomal proteolysis. Together with increased
276 autophagosome number and accumulation of Atg8-II, these data suggest that
277 autophagosome formation is promoted, whereas lysosomal degradation at the later stage
278 of autophagy is compromised in the fat body of Yki flies. To further assess lysosomal
279 alterations, we examined lysosome morphology and abundance in the fat body of Yki flies
280 using LysoTracker, which labels acidic lysosomes and autolysosomes. Consistent with
281 compromised lysosomal function, Yki fat bodies exhibited abnormally increased size and
282 number of lysosomes, and these alterations were suppressed by fat-body specific *CG5966*
283 depletion (Fig. 4b-d). Because a block in lysosomal degradation can arise from defective
284 autophagosome-lysosome fusion or intrinsic lysosomal dysfunction (Fig. S3a), we co-
285 stained autophagic and lysosomal vesicles to examine these possibilities. Co-localization
286 analysis revealed substantial overlap between enlarged autophagic vesicles and
287 lysosomes, indicating that the expanded vesicles in Yki fat bodies are predominantly
288 autolysosomes (autophagosome-lysosome hybrids) (Fig. 4e, f). Notably, the number of
289 autolysosomes were also increased in Yki flies, suggesting no defects in autophagosome-
290 lysosome fusion (Fig. 4g). Consistent with the role of CG5966 in supplying lipids for
291 autophagosome formation, its depletion in Yki flies reduced autolysosome number and
292 was accompanied by smaller autophagic vesicles and lysosomes (Fig. 3c; 4d, g). Together,
293 these results rule out autophagic flux blockade at the autophagosome formation or
294 autophagosome-lysosome fusion steps, instead indicate that the terminal degradation is
295 impaired due to lysosomal dysfunction.

296

297 **Ceramide accumulation underlies lysosomal dysfunction in Yki flies**

298 We next investigated why terminal lysosomal degradation is impaired in the fat body of Yki
299 flies. Intrinsic lysosomal dysfunction can result from several causes, including defective

300 lysosomal acidification and compromised hydrolase processing (Colacurcio and Nixon,
301 2016; Saftig and Klumperman, 2009). Surveying our Yki transcriptome and lipidomics
302 datasets, we found no evidence of altered expression in genes governing lysosomal
303 acidification (e.g., *Vha100-1*, *Vha16-1*, *VhaAC39-1*) or hydrolase processing (e.g., *Lerp*,
304 *Rab5*, *Rab6*, *Rab7*, *Syx17*); with one exception: *CtsL1* was upregulated (Fig. S4b). Together
305 with the accumulation of pro-CtsL, this pattern is consistent with a possible compensatory
306 response to impaired CtsL maturation. In contract, we noticed a significant increase in
307 sphingolipids among the major lipid classes (Fig S4c-g), with a double amount of whole-
308 body ceramide levels in Yki flies compared with controls (Fig. 4h). Excessive ceramides are
309 known to disrupt lysosomal function and blocking cargo degradation (Gabandé-Rodríguez
310 et al., 2014; Liu et al., 2016). These findings suggest a ceramide-driven mechanism for the
311 lysosomal defect in Yki flies. To test this hypothesis, we depleted *schlank*, the sole
312 ceramide synthase characterized in *Drosophila*, in the fat body and assessed lysosomal
313 function by CtsL maturation. As predicted, *schlank* knockdown reduced the accumulation
314 of pro-CtsL in Yki flies, indicating improved lysosomal proteolysis (Fig. 4i). Concordantly,
315 *schlank* depletion restored lysosome number and size to near-normal levels (Fig. 4j-l).
316 Importantly, co-staining of autophagic and lysosomal vesicles showed reduced
317 autolysosome number (Fig. 4m), and the enlarged autolysosomes were normalized close
318 to typical autophagic vesicle dimensions (Fig. 4n). Notably, *schlank* knockdown did not
319 change autophagic vesicle numbers (Fig. 4o), consistent with our model that
320 autophagosome biogenesis is mediated by CG5966. Together, these findings indicate that
321 *Schlank* depletion enhances lysosomal clearance and alleviates autophagic blockade in
322 *Yki* flies. We next accessed whether relieving the lysosomal blockade improves host
323 physiology. Without altering tumor burden or proliferation (Fig. 4p-r), *schlank* depletion
324 reduced bloating and total body fluid (Fig. 4p, s, t), restored climbing ability, and extended
325 survival in Yki flies (Fig. 4u, v). Together, these findings support a model in which ceramide
326 accumulation-induced lysosomal dysfunction blocks autophagic clearance; the
327 consequent accumulation of enlarged, dysfunctional autolysosomes contribute causally
328 to paraneoplastic syndrome pathology in the Yki model.

329

330 **The JAK–STAT pathway drives fat body autophagy dysregulation**

331 We next asked what upstream signal induces fat-body autophagy dysregulation. Many TG
332 lipases (e.g., *brummer/bmm*, fly homolog of *ATGL*) are upregulated when insulin signaling
333 is low to mobilize stored energy (Wang et al., 2011). Although Yki flies exhibit reduced
334 systemic insulin activity due to elevated circulating ImpL2 (an insulin-like peptide
335 antagonist) (Kwon et al., 2015), *CG5966* expression was not suppressed by restoring fat
336 body insulin signaling via overexpression of a constitutively active from of the insulin
337 receptor (*InRca*) (Fig. S5a). Beyond insulin, prior work showed increased Upd3/JAK-STAT
338 and Pvf1/Pvr-RTK signaling in Yki flies (Ding et al., 2021; Liu et al., 2022, 2025; Song et al.,
339 2019); we therefore tested whether these pathways regulate *CG5966*. Among these
340 candidates, *Upd3* overexpression in intestinal stem cells (ISCs) (*esg>Upd3*) led to an
341 upregulation of *CG5966* in the fat body (Fig. 5a). Consistently, fat body expression of
342 constitutively active from of Stat92E (*Lpp>Stat92E*^{act}*-HA*) increased *CG5966* expression
343 (Fig. 5b). Strikingly, the ceramide synthase *schlank* showed the same regulatory pattern
344 (Fig. 5c, d). These results suggest that the Upd3/JAK-STAT pathway induces expression of
345 both *CG5966* and *schlank* in wildtype flies.

346

347 To validate this regulatory axis in the tumor context, we used the dual binary systems: LexA-
348 LexAop to express Yki in ISCs and GAL4-UAS to deplete the JAK-STAT pathway components
349 *hop* (JAK) and *Stat92e* (STAT) in the fat body. As expected, inhibition of JAK-STAT pathway
350 reduced *CG5966* and *schlank* expression (Fig. 5e-h). Published Stat92e ChIP-seq dataset
351 (ENCODE, ENCSR290OJD/ENCFF873KIF) revealed putative Stat92E occupancy within
352 promoter and intronic regions of *CG5966* and *schlank* (Fig. 5i). In agreement, fat body ChIP
353 confirmed Stat92E association at these loci (Fig. 5j). Consistent with the gene expression
354 regulation, inhibiting JAK-STAT signaling in the fat body lowered whole-body ceramide (Fig.
355 5k), reduced the size and number of autophagic vesicles and lysosomes, decreased
356 autolysosome number (Fig. 5i-q), and cleared the accumulation of pro-CtsL (Fig. 5r),

indicating restored lysosomal maturation. Together, these data indicate that Upd3/JAK-STAT signaling upregulates two effectors of autophagy in the fat body: *CG5966*, which boosts autophagosome biogenesis; and *schlank*, which elevates ceramide and impairs lysosomal function, together driving autophagy dysregulation in Yki flies.

Conserved pathogenic mechanism in mouse models and humans

Public STAT3 ChIP-seq dataset (ENCODE, ENCSR000DEC) in human Hela cells indicates putative STAT3 occupancy within the promoter regions of *LPL* and *CERS5* (Fig. S5b, c), suggesting a conserved regulation in mammals. To test whether this JAK-STAT-mediated lipid-autophagy pathogenic axis is conserved, we employed a mouse IL-6 tumor model: C57BL/6 mice bearing Lewis lung carcinoma (LLC) tumors engineered either to secrete IL-6 (LLC+IL-6) or not (LLC). LLC+IL-6 mice exhibit rapid weight loss, indicating progress of paraneoplastic syndrome (Liu et al., 2025). To determine whether mammalian lipases functionally homologous to CG5966 act downstream of IL-6 in tumor-bearing mice, we profiled the expression of its putative orthologs (*Pnlip* and *Lpl*) in the liver as well as adipose tissue, the major TG storage site in mammals. *Pnlip*, predominantly expressed in the pancreas, was undetectable in adipose tissue or liver, whereas *Lpl* was induced in both tissues of LLC+IL-6 mice (Fig. 6a, b). These data indicate that IL-6 promotes lipolysis in both adipose tissue and liver, aligning with our observation of elevated lipolysis in the fly fat body, which is functionally analogous to these mammalian tissues. To evaluate functional conservation, we performed lipidomic profiling of adipose tissue and liver in LLC and LLC+IL-6 mice. In adipose tissue, TG species containing C16/C18 acyl chains were significantly reduced in LLC+IL-6 mice (Fig. 6c; Fig. S6a), suggesting preferential liberation of C16/18 fatty acids through activated lipolysis. A similar selective TG depletion occurred in liver (Fig. 6d; Fig. S6b), accompanied by significant enrichment of phospholipids (PC, PI, PE, PG) containing C16/C18 chains (Fig. 6e-h; Fig. S6c-e), mirroring our observation in flies. Together, these findings support a conserved IL-6-driven program that mobilizes C16/18 fatty acids from TG to supply specific phospholipid synthesis. Given that lipolysis substrates reside primarily in adipocytes in mammals, these results point to an adipose-

386 liver metabolic circuit in which adipocyte TG hydrolysis provides fatty acids that fuel
387 hepatic phospholipid biogenesis.

388

389 We next examined whether JAK-STAT dependent upregulation of hepatic ceramide
390 synthesis is also conserved in mice. Among the six *CerS* genes (*CerS1-6*), *CerS4*, *CerS5*,
391 and *CerS6* were upregulated in liver following IL-6 induction (Fig. 6i-k; Fig. S6f). Unlike the
392 fly enzyme schlank (with limited substrate bias), mammalian CerS isoforms exhibit distinct
393 acyl-chain specificities (Mizutani et al., 2005; Pewzner-Jung et al., 2010; Riebeling et al.,
394 2003). Concordant with the known C16 preference of CerS5/6 (Mizutani et al., 2005;
395 Pewzner-Jung et al., 2010; Riebeling et al., 2003), we observed a selective increase in C16:0
396 ceramide in LLC+IL-6 mice (Fig. 6h), supporting targeted ceramide production. Given
397 previous report that hepatic ceramides are synthesized from acyl-CoAs (Pewzner-Jung et
398 al., 2010), together with our observation that hepatic TG species containing C16:0 acyl
399 chains were significantly reduced (Fig. 6d), it is likely that elevated C16 ceramide synthesis
400 in LLC+IL-6 mice is fueled by palmitoyl-CoA derived from enhanced lipolysis.

401

402 Next, we asked whether autophagic flux is blocked in mouse tumor model similarly as
403 observed in our fly model. Immunoblot markers of autophagic flux indicated a late-stage
404 block at the autolysosome in livers of LLC+IL-6 mice (Fig. 6l), evidenced by: accumulation
405 of pro-CtsL, indicating impaired lysosomal maturation; elevated SQSTM1/p62, indicating
406 defective cargo degradation; incompletely glycosylated LAMP2, consistent with lysosomal
407 biogenesis/maturation defects; and increased LC3-II, which, in the context of rising p62,
408 supports impaired flux downstream of autophagosome formation (Klionsky et al., 2021).
409 Together, these findings indicate blocked autophagic clearance in the IL6 tumor-bearing
410 mice. To access the paraneoplastic consequences of these autophagy dysregulations, we
411 turned to an inducible lung-cancer model (*Kras*$^{LSL\text{-}G12D}$*/+; Lkb*$^{\wedge flox/flox}$; "KL" mice), in which
412 tumors were initiated by intranasal Ad-Cre. In this model, ~70% of mice display cachexia
413 (>15% body-weight loss) 5-6 weeks following the tumor induction (Goncalves et al., 2018).

414 We assessed the expression correlation of *CerS* and their weight loss in cachectic and non-
415 cachectic groups, and found that expression of *CerS4* and *CerS5*, which preferentially
416 synthesize C18-20 and C16 ceramides, respectively, were positively correlated with weight
417 loss (Fig. 6m, n), reinforcing their association with paraneoplastic syndrome progression.

418

419 Extending to humans, we analyzed non-diseased liver from GTEx project (226 participants).
420 Because IL-6 activates STAT3, we asked whether hepatic *CERS4/5/6* expression
421 corresponds with STAT3 activity. Expression of *CERS5* and *CERS6* positively correlated with
422 canonical IL-6/STAT3 targets (*CRP*, *HIF1A*, *TIMP1*) and with *STAT3* itself (Fig. 6o-r; Fig. S6g-j)
423 (Castell et al., 1990; Dien et al., 2006; Johnson et al., 2018; Yu et al., 2007), suggesting IL-6
424 driven regulation of *CERS5* and *CERS6* in the human liver. To explore the clinical relevance
425 of hepatic lipolysis and ceramide synthesis, we analyzed transcriptomic data from the
426 TCGA Pan-Cancer Hepatocellular Carcinoma cohort (372 participants) (Hoadley et al.,
427 2018; Liu et al., 2018). In alignment with our fly and mouse model findings, higher hepatic
428 *LPL* expression associated with worse survival (Fig. 6t). We then examined genes in human
429 *de novo* ceramide synthesis pathway (Fig. 6s): *CERS5* and *CERS6* were significantly
430 associated with worse survival (Fig. 6u, v; Fig. S6k-n), and higher expression of *DEGS1*,
431 which catalyzes the desaturation of dihydroceramide to ceramide (Fig. 6s), aligned with
432 adverse outcomes (Fig. 6w). By contrast, *DEGS2*, a bifunctional C4-hydroxylase/desaturase
433 with tissue-restricted roles (Ota et al., 2023; UniPort Q6QHC5), showed no such
434 association, consistent with its lower hepatic relevance (Fig. S6o). Collectively, these
435 cross-species data support a conserved mechanism: Upd3/IL-6/JAK-STAT signaling
436 induces *LPL* and *CerS* expression (notably CerS5/6), driving a late-stage autophagy block
437 that contributes to paraneoplastic syndrome.

438

439 **Discussion**

440 IL-6 is a central cytokine in the metabolic crosstalk between tumors and the host,
441 coordinating systemic inflammation and altered fuel handling that drive paraneoplastic

442 syndromes (Barton, 2001; Johnson et al., 2018). Our work builds upon previous studies by
443 identifying a novel, cytokine-driven lipid-autophagy axis that underlies paraneoplastic
444 hepatic dysfunction, specifically: (1) by charting paraneoplastic-syndrome associated
445 genes organism-wide, we identify two key drivers: the triglyceride lipase *calm*/*CG5966*
446 (putative human *LPL* ortholog) and the ceramide synthase *schlank* (human *CERS* ortholog);
447 (2) we reveal a previously unrecognized Upd3/JAK-STAT control of hepatic lipid metabolism
448 through direct transcriptional upregulation of both genes; (3) we show that this lipid
449 reprogramming initiates autophagosome formation yet blocks autophagic completion,
450 leading to a pathologic buildup of enlarged, dysfunctional autolysosomes and
451 consequently hepatic injury; (4) we validate conservation in preclinical mouse models,
452 where IL-6 elevates hepatic *Lpl* and *CerS* alongside a late-stage autophagy block; (5) we
453 extend these findings to humans, showing that higher hepatic *LPL* and *CERS* expression
454 correlates with poorer survival in hepatocellular carcinoma, thereby nominating the IL-
455 6/LPL-CERS axis as a tractable therapeutic target.

456

457 JAK-STAT signaling orchestrates systemic energy mobilization through coordinated actions
458 across tissues. Through STAT3 activation, Leukemia inhibitory factor (LIF) suppresses
459 hepatic lipogenic gene expression and increases adipose triglyceride lipase (ATGL) activity
460 in adipose tissue, thereby promoting FAs release from TG (Arora et al., 2018; Yang et al.,
461 2024). Because IL-6 also activates STAT3, similar repression of lipogenesis and activation
462 of lipolysis via ATGL and/or other lipases are expected with enhanced IL-6 signaling.
463 Indeed, our data show that IL-6 upregulates *LPL* in adipose tissue and liver, which may act
464 with ATGL to promote free FAs release from TG. Under physiological conditions, excess FAs
465 are re-esterified into TAG and phospholipids or oxidized in mitochondria via β-oxidation to
466 feed the TCA cycle (Houten and Wanders, 2010; Lee and Ridgway, 2020). We previously
467 showed that hepatic IL-6/JAK-STAT3 signaling induces gluconeogenic programs and
468 elevates *PDK3*, which inhibits pyruvate dehydrogenase and restricts glycolytic acetyl-CoA
469 entry into the TCA cycle (Liu et al., 2025). Thus, upon activation of JAK-STAT pathway,
470 hepatocytes may shift substrate of TCA cycle from glucose (glycolysis-derived) to fatty

acids (β-oxidation-derived). While this may be adaptive during acute stress (Qing et al., 2020), chronic IL-6 signaling imposes sustained FA influx that can exceed hepatic β-oxidation capacity (Kerner et al., 2008), prompting diversion of surplus FAs into alternative lipid pathways, including phospholipid and ceramide synthesis. We therefore propose that IL-6's normally adaptive substrate-mobilizing role becomes maladaptive in cancer: excess FAs that cannot be efficiently oxidized are progressively redirected into membrane lipids and bioactive sphingolipids, predisposing to lipid-driven organelle dysfunction.

Hepatic lipid metabolic reprogramming is an active driver of paraneoplastic pathology. Although depletion of storage lipid is frequently observed in cancer and often interpreted solely as a signature wasting phenotype accompanied by disease progression, our findings reveal that TG depletion and reprogramming of phospholipid and ceramide metabolism contribute causally to organelle dysfunction, uncovering a novel mechanism contributing to hepatic dysfunction and systemic paraneoplastic disorders. In Yki flies, fatty-acid overload augments the membrane lipids supply required for autophagosome formation. In line with the lipid composition of autophagic structures in flies, where PE species with total carbon 32 and 34 predominate (C16/C16, C16/C18, C14/C18) (Laczkó-Dobos et al., 2021), we show that CG5966 preferentially mobilizes C16 and C18 fatty acids from TG, enriching C16- and C18-containing PE to supply membranes for autophagosome formation. Notably, this heightened initiation is tolerated, as *CG5966* overexpression alone in flies does not trigger autophagy dysfunction or induces paraneoplastic phenotypes. By contrast, in the context of Yki, CG5966-mediated membrane lipid supply and concomitant ceramide synthesis is deleterious. Sustained ceramide accumulation compromises lysosomal function, inducing membrane permeabilization, disrupting cathepsin processing, and blocking late-stage autophagic clearance (Gabandé-Rodríguez et al., 2014; Liu et al., 2016). Accordingly, we observe defective lysosomal maturation in Yki flies and in tumor-bearing mice, indicating that cancer-induced lipid reprogramming actively drives autophagy failure and hepatic dysfunction rather than representing a mere by-product of systemic disease.

IL-6/ceramide-induced lysosomal dysfunction may constitute a common lipotoxic pathology across liver diseases. Ceramide synthases are sophisticatedly regulated, integrating hormonal, stress, and kinase signals. For instance, their transcription is controlled by factors like 17β-estradiol, GPER1, and FOXP3 (Qi et al., 2021; Wegner et al., 2014), and their activity is modulated post-translationally by phosphorylation via kinases such as CK2 and PKC (Fresques et al., 2015; Mullen et al., 2012). Our data position IL-6/JAK–STAT as a previously unrecognized upstream regulator of hepatic CERS, adding a critical inflammatory layer to this regulatory network. Notably, *CERS5* and *CERS6* emerge as actionable effectors of IL-6 associated hepatic dysfunction: higher *CERS5/6* expression correlates with reduced survival in hepatocellular carcinoma. A possible mechanistic basis is that these isoforms preferentially generate C16-ceramide, a species implicated in hepatic insulin resistance, steatosis, and inflammation (Chavez and Summers, 2012; Pewzner-Jung et al., 2010) and in the pathogenesis of obesity and type 2 diabetes (Raichur et al., 2019). Moreover, IL-6 has context-dependent roles in obesity and diabetes (Alexaki, 2024; Wueest and Konrad, 2020), suggesting that the IL-6/CERS axis may underlie a shared lipotoxic program when IL-6 drives liver dysregulation in these settings. Thus, whether hepatic autophagy is similarly impaired in these diseases warrants further investigation. Nevertheless, these observations nominate selective CERS5/6 inhibition as a rational strategy to mitigate lipotoxic stress and restore autophagy-lysosome competence in IL-6 related hepatic dysfunction.

In conclusion, we delineate a mechanistic link from chronic inflammation to failure of lipid homeostasis and lysosome-limited autophagy, identifying the IL-6/CERS axis as a key driver and therapeutic entry point of cancer-associated hepatic dysfunction.

Acknowledgments

We thank Mujeeb Qadiri, Baolong Xia, Christians Villalta, Stephanie Mohr, Jonathan Zirin, Luping Liu, Litz Brown, and all members of the Perrimon Lab for their critical suggestions and help on this research. We thank Paula Montero Llopis and Microscopy Resources on the North Quad (MicRoN) core facility at Harvard Medical School for advice and help on confocal imaging. Young Yon Kwon, Yanshan Liang and Sheng Hui Lab for advice and help on lipidomics, and the *Drosophila* RNAi Screening Center (DRSC) and Bloomington Drosophila Stock Center (BDSC) for providing fly stocks used in this study. We thank Erika Bach (NYU School of Medicine) for the generous gift of Stat92E fly stocks. This work is funded in part by R01 DK136945, R01 AR057352, the Cancer Grand Challenges partnership funded by Cancer Research UK (CGCATF-2021/100022), and the National Cancer Institute (1 OT2 CA278685-01). Y.L. is supported by Charles A. King Trust. T. M. is supported by the Cystinosis Research Foundation and the Glenn Foundation for Medical Research Postdoctoral Fellowship in Aging Research. N.P. is an investigator of the Howard Hughes Medical Institute.

This article is subject to HHMI's Immediate Access to Research policy, which requires that this article be made publicly available as initial and revised preprints deposited on a designated preprint server under a CC BY 4.0 license.

Author Contributions

Y.L., T.M, and N.P. conceived the study and designed the experiments. Y.L. and T.M. conducted the majority of the experiments and the data analysis. Y.L. and A.W. carried out the mouse experiments. A.H.K performed AFM analysis. Y.L., T.M. and Y.H. were responsible for the bioinformatics analysis. J. M. A. helped for the lipidomics analysis. R.B generated the transgenic fly strains. Z.J.Z and X.M.S. helped for western blotting and

plasmid construction. Y.L., T.M. and N.P. interpreted the results and wrote the manuscript with contributions and feedback from all authors. All authors reviewed and approved the final manuscript.

Materials and Methods

Drosophila strains

All flies were maintained on standard cornmeal fly food containing yeast and agar. Crosses were reared at 18°C to inhibit Gal4 and LexA. Adult offspring flies were collected 2 days after emerging, then kept at 18°C for an additional day and subsequently shifted to 29°C for indicated days to induce transgene and/or RNAi expression. Experimental fly food was changed every other day. Stocks used in this study include *esg-LexA::GAD* (BDSC 66632), *tub-Gal80ts, Lpp-Gal4* (Song et al., 2017), *LexAop-Yki3SA-GFP* (Saavedra et al., 2021), *UAS-CG5966-RNAi* (RNAi #1: VDRC 13163, RNAi #2: VDRC 13164), *UAS-hop-RNAi* (BDSC 32966), *UAS-Stat92e-RNAi* (BDSC 33637), *UAS-schank-RNAi* (BDSC 29340), *UAS-Atg1-RNAi* (BDSC 26731), *UAS-HA-Stat92E* dominant-active form (Ekas et al., 2010), *UAS-Upd3* (Woodcock et al., 2015), and *UAS-Pvf1*(Xu et al., 2022). The *w1118* strain served as the control. Female flies are used in all experiments as they showed a more significant and consistent bloating phenotype.

Plasmid and transgenic *Drosophila* strains

The full-length cDNA of *CG5966* (FlyBase ID: FBcl0163613) was obtained from DGRC (Stock 1514588). The insert was first cloned into pENTR-TOPO (Thermo Fisher) following the manufacturer's protocol, then transferred into the *pWALIUM10-moe UAS* destination vector by Gateway LR recombination to generate *UAS-CG5966*. Positive clones were verified by colony PCR and complete Sanger sequencing. Endotoxin-reduced plasmid DNA

577 was prepared by EndoFree midiprep for embryo injections. ΦC31 integrase–mediated
578 transgenesis was used to integrate *UAS-CG5966* into standard attP docking sites: attP40
579 on chromosome 2L (25C7) or attP2 on chromosome 3L (68A4). Plasmid DNA was injected
580 into pre-blastoderm embryos by in-house microinjection. Surviving G_0 adults were crossed
581 individually to balancer stocks, and transformants were identified in the G_1 by *mini-white*
582 marker selection. GAL4-dependent overexpression of *CG5966* was verified in the fat body
583 by RT-qPCR.

584

585 **Lipidomics**

586 Lipidomics and metabolomics of fly samples were performed using the classic Folch
587 method (Folch et al., 1957). For each sample, 15 adult flies or 40 abdomens were used for
588 lipidomics and metabolomics. Samples were homogenized in a 1 mL dounce homogenizer
589 (TIGHT) on ice in 0.6 mL chloroform and 0.3 mL methanol (2:1 chloroform-methanol
590 mixture). Homogenized samples were transferred to a 15 mL glass tube with a Teflon cap,
591 with additional 0.6 mL chloroform and 0.3 mL methanol to make a final volume of 1.8 mL.
592 Samples were vortexed briefly and incubated on a rotator for 30 minutes at room
593 temperature. After incubation, 0.2 volumes (0.36 mL) of HPLC-grade deionized water
594 (HPLC dH2O) were added. Samples were then vortexed three times for 5 seconds, followed
595 by centrifugation 10 minutes at 1000 g at 4°C. Non-polar lipids solution (the lower phase)
596 was transferred to a 1.85 mL glass tube using a glass pipette, then dried under nitrogen gas.
597 Dried lipids pellets were stored at -80°C with nitrogen to prevent oxidation. Before
598 injection, pellets were resuspended in 35 µL of HPLC-grade 50% methanol/50% isopropyl
599 alcohol (IPA) and injected and analyzed using untargeted LC-MS/MS on a Thermo
600 QExactive Plus Orbitrap mass spectrometer. Lipid molecules were identified using
601 LipidSearch version 4.2 (Thermo Scientific). Ion intensity was quantified by measuring the
602 area size of identified peaks.

603

604 **Protein lysate preparation and Western blot**

605 30 abdomens with gonads and guts removed were dissected and lysed in RIPA lysis buffer
606 (50 mM Tris, pH = 8.0, 150 mM NaCl, 0.1% SDS, 0.5% sodium deoxycholate, 1% Triton X-
607 100, 1× complete ULTRA Mini EDTA-free protease inhibitor (Roche), and 1 mM PMSF).
608 Dissected tissues in RIPA buffer were mixed with zirconium oxide beads (NextAdvance) and
609 homogenized using a TissueLyser II (Qiagen). Homogenates were incubated on ice for 15
610 min and centrifuged for 15 min at 16,000 × g at 4 °C. Supernatants were transferred to new
611 tubes, and protein concentrations were determined using the BCA Protein Assay Kit
612 (Pierce) according to the manufacturer's instructions. Samples were diluted to equal
613 protein concentrations with RIPA buffer and stored at –80 °C. Equal amounts of total
614 protein were mixed with 4× Laemmli sample buffer (Bio-Rad) containing 10% β-
615 mercaptoethanol to a final 1× concentration, boiled at 95 °C for 5 min, and centrifuged at
616 16,000× g for 15 min at 4 °C. Supernatants were transferred to new tubes. Equal amounts
617 of sample were loaded to a Mini-PROTEAN TGX Stain-Free Precast Gels (Bio-Rad) and ran
618 using 1× Tris/Tricine/SDS Running Buffer (Bio-Rad) according to the manufacturer's
619 instructions. Spectra Multicolor Broad Range Protein Ladder (ThermoFish) was used as a
620 molecular weight marker. The samples on the gel were transferred to a FL PVDF membrane
621 using Tris/Glycine Buffer (Millipore) for 16 min, according to the manufacturer's
622 instructions. The membrane was then blocked with 1% Casein in 1× Tris Buffered Saline
623 (TBS) (Bio-Rad) for 1 hour at room temperature. Next, the membrane was incubated in a
624 primary antibody dilution in 1% Casein in 1× TBS overnight at 4 °C with gentle shaking.
625 Primary antibodies were used at the following concentrations: 1:1000 mouse anti-Ctsl
626 (R&D Systems, MAB22591), 1:2000 rabbit anti-Atg8 (Abcam, ab109364). Next, the
627 membrane was washed three times quickly in TBST, followed by three 10-min washes in
628 TBST with gentle shaking. The membrane was then incubated with fluorescently labeled
629 secondary antibody in 1% Casein in 1× TBS for 1 h at room temperature with gentle
630 shaking. The dilution of the fluorescently labeled secondary antibody was used as follow:
631 1:2500 hFAB™ Rhodamine; 1:2500 Goat anti-Rabbit IgG (H+L) Secondary Antibody,
632 DyLight™ 800 4X PEG; 1:2500 IRDye 680RD Goat anti-Mouse IgG Secondary Antibody. After
633 incubation, the membrane was washed three times quickly in TBST, followed by three 10-

634 min washes in TBST with gentle shaking. Then, the membranes were imaged using a Biorad
635 Chemidoc MP imager.

636

637 **Quantitative RT-PCR of fly samples**

638 Nucleospin RNA kit (Macherey-Nagel) was used to extract RNA from fly samples according
639 to the manufacturer's protocol. cDNA was synthesized using iScript™ cDNA Synthesis Kit
640 (Bio-Rad, 1708890) according to the manufacturer's protocol. qPCR was performed with
641 Thermal Cycler CFX 96 Real-Time System qPCR machine using iQ™ SYBR® Green Supermix
642 (Bio-Rad). *RP49* and *CG13220* were used as housekeeping genes. qPCR primers used are:

643 rp49-qF ATCGGTTACGGATCGAACAA

644 rp49-qR GACAATCTCCTTGCGCTTCT

645 CG13220-qF GCATATGCGACAAAGTGGGCC

646 CG13220-qR AACATTCACCGCAAGGGCTCC

647 CG5966-qF CGGGCTTGGCATCAATATGCG

648 CG5966-qR GTCTTCTTCTTGACCACATCCTGG

649 Schlank-qF TGTCATGCTGGTCCGCTAC

650 Schlank-qR ACATTTGCCGCTTTCTTAGGC

651

652 **Body fluid measurements**

653 Body fluid measurement was followed a previous protocol (Liu et al., 2025). Briefly, flies
654 were weighted before dried at 65 °C for 5 hours, and then weighted again. Body fluid is
655 calculated by subtracting the second read from the first one.

656

657 **Climbing index and survival curve of flies**

658 To assess the climbing ability, flies were transferred to a fresh vial and then tapped down to
659 the bottom. Vials were imaged after 4 seconds. The percentages of flies in the upper 2/3 of
660 the vial were recorded. The climbing index was generated from 3-4 independent vials for
661 each genotype tested. Survival of flies was analyzed by calculating the percentage of flies
662 alive in each vial, and 3 vials of 10-13 flies from each genotype were tested and flies were
663 transferred to vials contain fresh food every other day or daily.

664

665 **Gut and fly imaging**

666 Adult fly guts were dissected in cold PBS and immediately fixed for 30 minutes in 1X PBS
667 contain 4% formaldehyde. Guts were washed three times with 1X PBS contain 0.3% Triton
668 X-100 (PBT) and then mounted in Vectashield with DAPI (Vector Laboratories, H-1200). For
669 pH3 staining, washed guts were incubated with blocking buffer (5% NDS in 1X PBS contain
670 0.3% Triton X-100) for 2 hours at room temperature, incubated with rabbit anti-pH3 (1:500,
671 CST 9701S) antibody overnight at 4°C. Guts were washed three times in PBT next day before
672 incubating with secondary antibody, donkey anti-rabbit 565 (1:2000, Molecular Probes
673 A31572), for 1 hour. After three final washes with PBT, guts were mounted in Vectashield
674 with DAPI (Vector Laboratories, H-1200). Confocal images were taken with Nikon Ti2
675 Spinning Disk with Nikon Elements Acquisition Software AR (v5.02). Tumors were
676 quantified by measuring the average GFP signaling strength of gut tumors from individual
677 flies using Fiji-imageJ. Adult fly phenotypes were imaged using a ZEISS Axiozoom V16
678 fluorescence microscope. Bloating was quantified by the ratio between abdomen and head
679 compartment size using Fiji-imageJ.

680

681 **Live imaging of autophagic vesicle and lysosome**

682 For live imaging of autophagy and lysosomes, abdominal cuticles were dissected in cold
683 Schneider's insect medium. Samples were then incubated for 10 minutes at room

684 temperature in a staining buffer composed of Schneider's medium, CYTO-ID® Autophagy
685 Detection Reagent (1:1000, Enzo Life Sciences ENZ-KIT175), Hoechst nuclear stain
686 (1:1000), and LysoTracker™ Deep Red (500 nM, Thermo Fisher Scientific L12492). Following
687 incubation, the samples were rinsed once with fresh Schneider's medium and then twice
688 with phosphate-buffered saline (PBS). Finally, the stained cuticles were transferred to a
689 glass slide with mounting medium, coverslipped, and immediately visualized using a Nikon
690 Ti2 Spinning Disk confocal microscope.

691

692 **Chromatin Immunoprecipitation**

693 ChIP assay was performed with the SimpleChIP® Plus Enzymatic Chromatin IP Kit (Cell
694 Signaling, 9005). Fat bodies from 50 adult flies were collected for each sample. Fat body
695 expressing HA-tagged dominant-active Stat92e were dissected and flash-frozen in liquid
696 nitrogen. Cross-linked was done with 1.5% formaldehyde for 20 minutes at room
697 temperature. Cross-linking was stopped by adding glycine solution for 5 minutes at RT,
698 samples were washed twice with 1 ml 1X PBS containing 1X Protease Inhibitor Cocktail and
699 homogenized using 1 ml dounce homogenizer to release nuclei. Samples were lysed with
700 Diagenode Bioruptor sonicator to retrieve cross-linked chromatin. Chromatins were diluted
701 in 1X ChIP buffer before incubating with 10 ul HA-Tag (C29F4) Rabbit mAb (Cell Signaling,
702 3724) or Normal Rabbit IgG (Cell Signaling, 2729) overnight with rotation at 4°C. Next day,
703 each immunoprecipitation was incubated for 2 hours with 30 ul ChIP-Grade Protein G
704 Magnetic Beads (Cell Signaling, 9006) at 4 °C with rotation. Beads were then washed and
705 incubated in 150 µl 1X ChIP Elution Buffer at 65 °C for 30 minutes with vortexing (1200 rpm)
706 to elute the chromatin. 6 µl 5M NaCl and 2 µl Proteinase K was added to the eluted
707 chromatin supernatant to reverse cross-links and incubated 2 hours at 65°C. DNA was then
708 purified from each sample using Spin Columns provided by the kit. 1 ul DNA sample was
709 used as template for qPCR to detect enrichments of certain DNA regions. qPCR of a
710 fragment in the Sam-S gene region was used as the negative control. Primers used are:

711 Sam-S-qF AAA CTT TGA CCT CAG GCC C

712 Sam-S-qR CGC TGG TAT ATC GGC TGG

713 Schlank-ChIPF1 CATGTGCTGACAACAATTGGAC

714 Schlank-ChIPR1 AGCAAACTTCATCGTTGAGACC

715 Schlank-ChIPF2 GCCATAAGCGCAAGTTAACGAG

716 Schlank-ChIPR2 CACTAATGCACACTCACAGCG

717 CG5966-ChIP-F CAGATCGGCGGAGATATACACG

718 CG5966-ChIP-R GTCTCGAGTGTGCCGTTAGC

719

720 **Mouse models**

721 The *Kras*$^{G12D/+}$; *Lkb1*$^{f/f}$ mice described before (Ji et al., 2007) were further backcrossed to FVB
722 mice. Tumor induction in adult 12- to 20-week-old FVB mice was achieved by intranasal
723 administration of 75 µL of PBS containing 2.5 × 10^7 pfu of Adenovirus CMV-Cre (Ad5CMV-
724 Cre) obtained from the University of Iowa Gene Transfer Vector Core (Iowa City, IA) and
725 1 mM $CaCl_2$. Male mice were used for liver RNAseq. The *Kras*$^{G12D/+}$; *Lkb1*$^{f/f}$ mice experiments
726 were approved by the Institutional Animal Care and Use Committee (IACUC) of Weill
727 Cornell Medical College and maintained as approved by the Institutional Animal Care and
728 Use Committee (IACUC) at Weill Cornell Medicine (NYC).

729 C57BL/6J mice were obtained from the Jackson Laboratory (Strain #000664). 2 x 10^6 Lewis
730 Lung Carcinoma (LLC) cells or LLC cells edited to produce IL-6 (LLC-IL6) were
731 subcutaneously inoculated into their right flank after a week of acclimation. Mice were kept
732 in pathogen-free conditions on a 24 hour 12:12 light-dark cycle. 9 weeks old male C57BL/6J
733 mice were used in the experiments. C57BL/6J mice experiments were approved by the
734 Institutional Animal Care and Use Committee (IACUC) at Cold Spring Harbor Laboratory
735 (CSHL) and were conducted in accordance with the National Institutes of Health Guide for
736 the Care and Use of Laboratory Animals. Body weights and clinical signs of cachexia were
737 monitored daily. Handling was kept to a minimum. Mice were sacrificed when tumor size

738 exceeded 2 cm length, when weight loss exceeded 15% from peak weight, or when showing
739 clinical signs of discomfort indicative of cachectic endpoint as stated by the Animal
740 Cachexia Score (ACASCO): piloerection, diarrhea or constipation, hunched posture,
741 tremors, and closed eyes. Death was confirmed by cervical dislocation.

742

743 **Lewis Lung Carcinoma (LLC) cell line**

744 LLC cells were purchased from American Type Culture Collection (ATCC), cultured in
745 complete growth medium consisting of Dulbecco's Modified Eagle Medium (DMEM)
746 (#10027CV; Corning) containing 1x Penicillin-Streptomycin solution (#15-140-122; Thermo
747 Fisher) and 10% of Heat-Inactivated Fetal Bovine Serum (FBS) (#10-438-026; Thermo
748 Fisher). LLC cells were transfected with 500ng of plasmid (comprising 2.5:1 PB-IL6 plasmid
749 and PBase plasmids) using Lipofectamine 3000 (Thermo Fisher) according to the
750 manufacturer's protocol. PBase plasmid was obtained from System Biosciences
751 (#PB210PA-1) and PB-IL6 was obtained from VectorBuilding comprising mouse Il6 cDNA
752 driven by EF1a promoter and flanked by piggyBac elements. 48 hours after transfection, the
753 media was changed and replaced with DMEM media supplemented with 3 μg/ml
754 puromycin. After 14 days of antibiotic selection, monoclonal populations were isolated by
755 serial dilutions in a 96-well plate. To identify clones with constitutive IL-6 expression, we
756 measured IL-6 in the cell supernatant for each clone using the Mouse IL-6 ELISA Kit
757 (#ab222503; Abcam).1x Trypsin-EDTA (#15400054; Thermo Fisher) was used for cell
758 dissociation. Cells were resuspended in FBS-free DMEM and counted using a Vi-Cell
759 counter prior to subcutaneous injection. For each C57BL/6J mouse, $2x10^6$ viable cells
760 diluted in 100μL DMEM into the right flank.

761

762 **Lipid extraction and profiling in mice**

763 Lipid extracts were analyzed using a Dionex Ultimate 3000 RSLC system (Thermo Scientific)
764 coupled with a QExactive mass spectrometer (Thermo Scientific, Waltham, MA, USA) mass

765 spectrometer. Chromatographic separation was achieved on an ACQUITY UPLC CSH C18
766 column (130Å, 1.7 μm, 2.1 mm × 100 mm) with an ACQUITY UPLC CSH C18 VanGuard pre-
767 column (130Å, 1.7 μm, 2.1 mm × 5 mm) (Waters, Milford, MA) with column temperature at
768 50 ˚C. For the gradient, mobile phase A consisted of an acetonitrile-water mixture (6:4), and
769 mobile phase B was a 2-propanol-acetonitrile mixture (9:1), both phases containing 10 mM
770 ammonium formate and 0.1% formic acid. The linear elution gradient was: 0-3 min, 20% B;
771 3- 7 min, 20-55% B; 7-15 min, 55-65% B; 15-21 min, 65-70% B; 21-24 min, 70-100% B; and
772 24-26 min, 100% B, 26-28 min, 100-20% B, 28-30 min, 20% B, with a flow rate of 0.35 mL/
773 min. The autosampler was at 4˚C. The injection volume was 5 μL. Needle wash was applied
774 between samples using a mixture of dichloromethane-isopropanol-acetonitrile (1:1:1).

775

776 ESI-MS analysis was performed in positive and negative ionization polarities using a
777 combined full mass scan and data-dependent MS/MS (Top 10) (Full MS/dd-MS^2) approach.
778 The experimental conditions for full scanning were as follows: resolving power, 70,000;
779 automatic gain control (AGC) target, 1×10^6; and maximum injection time (IT), 100 ms. The
780 scan range of the instrument was set to m/z 100-1200 in both positive and negative ion
781 modes. The experimental conditions for the data-dependent product ion scanning were as
782 follows: resolving power, 17,500; AGC target, 5×10^4; and maximum IT, 50 ms. The isolation
783 width and stepped normalized collision energy (NCE) were set to 1.0 m/z, and 10, 20, and 40
784 eV. The intensity threshold of precursor ions for dd-MS2 analysis and the dynamic exclusion
785 were set to 1.6×10^5 and 10 s. The ionization conditions in the positive mode were as follows:
786 sheath gas flow rate, 50 arb; auxiliary (AUX) gas flow rate, 15 arb; sweep gas flow rate, 1 arb;
787 ion spray voltage, 3.5 kV; AUX gas heater temperature, 325 ˚C; capillary temperature, 350 ˚C;
788 and S-lens RF level, 55. The ionization conditions in the negative mode were as follows:
789 sheath gas flow rate, 45 arb; auxiliary (AUX) gas flow rate, 10 arb; sweep gas flow rate, 1 arb;
790 ion spray voltage, 2.5 kV; AUX gas heater temperature, 320 ˚C; capillary temperature, 320 ˚C;
791 and S-lens RF level, 55.

792 Thermo Scientific™ LipidSearch™ software version 5.0 was used for lipid identification and
793 quantitation. First, the product search mode was used during which lipids were identified
794 based on the exact mass of the precursor ions and the mass spectra resulting from product
795 ion scanning. The precursor and product tolerances were set to 10 and 10 ppm mass
796 windows. The absolute intensity threshold of precursor ions and the relative intensity
797 threshold of product ions were set to 30000 and 1%. Next, the search results from the
798 individual positive or negative ion files from each sample were aligned within a retention time
799 window (±0.25 min) and then all the data were merged for each annotated lipid with a
800 retention time correction tolerance of 0.5 min. The annotated lipids were then filtered to
801 reduce false positives by only including a total grade of A or B or C for PC and SM; otherwise
802 only including grade A or B.

803

804 **Bulk RNA-Sequencing from KL livers**

805 Total RNA was extracted from the liver using TRIzol (Thermo Fisher), followed by a clean-up
806 using RNeasy kit (Qiagen). 1mg RNA from each sample was submitted to the WCM
807 Genomics Resources Core Facility. Raw sequenced reads were aligned to the mouse
808 reference GRCm38 using STAR (v2.4.1d, 2-pass mode) aligner, and raw counts were
809 obtained using HTSeq (v0.6.1). Differential expression analysis, batch correction and
810 principal component analysis (PCA) were performed using R Studio Version 4.2.2 and
811 DESeq2 (v.1.38.3). Gene set enrichment analysis (GSEA) analysis was performed with the
812 R package fGSEA (10.18129/B9.bioc.fgsea), using the Reactome pathway database
813 contained in the 2022 release of Mouse Molecular Signatures Database from the Broad
814 Institute (https://www.gsea-msigdb.org/gsea/msigdb/mouse/collections.jsp).

815

816 **Quantitative RT-PCR of mouse samples**

817 For LLC and IL6-secreting LLC mouse liver samples, 100 mg tissue was lysed in 1 mL of
818 Qia-zol with Qiagen TissueLyser II at 20 Hz for 4 minutes. Samples were centrifuged at

819 12,000 g for 12 minutes at 4 C to separate aqueous layer from others. Approximately 600 ul
820 of RNA containing aqueous layer was collected and processed using Qiagen RNeasy lipid
821 RNA extraction kit and QiaCube machine. RNA were diluted in ddH20 to 100 ng/uL. cDNA
822 was synthesized using iScript™ cDNA Synthesis Kit (Bio-Rad, 1708890) according to the
823 manufacturer's protocol. qPCR was performed with Thermal Cycler CFX 96 Real-Time
824 System qPCR machine using iQ™ SYBR® Green Supermix (Bio-Rad). RN18s was used as
825 housekeeping gene. Primers used are:

826 Rn18s-qF GTAACCCGTTGAACCCCATT

827 Rn18s-qR CCATCCAATCGGTAGTAGCG

828 CerS1 qF CCACCACACACATCTTTCGG

829 CerS1 qR GGAGCAGGTAAGCGCAGTAG

830 CerS2 qF AGAGTGGGCTCTCTGGACG

831 CerS2 qR CCAGGGTTTATCCACAGTGAC

832 CerS3 qF CCTGGCTGCTATTAGTCTGATG

833 CerS3 qR CTGCTTCCATCCAGCATAGG

834 CerS4 qF CTGTGGTACTGTTGTTGCATGAC

835 CerS4 qR GCGCGTGTAGAAGAAGACTAAG

836 CerS5 qF GACTGCTTCCAAAGCCTTGAG

837 CerS5 qR GCAGTTGGCACCATTGCTAG

838 CerS6 qF CCGGAGTGGACAAAGCAAGA

839 CerS6 qR ATTGTGCGGAAGCCAAAACC

840 Pnlip qF CTGGGAGCAGTAGCTGGAAG

841 Pnlip qR AGCGGGTGTTGATCTGTGC

842 Lpl qF GGGAGTTTGGCTCCAGAGTTT

843 Lpl qR TGTGTCTTCAGGGGTCCTTAG

844

845 **Public datasets, Software, Quantification and Statistical Analyses**

846 Transcriptomic data from non-diseased liver samples of 226 individuals were obtained
847 from the Genotype-Tissue Expression (GTEx) Project. Transcriptomic data and
848 corresponding survival records were obtained from the Hepatocellular Carcinoma (LIHC)
849 cohort of 372 patients in the PanCancer Atlas of The Cancer Genome Atlas (TCGA) Program
850 (Hoadley et al., 2018; Liu et al., 2018). Sex and gender were not considered in the design of
851 present research, and related information was not collected for the analysis. Kaplan-Meier
852 survival curves were generated using the R packages survival and survminer. We used
853 Biorender and PyMOL for a subset of figures, and ChatGPT and Gemini were used to
854 proofread the text. The authors reviewed and edited the content as needed and take full
855 responsibility for the content of the publication. GraphPad Prism was used for generation
856 of figures, statistical analysis, and gene expression correlation analysis. Data distribution
857 was assumed to be normal, but this was not formally tested. Animals and samples were
858 randomly assigned to experimental groups, and the data collection was randomized. Data
859 collection and analysis were not performed blind to the conditions of the experiments.
860 Statistical analysis was done with student's t test (two experimental groups) or ordinary
861 one-way ANOVA (three or more experimental groups) by the default settings of GraphPad
862 Prism (ns indicates not significant, * indicates $p<0.05$, ** indicates $p<0.01$, *** indicates
863 $p<0.001$, **** indicates $p<0.0001$). Gene expression levels (qPCR) were normalized to the
864 mean of control samples. Error bars indicate the standard deviations with the mean as the
865 center. n indicates the number of biological replicates in each experiment, for fly
866 experiments, each biological replicates contains 10-16 flies otherwise noted; for mouse
867 experiment, each biological replicates is one mouse.

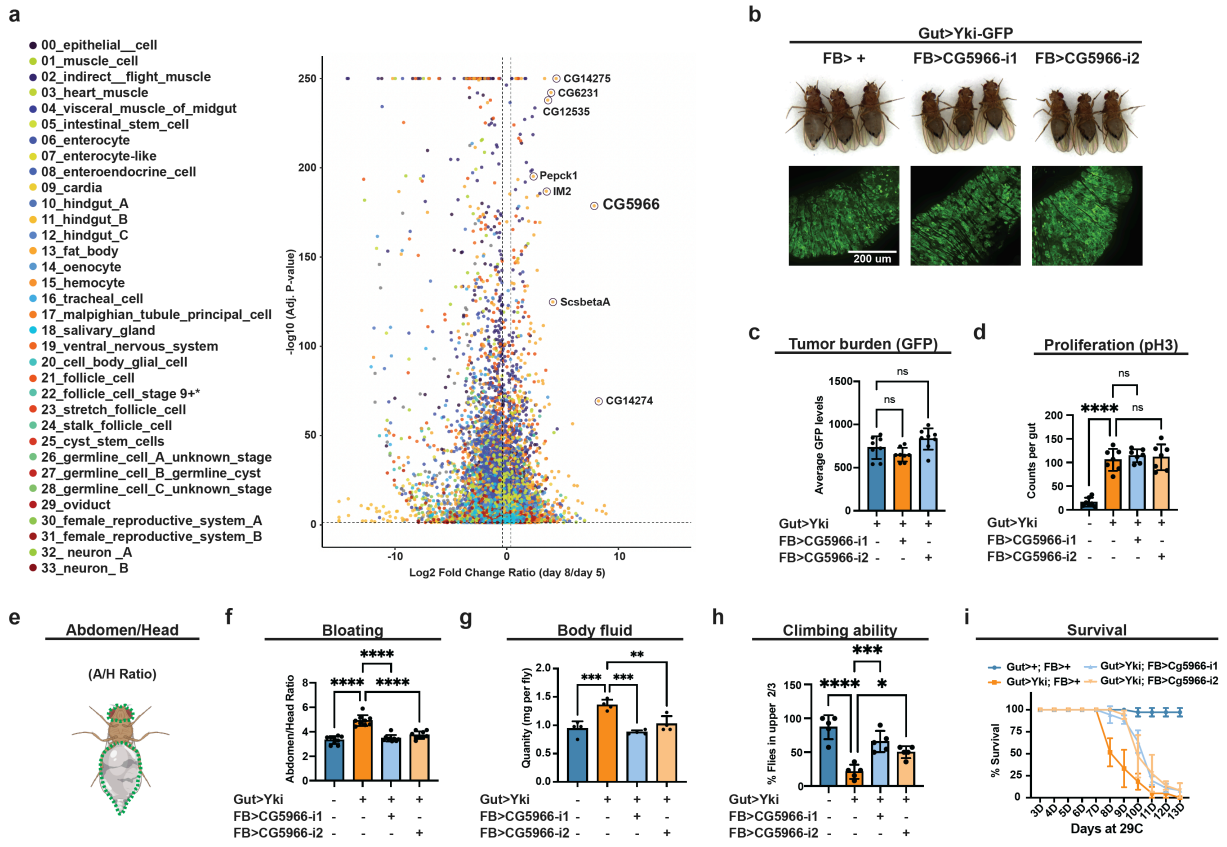
a
00_epithelial__cell
01_muscle_cell
02_indirect__flight_muscle
03_heart_muscle
04_visceral_muscle_of_midgut
05_intestinal_stem_cell
06_enterocyte
07_enterocyte-like
08_enteroendocrine_cell
09_cardia
10_hindgut_A
11_hindgut_B
12_hindgut_C
13_fat_body
14_oenocyte
15_hemocyte
16_tracheal_cell
17_malpighian_tubule_principal_cell
18_salivary_gland
19_ventral_nervous_system
20_cell_body_glial_cell
21_follicle_cell
22_follicle_cell_stage 9+*
23_stretch_follicle_cell
24_stalk_follicle_cell
25_cyst_stem_cells
26_germline_cell_A_unknown_stage
27_germline_cell_B_germline_cyst
28_germline_cell_C_unknown_stage
29_oviduct
30_female_reproductive_system_A
31_female_reproductive_system_B
32_ neuron _A
33_neuron_ B
CG14275
CG6231
CG12535
Pepck1
IM2
CG5966
ScsbetaA
CG14274
-log10 (Adj. P-value)
Log2 Fold Change Ratio (day 8/day 5)
b
Gut>Yki-GFP
FB> +
FB>CG5966-i1
FB>CG5966-i2
200 um
c
Tumor burden (GFP)
Average GFP levels
ns
Gut>Yki
FB>CG5966-i1
FB>CG5966-i2
d
Proliferation (pH3)
Counts per gut
****
e
Abdomen/Head
(A/H Ratio)
f
Bloating
Abdomen/Head Ratio
g
Body fluid
Quanity (mg per fly)
h
Climbing ability
% Flies in upper 2/3
i
Survival
Gut>+; FB>+
Gut>Yki; FB>+
Gut>Yki; FB>Cg5966-i1
Gut>Yki; FB>Cg5966-i2
% Survival
Days at 29C

868

869 **Figure 1. Identification of CG5966 as a paraneoplastic factor**

870 **a**, Progression association index of differential expressed genes across cell clusters. **b**,
871 Images of gut tumors and phenotypes of Yki flies with or without fat-body *CG5966*
872 depletion at day 6. **c**, Quantification of gut tumors (GFP signal, arbitrary units) of Yki flies
873 with or without fat-body *CG5966* depletion at day 6 (n = 8). **d**, Total pH3 counts per gut of
874 control flies and Yki flies with or without fat-body *CG5966* depletion at day 6 (n = 8). **e**, The
875 bloating quantification by abdomen/head (A/H) size ratio. **f**, Quantification of bloating
876 phenotypes of control flies and Yki flies with or without fat-body *CG5966* depletion at day 6
877 (A/H ratio, n=9). **g**, Body-fluid levels of Yki flies with or without fat-body *CG5966* depletion
878 at day 6 (n = 4). **h**,**i**, The climbing ability at day 6 (**h**) (n = 4) and survival curve (**i**) (n = 3) of
879 control flies, Yki flies, and Yki flies with fat-body *CG5966* depletion. *$p < 0.05$, **$p < 0.01$,
880 ***$p < 0.001$, ****$p < 0.0001$, ns indicates not significant. Error bars indicate SDs. n
881 indicates the number of biological replicates in each experiment.

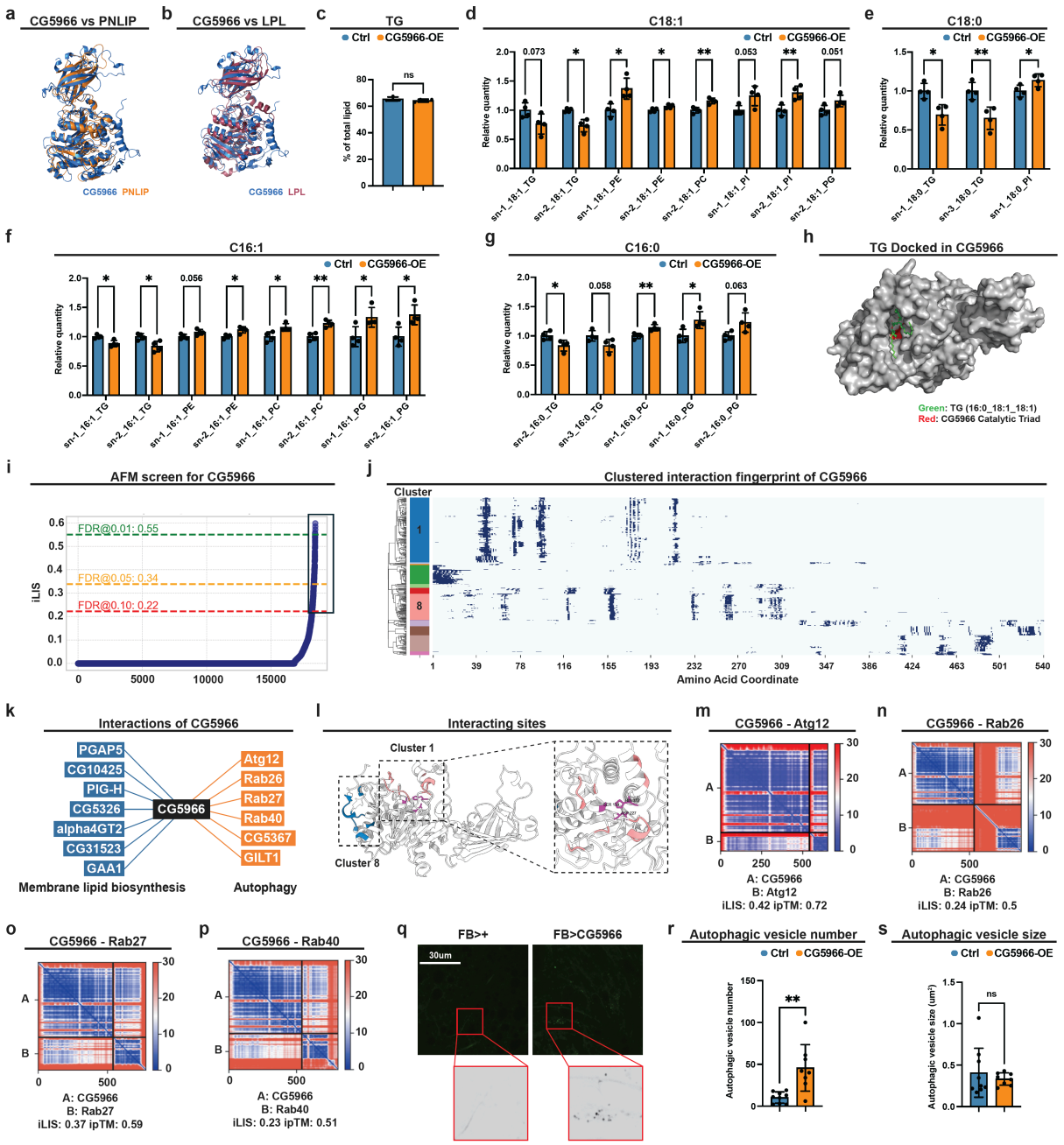
a
CG5966 vs PNLIP
CG5966 PNLIP
b
CG5966 vs LPL
CG5966 LPL
c
TG
Ctrl CG5966-OE
ns
% of total lipid
d
C18:1
Ctrl CG5966-OE
Relative quantity
sn-1_18:1_TG
sn-2_18:1_TG
sn-1_18:1_PE
sn-2_18:1_PE
sn-2_18:1_PC
sn-1_18:1_PI
sn-2_18:1_PI
sn-2_18:1_PG
e
C18:0
Ctrl CG5966-OE
Relative quantity
sn-1_18:0_TG
sn-3_18:0_TG
sn-1_18:0_PI
f
C16:1
Ctrl CG5966-OE
Relative quantity
sn-1_16:1_TG
sn-2_16:1_TG
sn-1_16:1_PE
sn-2_16:1_PE
sn-1_16:1_PC
sn-2_16:1_PC
sn-1_16:1_PG
sn-2_16:1_PG
g
C16:0
Ctrl CG5966-OE
Relative quantity
sn-2_16:0_TG
sn-3_16:0_TG
sn-1_16:0_PC
sn-1_16:0_PG
sn-2_16:0_PG
h
TG Docked in CG5966
Green: TG (16:0_18:1_18:1)
Red: CG5966 Catalytic Triad
i
AFM screen for CG5966
FDR@0.01: 0.55
FDR@0.05: 0.34
FDR@0.10: 0.22
iLIS
j
Clustered interaction fingerprint of CG5966
Cluster
Amino Acid Coordinate
k
Interactions of CG5966
PGAP5
CG10425
PIG-H
CG5326
alpha4GT2
CG31523
GAA1
CG5966
Atg12
Rab26
Rab27
Rab40
CG5367
GILT1
Membrane lipid biosynthesis
Autophagy
l
Interacting sites
Cluster 1
Cluster 8
m
CG5966 - Atg12
A: CG5966
B: Atg12
iLIS: 0.42 ipTM: 0.72
n
CG5966 - Rab26
A: CG5966
B: Rab26
iLIS: 0.24 ipTM: 0.5
o
CG5966 - Rab27
A: CG5966
B: Rab27
iLIS: 0.37 ipTM: 0.59
p
CG5966 - Rab40
A: CG5966
B: Rab40
iLIS: 0.23 ipTM: 0.51
q
FB>+
FB>CG5966
30um
r
Autophagic vesicle number
Ctrl CG5966-OE
Autophagic vesicle number
s
Autophagic vesicle size
Ctrl CG5966-OE
Autophagic vesicle size (um²)

882

883 **Figure 2. CG5966 is a triglyceride lipase that promotes autophagosome formation.**

884 **a**,**b**, 3D structural modeling using AlphaFold demonstrating similarity of human PNLIP (**a**)
885 and LPL (**b**) to CG5966. **c**, Relative levels of Abdomen TG levels of flies with or without fat-
886 body *CG5966* overexpression (n=4), data were retrieved from lipidomics analysis. **d**-**g**,
887 Relative levels of abdomen lipid species with C18:1 (**d**), C18:0 (**e**), C16:1 (**f**), and C16:0 (**g**)
888 acyl chains of flies with or without fat-body *CG5966* overexpression (n=4), data were
889 retrieved from lipidomics analysis. **h**, Molecular docking of TG (16:0/18:1/18:1) to CG5966
890 by the Boltz-2 docking model. **i**, AFM prediction of interacting partners of CG5966. **j**,
891 Cluster of predicted interacting partners of CG5966 based on interacting sites. Y-axis
892 present grouping of interacting patterners and X-axis indicate the interacting sites of
893 CG5966. **k**, Predicted interactions between CG5966 with membrane lipid biosynthesis and
894 autophagy regulators by AFM. **l**, Predicted interacting pocket of CG5966. **m**-**p**, AFM
895 prediction of interaction between CG5966 and Atg12 (**m**), Rab26 (**n**), Rab27 (**o**), Rab40 (**p**).
896 **q**, Live imaging of fat bodies with autophagic vesicle staining dye in flies with or without fat-
897 body *CG5966* overexpression at day 7. **r**, **s**, Quantification of autophagic vesicle numbers
898 (**r**) and sizes (**s**) in **q** (n>8). *$p < 0.05$, **$p < 0.01$, ***$p < 0.001$, ****$p < 0.0001$, ns indicates
899 not significant. Error bars indicate SDs. n indicates the number of biological replicates in
900 each experiment.

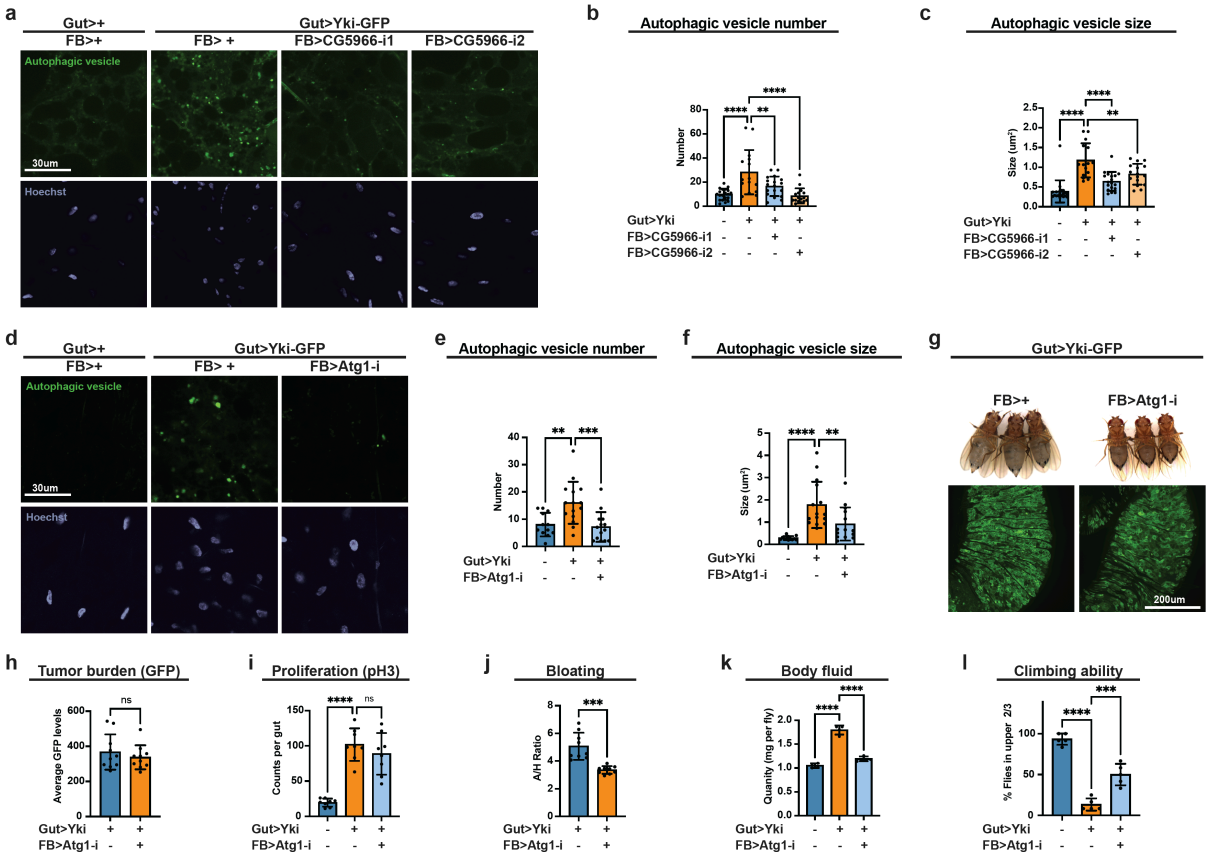
a
Gut>+
FB>+
Gut>Yki-GFP
FB> +
FB>CG5966-i1
FB>CG5966-i2
Autophagic vesicle
30um
Hoechst
b
Autophagic vesicle number
Number
Gut>Yki
FB>CG5966-i1
FB>CG5966-i2
c
Autophagic vesicle size
Size (um²)
d
Gut>+
FB>+
Gut>Yki-GFP
FB> +
FB>Atg1-i
e
Autophagic vesicle number
f
Autophagic vesicle size
g
Gut>Yki-GFP
FB>+
FB>Atg1-i
200um
h
Tumor burden (GFP)
Average GFP levels
i
Proliferation (pH3)
Counts per gut
j
Bloating
A/H Ratio
k
Body fluid
Quanity (mg per fly)
l
Climbing ability
% Flies in upper 2/3

901

Figure 3. CG5966 promotes autophagosome formation in the fat body of Yki flies.

a, Live imaging of fat bodies with autophagic vesicle staining dye in Yki flies with or without fat-body *CG5966* depletion at day 7. **b**, **c**, Quantification of autophagic vesicle numbers (**b**) and sizes (**c**) in **a** (n>15). **d**, Live imaging of fat bodies with autophagic vesicle staining dye in Yki flies with or without fat-body *Atg1* depletion at day 7. **e**, **f**, Quantification of autophagic vesicle numbers (**e**) and sizes (**f**) in **d** (n>15). **g**, Images of gut tumors and phenotypes of Yki flies with or without fat-body *Atg1* depletion at day 6. **h**, Quantification of gut tumors (GFP signal, arbitrary units) of Yki flies with or without fat-body *Atg1* depletion at day 6 (n = 8). **i**, Total pH3 counts per gut of control flies and Yki flies with or without fat-body Atg1 depletion at day 6 (n = 8). **j**, Quantification of bloating phenotypes of control flies and Yki flies with or without fat-body Atg1 depletion at day 6 (A/H ratio, n=9). **k**, Body-fluid levels of Yki flies with or without fat-body *Atg1* depletion at day 6 (n = 4). **l**, The climbing ability at day 6 (n = 4) of control flies, Yki flies, and Yki flies with fat-body *Atg1* depletion. *$p < 0.05$, **$p < 0.01$, ***$p < 0.001$, ****$p < 0.0001$, ns indicates not significant. Error bars indicate SDs. n indicates the number of biological replicates in each experiment.

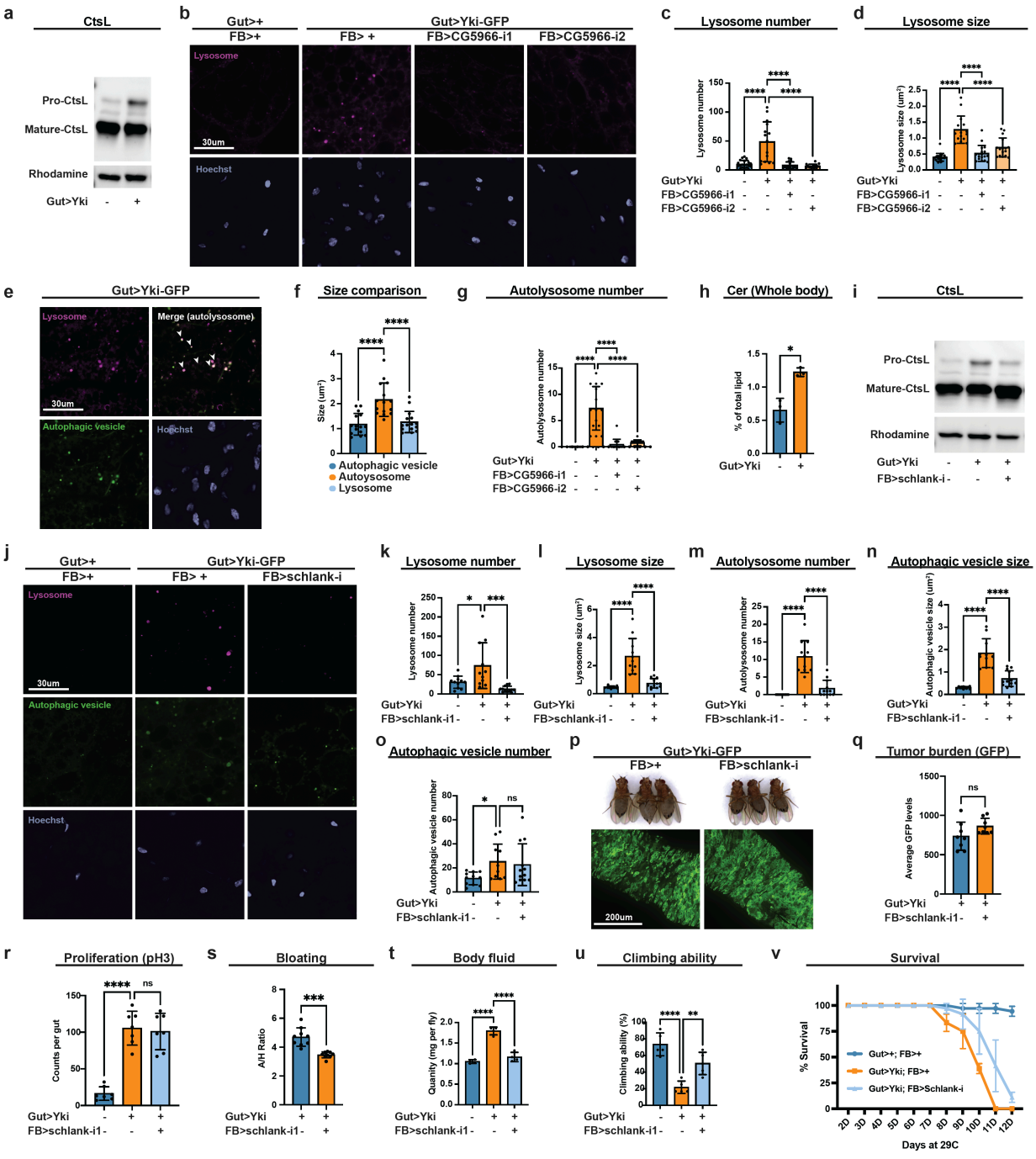
a
CtsL
Pro-CtsL
Mature-CtsL
Rhodamine
Gut>Yki - +
b
Gut>+
FB>+
Gut>Yki-GFP
FB> +
FB>CG5966-i1
FB>CG5966-i2
Lysosome
30um
Hoechst
c
Lysosome number
Lysosome number
Gut>Yki - + + +
FB>CG5966-i1 - - + -
FB>CG5966-i2 - - - +
d
Lysosome size
Lysosome size (um²)
Gut>Yki - + + +
FB>CG5966-i1 - - + -
FB>CG5966-i2 - - - +
e
Gut>Yki-GFP
Lysosome
Merge (autolysosome)
30um
Autophagic vesicle
Hoechst
f
Size comparison
Size (um²)
Autophagic vesicle
Autoysosome
Lysosome
g
Autolysosome number
Autolysosome number
Gut>Yki - + + +
FB>CG5966-i1 - - + -
FB>CG5966-i2 - - - +
h
Cer (Whole body)
% of total lipid
Gut>Yki - +
i
CtsL
Pro-CtsL
Mature-CtsL
Rhodamine
Gut>Yki - + +
FB>schlank-i - - +
j
Gut>+
FB>+
Gut>Yki-GFP
FB> +
FB>schlank-i
Lysosome
30um
Autophagic vesicle
Hoechst
k
Lysosome number
Lysosome number
Gut>Yki - + +
FB>schlank-i1 - - +
l
Lysosome size
Lysosome size (um²)
Gut>Yki - + +
FB>schlank-i1 - - +
m
Autolysosome number
Autolysosome number
Gut>Yki - + +
FB>schlank-i1 - - +
n
Autophagic vesicle size
Autophagic vesicle size (um²)
Gut>Yki - + +
FB>schlank-i1 - - +
o
Autophagic vesicle number
Autophagic vesicle number
Gut>Yki - + +
FB>schlank-i1 - - +
p
Gut>Yki-GFP
FB>+
FB>schlank-i
200um
q
Tumor burden (GFP)
Average GFP levels
Gut>Yki + +
FB>schlank-i1 - +
r
Proliferation (pH3)
Counts per gut
Gut>Yki - + +
FB>schlank-i1 - - +
s
Bloating
A/H Ratio
Gut>Yki + +
FB>schlank-i1 - +
t
Body fluid
Quanity (mg per fly)
Gut>Yki - + +
FB>schlank-i1 - - +
u
Climbing ability
Climbing ability (%)
Gut>Yki - + +
FB>schlank-i1 - - +
v
Survival
% Survival
Gut>+; FB>+
Gut>Yki; FB>+
Gut>Yki; FB>Schlank-i
2D 3D 4D 5D 6D 7D 8D 9D 10D 11D 12D
Days at 29C

917

Figure 4. Autophagic flux is blocked in Yki flies.

a, Western blot showing pro and matured forms of CtsL in Yki and control flies. Rhodamine was used as loading control. **b**, Live imaging of lysosomes in Yki flies with or without fat-body *CG5966* depletion at day 7. **c**, **d**, Quantification of lysosome numbers (**c**) and sizes (**d**) in **b** (n>15). **e**, Live imaging of lysosome and autophagic vesicles in Yki flies at day 7. **f**, Quantification of sizes of autophagic vesicles, autolysosome and lysosome in Yki flies (n>15). **g**, Quantification of autolysosome numbers in Yki flies with or without fat-body *CG5966* depletion at day 7 (n>15). **h**, Relative levels of whole-body ceramide levels of Yki and control flies (n=3), data were retrieved from lipidomics analysis. **i**, Western blot showing pro and matured forms of CtsL in control flies, Yki flies with or without fat-body *schlank* depletion at day 7. Rhodamine was used as loading control. **j**, Live imaging of lysosomes and autophagic vesicles in Yki flies with or without fat-body *schlank* depletion at day 7. **k**-**n**, Quantification of lysosome numbers (**k**) and sizes (**l**), autophagic vesicle numbers (**m**) and sizes (**n**), autolysosome numbers (**o**) in **j** (n>15). **p**, Images of gut tumors and phenotypes of Yki flies with or without fat-body *schlank* depletion at day 6. **q**, Quantification of gut tumors (GFP signal, arbitrary units) of Yki flies with or without fat-body *schlank* depletion at day 6 (n = 8). **r**, Total pH3 counts per gut of control flies and Yki flies with or without fat-body *schlank* depletion at day 6 (n = 8). **s**, Quantification of bloating phenotypes of control flies and Yki flies with or without fat-body *schlank* depletion at day 6 (A/H ratio, n=9). **t**, Body-fluid levels of Yki flies with or without fat-body *schlank* depletion at day 6 (n = 4). **u**, **v**, The climbing ability at day 6 (**u**) (n = 4) and survival curve (**v**) (n = 3) of control flies, Yki flies, and Yki flies with fat-body *schlank* depletion. *$p < 0.05$, **$p < 0.01$, ***$p < 0.001$, ****$p < 0.0001$, ns indicates not significant. Error bars indicate SDs. n indicates the number of biological replicates in each experiment.

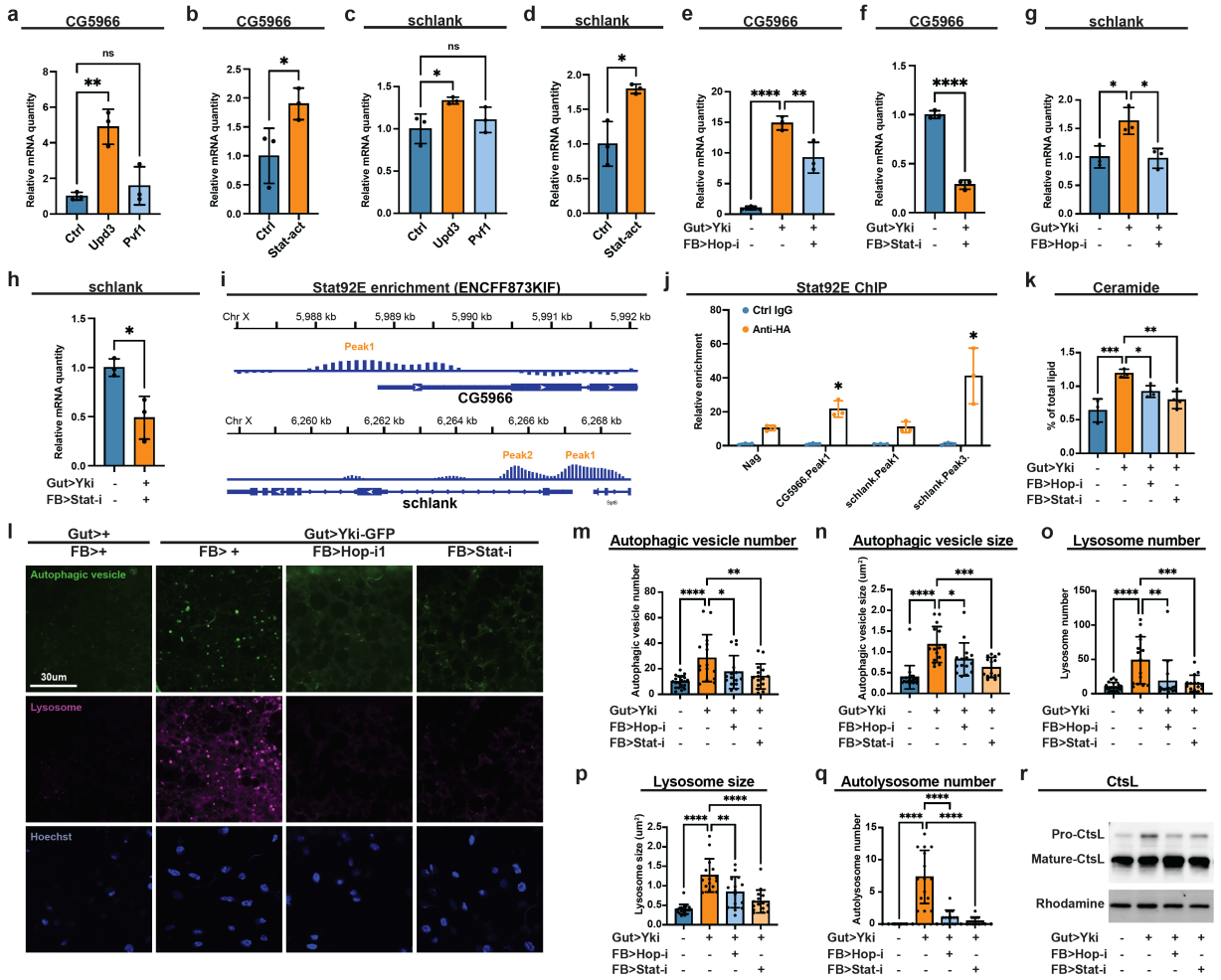
a
CG5966
Relative mRNA quantity
ns
**
Ctrl
Upd3
Pvf1
b
CG5966
*
Ctrl
Stat-act
c
schlank
ns
*
Ctrl
Upd3
Pvf1
d
schlank
*
Ctrl
Stat-act
e
CG5966
****
**
Gut>Yki
FB>Hop-i
f
CG5966
****
Gut>Yki
FB>Stat-i
g
schlank
*
*
Gut>Yki
FB>Hop-i
h
schlank
*
Gut>Yki
FB>Stat-i
i
Stat92E enrichment (ENCFF873KIF)
Chr X
5,988 kb
5,989 kb
5,990 kb
5,991 kb
5,992 kb
Peak1
CG5966
Chr X
6,260 kb
6,262 kb
6,264 kb
6,266 kb
6,268 kb
Peak2
Peak1
schlank
j
Stat92E ChIP
Ctrl IgG
Anti-HA
Relative enrichment
Nag
CG5966.Peak1
schlank.Peak1
schlank.Peak3
k
Ceramide
% of total lipid
***
*
**
Gut>Yki
FB>Hop-i
FB>Stat-i
l
Gut>+
FB>+
Gut>Yki-GFP
FB> +
FB>Hop-i1
FB>Stat-i
Autophagic vesicle
30um
Lysosome
Hoechst
m
Autophagic vesicle number
****
*
**
Gut>Yki
FB>Hop-i
FB>Stat-i
n
Autophagic vesicle size
Autophagic vesicle size (um²)
****
*
***
Gut>Yki
FB>Hop-i
FB>Stat-i
o
Lysosome number
Lysosome number
****
**
***
Gut>Yki
FB>Hop-i
FB>Stat-i
p
Lysosome size
Lysosome size (um²)
****
**
****
Gut>Yki
FB>Hop-i
FB>Stat-i
q
Autolysosome number
Autolysosome number
****
****
****
Gut>Yki
FB>Hop-i
FB>Stat-i
r
CtsL
Pro-CtsL
Mature-CtsL
Rhodamine
Gut>Yki
FB>Hop-i
FB>Stat-i

942

943 **Figure 5. The JAK–STAT pathway regulates *CG5966* and *schlank* expression**

944 **in the fat body.**

945 **a**, **c**, qRT–PCR of *CG5966* (**a**) and *schlank* (**c**) mRNA in the fat body of flies with or without
946 ISC *Upd3* or *Pvf1* expression (*esg>Upd3* or *Pvf1*) at day 8 (n = 3). **b**, **d**, *CG5966* (**b**) and
947 *schlank* (**d**) mRNA in the fat body of flies with or without fat-body Stat92E-act (constitutive-
948 activated form of Stat92e) expression at day 8 (n = 3). **e**, **g**, *CG5966* (**e**) and *schlank* (**g**)
949 mRNA in the fat body of control, Yki flies, and Yki flies with fat-body *hop* depletion at day 6
950 (n = 3). **f**, **h**, *CG5966* (**f**) and *schlank* (**h**) mRNA in the fat body of Yki flies with or without fat-
951 body *Stat92e* depletion at day 6 (n = 3). **i**, Data from the ChIP-seq database indicating
952 enrichment of Stat92e binding at the *CG5966* and *schlank* promoter and gene regions. **j**,
953 ChIP revealed the enrichment of HA-tagged Stat92E-act binding at the *CG5966* and
954 *schlank* promoter and gene regions, shown by fold changes relative to control IgG at day 8
955 (n = 3). Neg, negative control. **k**, Relative levels of whole-body ceramide levels of control,
956 Yki flies, and Yki flies with fat-body *hop or Stat92E* depletion at day 6 (n > 3), data were
957 retrieved from lipidomics analysis. **l**, Live imaging of lysosome and autophagic vesicles in
958 Yki flies with or without fat-body *hop* or *Stat92e* depletion at day 7. **m**-**q**, Quantification of
959 autophagic vesicle numbers (**m**) and sizes (**n**), lysosome numbers (**o**) and sizes (**p**), and
960 autolysosome numbers (**q**) in **l** (n > 15). **r**, Western blot showing pro and matured forms of
961 CtsL in control flies, Yki flies with or without fat-body *hop* or *Stat92e* depletion at day 7.
962 Rhodamine was used as loading control. The same membrane was probed sequentially
963 with Atg8 antibody in S4a, loading control is shared. *p < 0.05, **p < 0.01, ***p < 0.001,
964 ****p < 0.0001, ns indicates not significant. Error bars indicate SDs. n indicates the number
965 of biological replicates in each experiment.

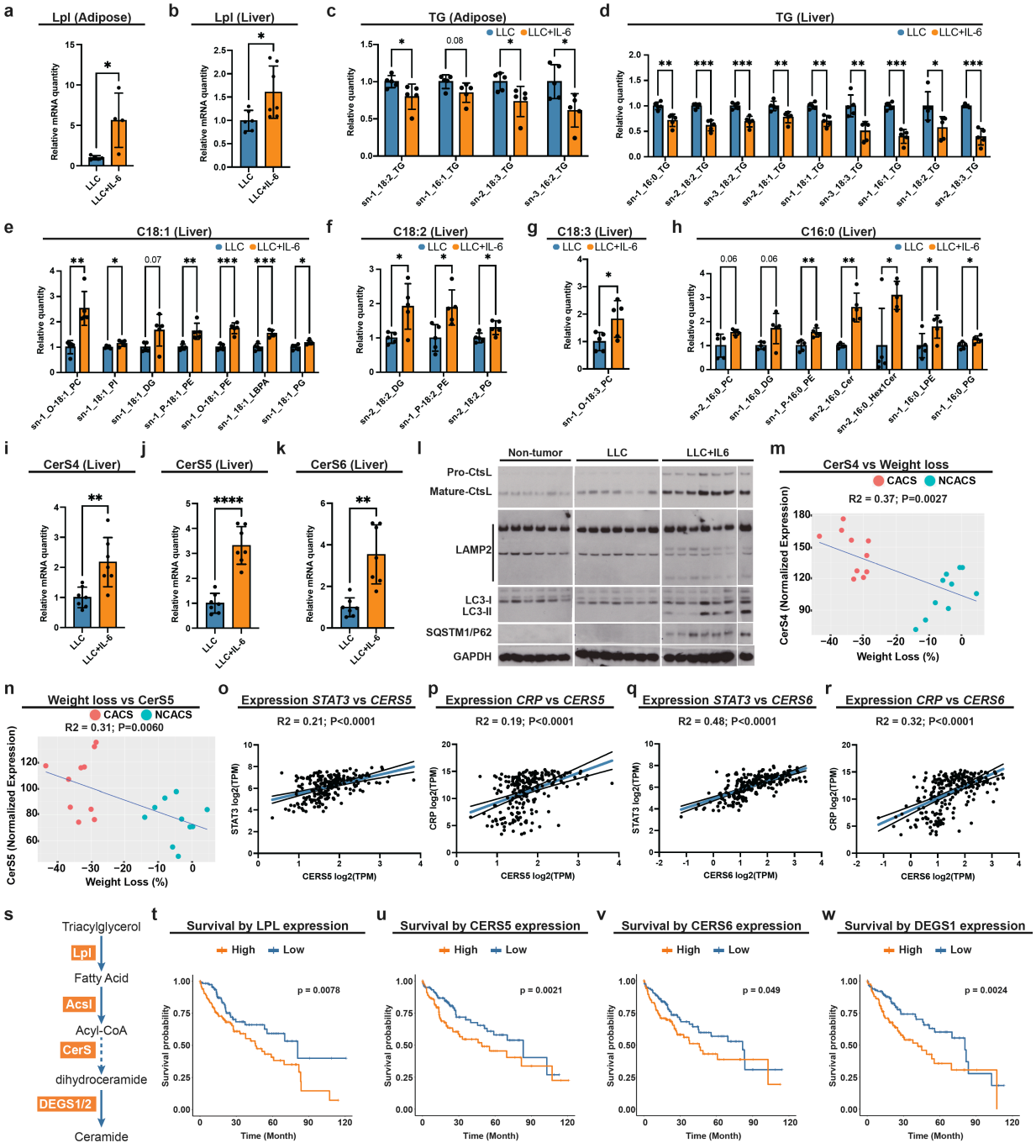
a
Lpl (Adipose)
Relative mRNA quantity
LLC
LLC+IL-6
b
Lpl (Liver)
c
TG (Adipose)
Relative quantity
sn-1_18:2_TG
sn-1_16:1_TG
sn-2_18:3_TG
sn-3_18:2_TG
d
TG (Liver)
sn-1_16:0_TG
sn-2_18:2_TG
sn-3_18:2_TG
sn-2_18:1_TG
sn-1_18:1_TG
sn-3_18:3_TG
sn-1_16:1_TG
sn-1_18:2_TG
sn-2_18:3_TG
e
C18:1 (Liver)
sn-1_O-18:1_PC
sn-1_18:1_PI
sn-1_18:1_DG
sn-1_P-18:1_PE
sn-1_O-18:1_PE
sn-1_18:1_LBPA
sn-1_18:1_PG
f
C18:2 (Liver)
sn-2_18:2_DG
sn-1_P-18:2_PE
sn-2_18:2_PG
g
C18:3 (Liver)
sn-1_O-18:3_PC
h
C16:0 (Liver)
sn-2_16:0_PC
sn-1_16:0_DG
sn-1_P-16:0_PE
sn-2_16:0_Cer
sn-2_16:0_HexCer
sn-1_16:0_LPE
sn-1_16:0_PG
i
CerS4 (Liver)
j
CerS5 (Liver)
k
CerS6 (Liver)
l
Non-tumor
LLC
LLC+IL6
Pro-CtsL
Mature-CtsL
LAMP2
LC3-I
LC3-II
SQSTM1/P62
GAPDH
m
CerS4 vs Weight loss
CACS
NCACS
R2 = 0.37; P=0.0027
CerS4 (Normalized Expression)
Weight Loss (%)
n
Weight loss vs CerS5
R2 = 0.31; P=0.0060
CerS5 (Normalized Expression)
o
Expression STAT3 vs CERS5
R2 = 0.21; P<0.0001
STAT3 log2(TPM)
CERS5 log2(TPM)
p
Expression CRP vs CERS5
R2 = 0.19; P<0.0001
CRP log2(TPM)
q
Expression STAT3 vs CERS6
R2 = 0.48; P<0.0001
CERS6 log2(TPM)
r
Expression CRP vs CERS6
R2 = 0.32; P<0.0001
s
Triacylglycerol
Lpl
Fatty Acid
AcsI
Acyl-CoA
CerS
dihydroceramide
DEGS1/2
Ceramide
t
Survival by LPL expression
High
Low
p = 0.0078
Survival probability
Time (Month)
u
Survival by CERS5 expression
p = 0.0021
v
Survival by CERS6 expression
p = 0.049
w
Survival by DEGS1 expression
p = 0.0024

967 **Figure 6. Conserved pathogenic mechanism in mouse models and humans.**

968 **a**, **b**, qRT–PCR of *Lpl* mRNA in adipose tissue (**a**) and liver (**b**) B6 mice injected with LLC
969 cells with (n = 4) or without (n = 5) and IL-6 expression. **c**,**d**, Relative levels of adipose (**c**)
970 and liver (**d**) TG species of B6 mice injected with LLC cells with or without IL-6 expression
971 (n=5). **e**-**h**, Relative levels of liver lipid species with C18:1 (**e**), C18:2 (**f**), C18:3 (**g**), and
972 C16:0 (**h**) acyl chains of B6 mice injected with LLC cells with or without IL-6 expression
973 (n=5). **i**-**k**, qRT–PCR of *CerS4* (**i**), *CerS5* (**j**), *CerS6* (**k**) mRNA in liver of B6 mice injected with
974 LLC cells with or without IL-6 expression (n = 7). **i**, Western blot showing forms of CtsL,
975 LAMP2, LC3, and P62 in liver of B6 mice injected with LLC cells with or without IL-6
976 expression, with the loading control GAPDH. **m**,**n**, Correlation plots showing the positive
977 relationship between liver *CerS4* (**m**) and *CerS5* (**n**) expression (n = 10) versus weight loss of
978 KL mice. **o**-**r**, Correlation plots showing the positive relationship between expression of
979 *STAT3* and *CerS5* (**o**), *CPR* and *CerS5* (**p**), *STAT3* and *CerS6* (**q**), *CPR* and *CerS6* (**r**) in non-
980 diseased liver samples of 226 participants in the GTEx Project. TPM, transcript per million.
981 **s**, Pathway map showing *de novo* ceramide synthesis pathway in human. **t**-**w**, Kaplan–
982 Meier survival curves displaying the estimated survival probabilities of people with
983 hepatocellular carcinoma with low (bottom third) and high (top third) hepatic expression of
984 *LPL* (**t**), *CERS5* (**u**), *CERS6* (**v**), and *DEGS1* (**w**). *$p < 0.05$, **$p < 0.01$, ***$p < 0.001$, ****$p <$
985 0.0001, ns indicates not significant. Error bars indicate SDs. n indicates the number of
986 biological replicates in each experiment.

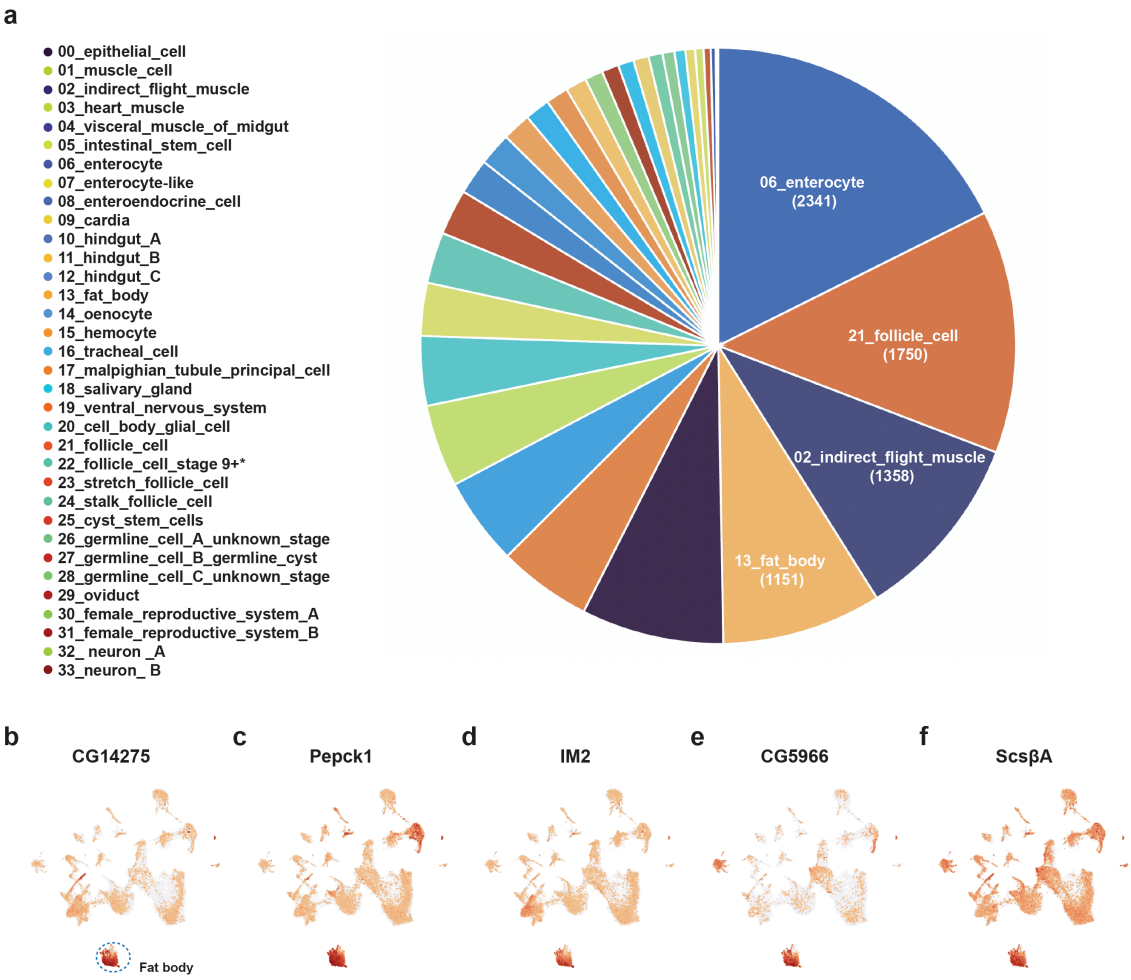
a
00_epithelial_cell
01_muscle_cell
02_indirect_flight_muscle
03_heart_muscle
04_visceral_muscle_of_midgut
05_intestinal_stem_cell
06_enterocyte
07_enterocyte-like
08_enteroendocrine_cell
09_cardia
10_hindgut_A
11_hindgut_B
12_hindgut_C
13_fat_body
14_oenocyte
15_hemocyte
16_tracheal_cell
17_malpighian_tubule_principal_cell
18_salivary_gland
19_ventral_nervous_system
20_cell_body_glial_cell
21_follicle_cell
22_follicle_cell_stage 9+*
23_stretch_follicle_cell
24_stalk_follicle_cell
25_cyst_stem_cells
26_germline_cell_A_unknown_stage
27_germline_cell_B_germline_cyst
28_germline_cell_C_unknown_stage
29_oviduct
30_female_reproductive_system_A
31_female_reproductive_system_B
32_ neuron _A
33_neuron_ B
06_enterocyte
(2341)
21_follicle_cell
(1750)
02_indirect_flight_muscle
(1358)
13_fat_body
(1151)
b
CG14275
Fat body
c
Pepck1
d
IM2
e
CG5966
f
ScsβA

987

988 **Figure S1, related to Figure 1.**

989 **a**, Distribution of progression associated genes across cell clusters. **b**-**f**, Expression of
990 CG14275 (**b**), Pepck1 (**c**), IM2 (**d**), CG5966 (**e**), ScsbetaA (**f**) across cell clusters, data retried
991 from snRNA-seq.

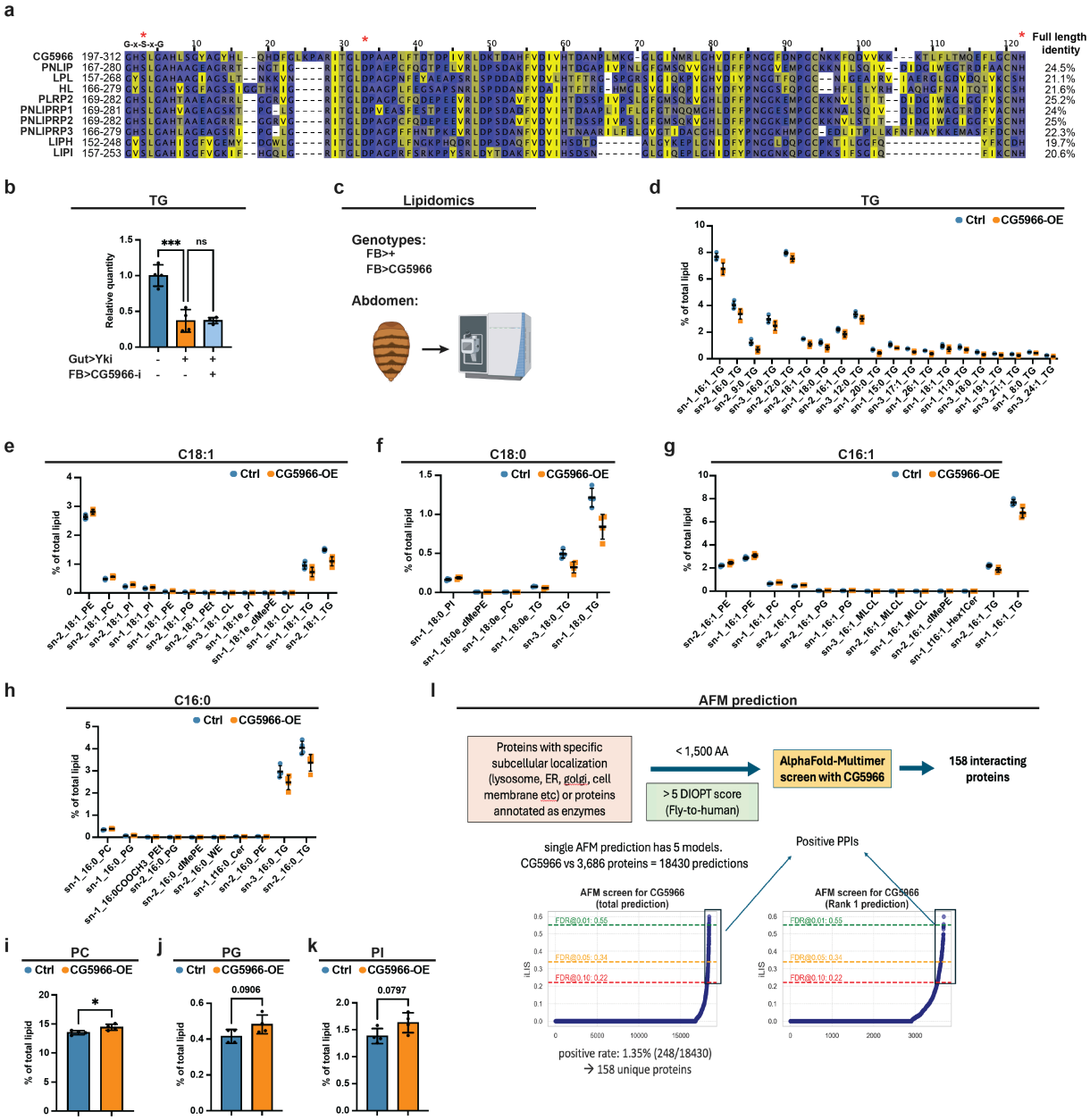
a
Full length identity
CG5966
PNLIP
LPL
HL
PLRP2
PNLIPRP1
PNLIPRP2
PNLIPRP3
LIPH
LIPI
24.5%
21.1%
21.6%
25.2%
24%
25%
22.3%
19.7%
20.6%
b
TG
Relative quantity
***
ns
Gut>Yki
FB>CG5966-i
c
Lipidomics
Genotypes:
FB>+
FB>CG5966
Abdomen:
d
TG
Ctrl
CG5966-OE
% of total lipid
e
C18:1
f
C18:0
g
C16:1
h
C16:0
i
PC
j
PG
k
PI
0.0906
0.0797
l
AFM prediction
Proteins with specific subcellular localization (lysosome, ER, golgi, cell membrane etc) or proteins annotated as enzymes
< 1,500 AA
> 5 DIOPT score (Fly-to-human)
AlphaFold-Multimer screen with CG5966
158 interacting proteins
single AFM prediction has 5 models.
CG5966 vs 3,686 proteins = 18430 predictions
Positive PPIs
AFM screen for CG5966 (total prediction)
AFM screen for CG5966 (Rank 1 prediction)
iLIS
positive rate: 1.35% (248/18430)
→ 158 unique proteins

992

993 **Figure S2, related to Figure 2.**

994 **a**, Amino acid sequence alignments showing similarity of human lipases to *CG5966*. **b**,
995 Whole-body TG levels of Yki flies with or without fat-body *CG5966* depletion at day 6 (n = 4).
996 **c**, Lipidomics analysis setting. **d**-**h**, Proportions of significantly changed abdomen TG
997 species (**d**), and lipid species containing C18:1 (**e**), C18:0 (**f**), C16:1 (**g**), or C16:0 (**h**) acyl
998 chains in flies with or without fat-body *CG5966* overexpression (n=4), data were retrieved
999 from lipidomics analysis. **i**-**k**, Proportions of abdomen PC (**i**), PG (**j**), PI (**k**) of flies with or
1000 without fat-body CG5966 overexpression (n=4), data were retrieved from lipidomics
1001 analysis. **l**, AFM analysis setting. *$p < 0.05$, **$p < 0.01$, ***$p < 0.001$, ****$p < 0.0001$, ns
1002 indicates not significant. Error bars indicate SDs. n indicates the number of biological
1003 replicates in each experiment.

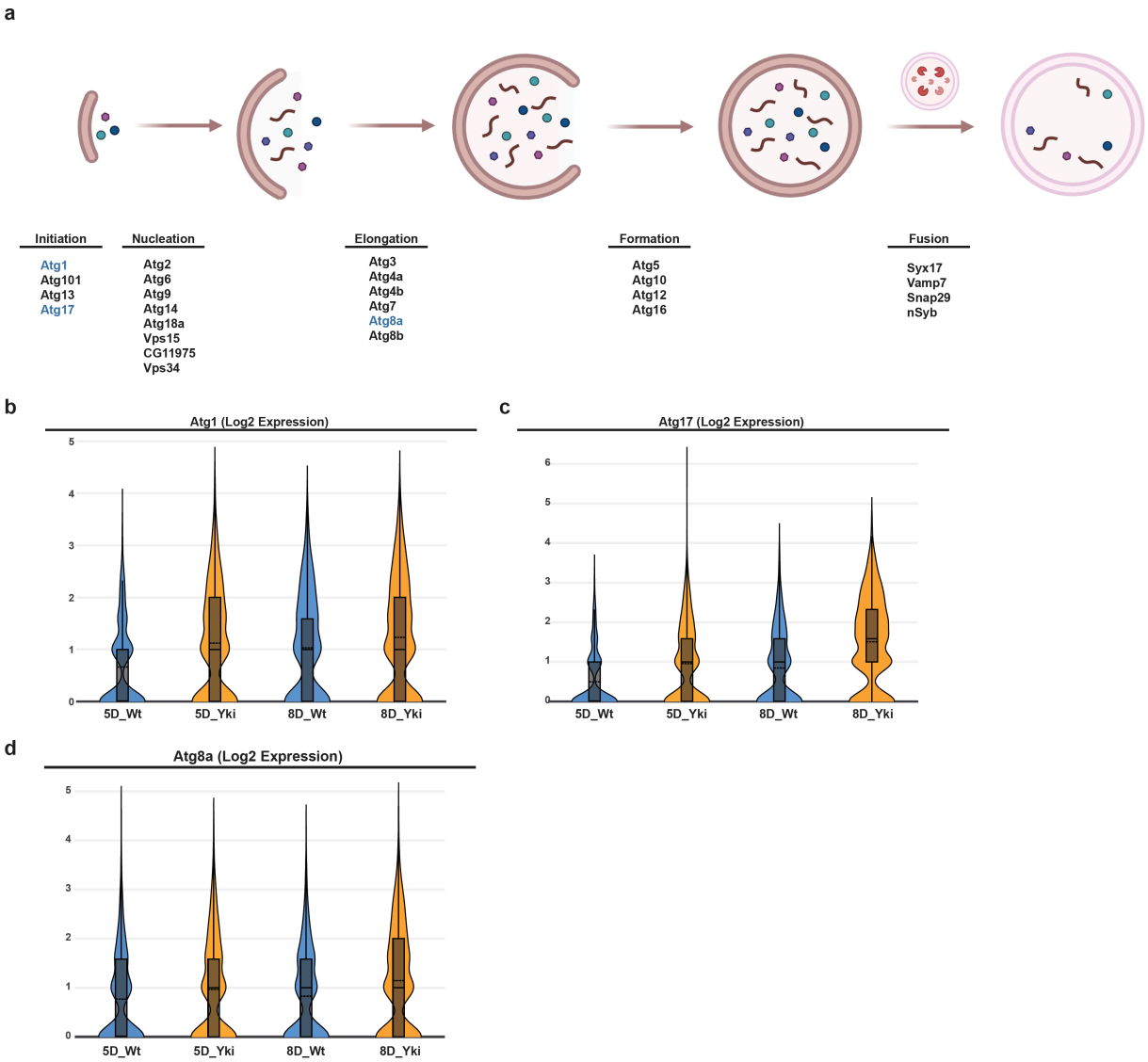
a
Initiation
Atg1
Atg101
Atg13
Atg17
Nucleation
Atg2
Atg6
Atg9
Atg14
Atg18a
Vps15
CG11975
Vps34
Elongation
Atg3
Atg4a
Atg4b
Atg7
Atg8a
Atg8b
Formation
Atg5
Atg10
Atg12
Atg16
Fusion
Syx17
Vamp7
Snap29
nSyb
b
Atg1 (Log2 Expression)
5D_Wt
5D_Yki
8D_Wt
8D_Yki
c
Atg17 (Log2 Expression)
5D_Wt
5D_Yki
8D_Wt
8D_Yki
d
Atg8a (Log2 Expression)
5D_Wt
5D_Yki
8D_Wt
8D_Yki

1004

1005 **Figure S3, related to Figure 3.**

1006 **a**, A schematic of autophagy in *Drosophila*, genes upregulated in Yki are labeled in blue,
1007 other genes are not significantly changed. **b-d**, Log2 expression of *Atg1* (**b**), *Atg17* (**c**), and
1008 *Atg8a* (**d**) in day 5 and day 8 control and Yki flies, data were retrieved from snRNAseq
1009 analysis.

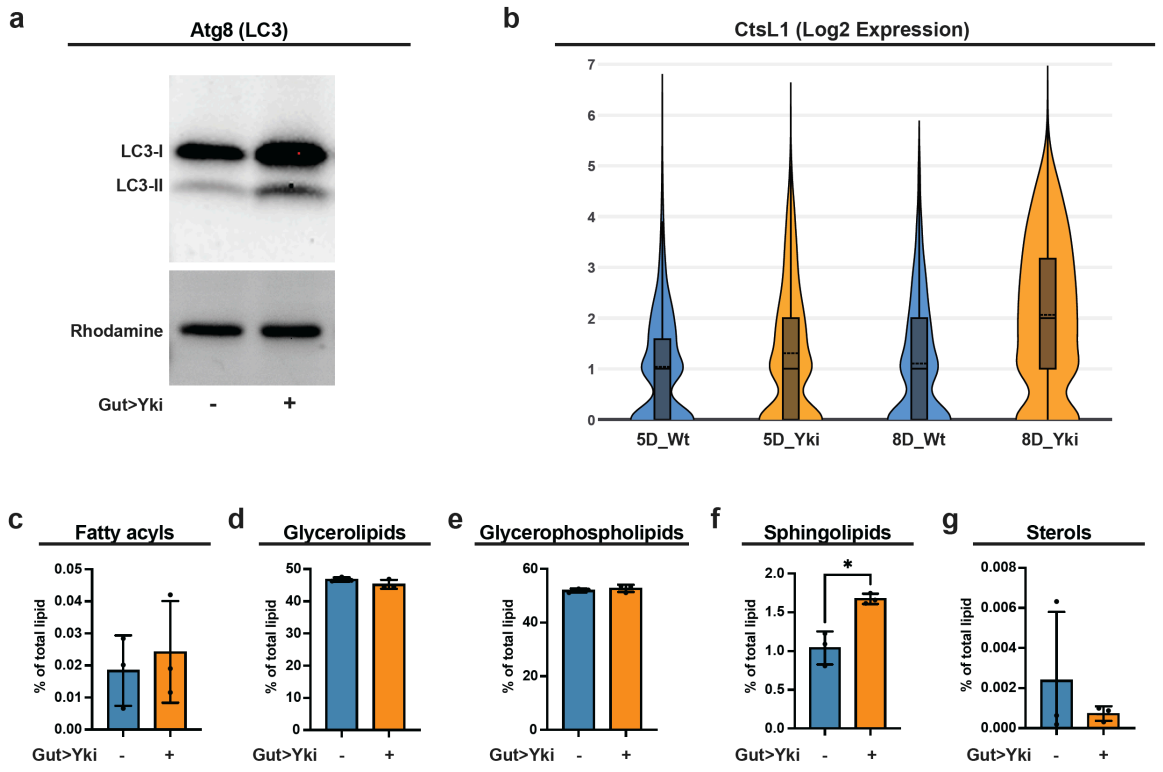
a
Atg8 (LC3)
LC3-I
LC3-II
Rhodamine
Gut>Yki
-
+
b
CtsL1 (Log2 Expression)
7
6
5
4
3
2
1
0
5D_Wt
5D_Yki
8D_Wt
8D_Yki
c
Fatty acyls
% of total lipid
0.05
0.04
0.03
0.02
0.01
0.00
Gut>Yki
-
+
d
Glycerolipids
% of total lipid
50
40
30
20
10
0
Gut>Yki
-
+
e
Glycerophospholipids
% of total lipid
60
40
20
0
Gut>Yki
-
+
f
Sphingolipids
*
% of total lipid
2.0
1.5
1.0
0.5
0.0
Gut>Yki
-
+
g
Sterols
% of total lipid
0.008
0.006
0.004
0.002
0.000
Gut>Yki
-
+

1010

1011 **Figure S4, related to Figure 4.**

1012 **a**, Western blot of Atg8 (LC3) of abdomen samples from control and Yki flies. Rhodamine
1013 was used as loading control. **b**, Log2 expression of *CtsL1* in day 5 and day 8 control and Yki
1014 flies, data were retrieved from snRNAseq analysis. **c**-**g**, Whole-body proportions of lipid
1015 subgroups fatty acyls (**c**), glycerolipids (**d**), glycerophospholipids (**e**), sphingolipids (**f**), and
1016 sterols (**g**) in control and Yki flies, data were retrieved from lipidomics analysis.

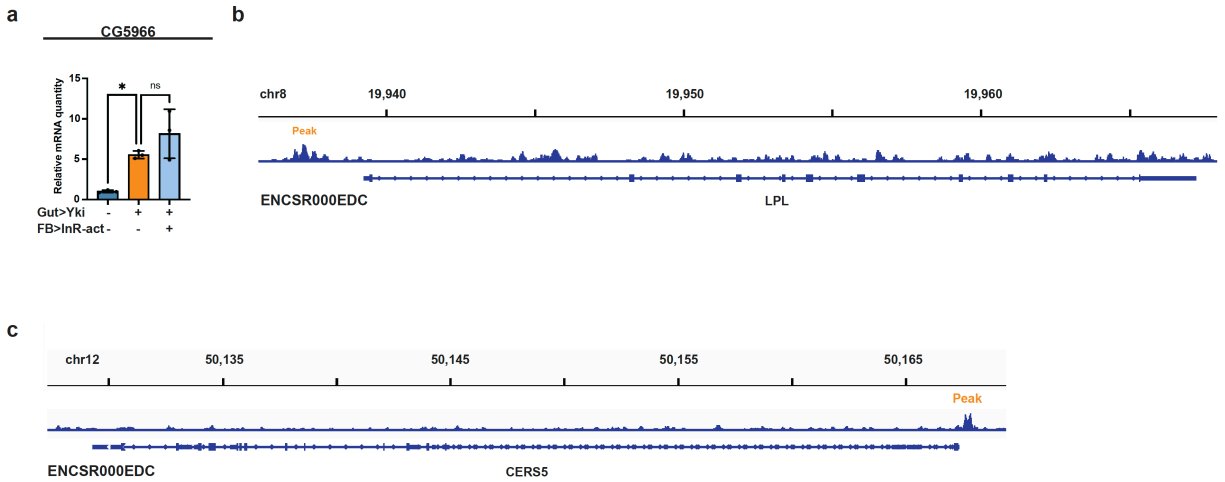
a
CG5966
Relative mRNA quantity
15
10
5
0
*
ns
Gut>Yki - + +
FB>InR-act - - +
b
chr8
19,940
19,950
19,960
Peak
ENCSR000EDC
LPL
c
chr12
50,135
50,145
50,155
50,165
Peak
ENCSR000EDC
CERS5

1017

1018 **Figure S5, related to Figure 5.**

1019 **a**, *CG5966* mRNA expression in the fat body of control, Yki flies, and Yki flies with fat-body
1020 *InR-act* (active form of InR) expression at day 6 (n = 3). *p < 0.05, **p < 0.01, ***p < 0.001,
1021 ****p < 0.0001, ns indicates not significant. Error bars indicate SDs. n indicates biological
1022 replicates. **b**,**c**, Data from the ChIP-seq data (ENCSR000EDC) indicating enrichment of
1023 STAT3 binding at the *LPL* (**b**) and *CERS5* (**c**) promoter and gene regions.

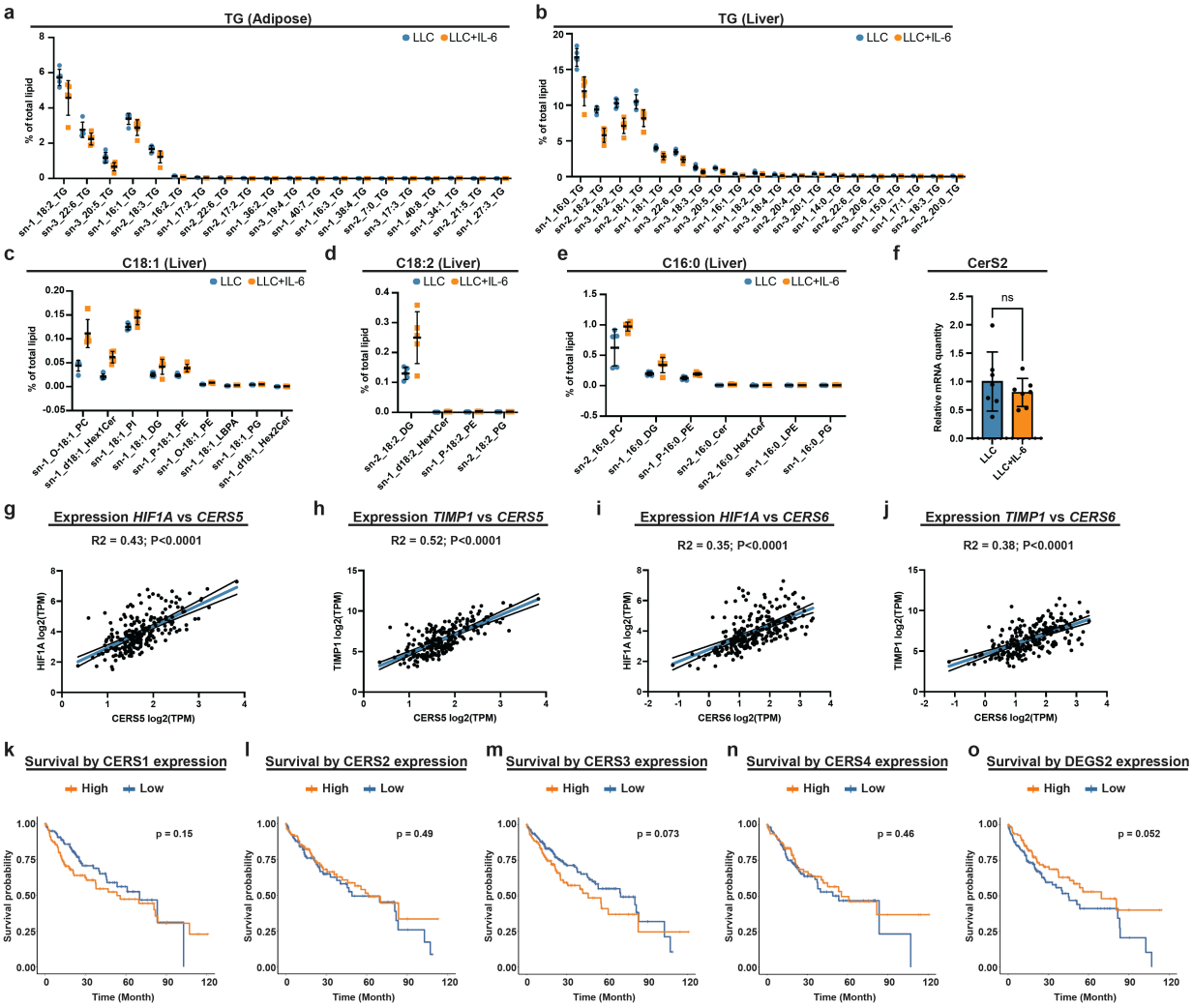
a
TG (Adipose)
LLC
LLC+IL-6
% of total lipid
sn-1_18:2_TG
sn-3_22:6_TG
sn-3_20:5_TG
sn-1_16:1_TG
sn-2_18:3_TG
sn-3_16:2_TG
sn-1_17:2_TG
sn-2_22:6_TG
sn-2_17:2_TG
sn-1_36:2_TG
sn-3_19:4_TG
sn-1_40:7_TG
sn-1_16:3_TG
sn-1_38:4_TG
sn-2_7:0_TG
sn-3_17:3_TG
sn-1_40:8_TG
sn-1_34:1_TG
sn-2_21:5_TG
sn-1_27:3_TG
b
TG (Liver)
LLC
LLC+IL-6
% of total lipid
sn-1_16:0_TG
sn-2_18:2_TG
sn-3_18:2_TG
sn-2_18:1_TG
sn-1_18:1_TG
sn-3_22:6_TG
sn-3_18:3_TG
sn-3_20:5_TG
sn-1_16:1_TG
sn-1_18:2_TG
sn-3_18:4_TG
sn-2_20:3_TG
sn-3_20:1_TG
sn-1_14:0_TG
sn-2_22:6_TG
sn-3_20:4_TG
sn-1_15:0_TG
sn-1_17:1_TG
sn-2_18:3_TG
sn-2_20:0_TG
c
C18:1 (Liver)
LLC
LLC+IL-6
% of total lipid
sn-1_O-18:1_PC
sn-1_d18:1_Hex1Cer
sn-1_18:1_PI
sn-1_18:1_DG
sn-1_P-18:1_PE
sn-1_O-18:1_PE
sn-1_18:1_LBPA
sn-1_18:1_PG
sn-1_d18:1_Hex2Cer
d
C18:2 (Liver)
LLC
LLC+IL-6
% of total lipid
sn-2_18:2_DG
sn-1_d18:2_Hex1Cer
sn-1_P-18:2_PE
sn-2_18:2_PG
e
C16:0 (Liver)
LLC
LLC+IL-6
% of total lipid
sn-2_16:0_PC
sn-1_16:0_DG
sn-1_P-16:0_PE
sn-2_16:0_Cer
sn-2_16:0_Hex1Cer
sn-1_16:0_LPE
sn-1_16:0_PG
f
CerS2
ns
Relative mRNA quantity
LLC
LLC+IL-6
g
Expression HIF1A vs CERS5
R2 = 0.43; P<0.0001
HIF1A log2(TPM)
CERS5 log2(TPM)
h
Expression TIMP1 vs CERS5
R2 = 0.52; P<0.0001
TIMP1 log2(TPM)
CERS5 log2(TPM)
i
Expression HIF1A vs CERS6
R2 = 0.35; P<0.0001
HIF1A log2(TPM)
CERS6 log2(TPM)
j
Expression TIMP1 vs CERS6
R2 = 0.38; P<0.0001
TIMP1 log2(TPM)
CERS6 log2(TPM)
k
Survival by CERS1 expression
High
Low
p = 0.15
Survival probability
Time (Month)
l
Survival by CERS2 expression
High
Low
p = 0.49
Survival probability
Time (Month)
m
Survival by CERS3 expression
High
Low
p = 0.073
Survival probability
Time (Month)
n
Survival by CERS4 expression
High
Low
p = 0.46
Survival probability
Time (Month)
o
Survival by DEGS2 expression
High
Low
p = 0.052
Survival probability
Time (Month)

1024

1025 **Figure S6. related to Figure 6.**

1026 **a**,**b**, Proportions of significantly changed adipose (**a**) and liver (**b**) TG levels of B6 mice
1027 injected with LLC cells with or without IL-6 expression (n=5). **c**-**e**, Proportions of
1028 significantly changed lipid species containing C18:1 (**c**), C18:2 (**d**), or C16:0 (**e**) acyl chains
1029 of B6 mice injected with LLC cells with or without IL-6 expression in liver (n=5). **f**, qRT–PCR
1030 of *CerS2* mRNA in liver of B6 mice injected with LLC cells with or without IL-6 expression (n
1031 = 7). **g**-**j**, Correlation plots showing the positive relationship between expression of *HIF1A*
1032 and *CerS5* (**g**), *TIMP1* and *CerS5* (**h**), *HIF1A* and *CerS6* (**i**), *TIMP1* and *CerS6* (**j**) in non-
1033 diseased liver samples of 226 participants in the GTEx Project. TPM, transcript per million.
1034 **k**-**o**, Kaplan–Meier survival curves displaying the estimated survival probabilities of people
1035 with hepatocellular carcinoma with low (bottom third) and high (top third) hepatic
1036 expression of *CERS1* (**k**), *CERS2* (**l**), *CERS3* (**m**), *CERS4* (**n**), and *DEGS2* (**o**). *$p < 0.05$, **$p <$
1037 0.01, ***$p < 0.001$, ****$p < 0.0001$, ns indicates not significant. Error bars indicate SDs. n
1038 indicates the number of biological replicates in each experiment.

References

Alexaki, V.I., 2024. Adipose tissue-derived mediators of systemic inflammation and metabolic control. Curr. Opin. Endocr. Metab. Res. 37, 100560. https://doi.org/10.1016/j.coemr.2024.100560

Arora, G.K., Gupta, A., Narayanan, S., Guo, T., Iyengar, P., Infante, R.E., 2018. Cachexia-associated adipose loss induced by tumor-secreted leukemia inhibitory factor is counterbalanced by decreased leptin. JCI Insight 3. https://doi.org/10.1172/jci.insight.121221

Barton, B.E., 2001. IL-6-like cytokines and cancer cachexia. Immunol. Res. 23, 41–58. https://doi.org/10.1385/IR:23:1:41

Bilder, D., Ong, K., Hsi, T.-C., Adiga, K., Kim, J., 2021. Tumour–host interactions through the lens of Drosophila. Nat. Rev. Cancer 1–14. https://doi.org/10.1038/s41568-021-00387-5

Castell, J.V., Gómez-Lechón, M.J., David, M., Fabra, R., Trullenque, R., Heinrich, P.C., 1990. Acute-phase response of human hepatocytes: regulation of acute-phase protein synthesis by interleukin-6. Hepatol. Baltim. Md 12, 1179–1186. https://doi.org/10.1002/hep.1840120517

Chavez, J.A., Summers, S.A., 2012. A ceramide-centric view of insulin resistance. Cell Metab. 15, 585–594. https://doi.org/10.1016/j.cmet.2012.04.002

Cheng, C., Liu, Y., Chen, Y., Li, J., Xu, W., Perrimon, N., Song, W., 2025. The Power of Drosophila in Modeling Cancer Cachexia, in: Deng, W.-M., Gonzaléz, C. (Eds.), The Drosophila Model in Cancer: Volume II. Springer Nature Switzerland, Cham, pp. 83–100. https://doi.org/10.1007/978-3-031-97035-1_5

Colacurcio, D.J., Nixon, R.A., 2016. Disorders of lysosomal acidification - the emerging role of v-ATPase in aging and neurodegenerative disease. Ageing Res. Rev. 32, 75–88. https://doi.org/10.1016/j.arr.2016.05.004

Dien, J., Amin, H.M., Chiu, N., Wong, W., Frantz, C., Chiu, B., Mackey, J.R., Lai, R., 2006. Signal Transducers and Activators of Transcription-3 Up-Regulates Tissue Inhibitor of Metalloproteinase-1 Expression and Decreases Invasiveness of Breast Cancer. Am. J. Pathol. 169, 633–642. https://doi.org/10.2353/ajpath.2006.051109

Ding, G., Xiang, X., Hu, Y., Xiao, G., Chen, Y., Binari, R., Comjean, A., Li, J., Rushworth, E., Fu, Z., Mohr, S.E., Perrimon, N., Song, W., 2021. Coordination of tumor growth and host wasting by tumor-derived Upd3. Cell Rep. 36, 109553. https://doi.org/10.1016/j.celrep.2021.109553

Dong, W., He, B., Qian, H., Liu, Q., Wang, D., Li, J., Wei, Z., Wang, Z., Xu, Z., Wu, G., Qian, G., Wang, G., 2018. RAB26-dependent autophagy protects adherens junctional integrity in acute lung injury. Autophagy 14, 1677–1692. https://doi.org/10.1080/15548627.2018.1476811

Ekas, L.A., Cardozo, T.J., Flaherty, M.S., McMillan, E.A., Gonsalves, F.C., Bach, E.A., 2010. Characterization of a dominant-active STAT that promotes tumorigenesis in Drosophila. Dev. Biol. 344, 621–636. https://doi.org/10.1016/j.ydbio.2010.05.497

Evans, R., O'Neill, M., Pritzel, A., Antropova, N., Senior, A., Green, T., Žídek, A., Bates, R., Blackwell, S., Yim, J., Ronneberger, O., Bodenstein, S., Zielinski, M., Bridgland, A.,

Potapenko, A., Cowie, A., Tunyasuvunakool, K., Jain, R., Clancy, E., Kohli, P., Jumper, J., Hassabis, D., 2021. Protein complex prediction with AlphaFold-Multimer. https://doi.org/10.1101/2021.10.04.463034

Fearon, K.C.H., Glass, D.J., Guttridge, D.C., 2012. Cancer Cachexia: Mediators, Signaling, and Metabolic Pathways. Cell Metab. 16, 153–166. https://doi.org/10.1016/j.cmet.2012.06.011

Ferrer, M., Mourikis, N., Davidson, E.E., Kleeman, S.O., Zaccaria, M., Habel, J., Rubino, R., Gao, Q., Flint, T.R., Young, L., Connell, C.M., Lukey, M.J., Goncalves, M.D., White, E.P., Venkitaraman, A.R., Janowitz, T., 2023. Ketogenic diet promotes tumor ferroptosis but induces relative corticosterone deficiency that accelerates cachexia. Cell Metab. 35, 1147-1162.e7. https://doi.org/10.1016/j.cmet.2023.05.008

Flint, T.R., Janowitz, T., Connell, C.M., Roberts, E.W., Denton, A.E., Coll, A.P., Jodrell, D.I., Fearon, D.T., 2016. Tumor-Induced IL-6 Reprograms Host Metabolism to Suppress Anti-tumor Immunity. Cell Metab. 24, 672–684. https://doi.org/10.1016/j.cmet.2016.10.010

Fresques, T., Niles, B., Aronova, S., Mogri, H., Rakhshandehroo, T., Powers, T., 2015. Regulation of Ceramide Synthase by Casein Kinase 2-dependent Phosphorylation in Saccharomyces cerevisiae. J. Biol. Chem. 290, 1395–1403. https://doi.org/10.1074/jbc.M114.621086

Gabandé-Rodríguez, E., Boya, P., Labrador, V., Dotti, C.G., Ledesma, M.D., 2014. High sphingomyelin levels induce lysosomal damage and autophagy dysfunction in Niemann Pick disease type A. Cell Death Differ. 21, 864–875. https://doi.org/10.1038/cdd.2014.4

Gillingham, A.K., Sinka, R., Torres, I.L., Lilley, K.S., Munro, S., 2014. Toward a Comprehensive Map of the Effectors of Rab GTPases. Dev. Cell 31, 358–373. https://doi.org/10.1016/j.devcel.2014.10.007

Goncalves, M.D., Hwang, S.-K., Pauli, C., Murphy, C.J., Cheng, Z., Hopkins, B.D., Wu, D., Loughran, R.M., Emerling, B.M., Zhang, G., Fearon, D.T., Cantley, L.C., 2018. Fenofibrate prevents skeletal muscle loss in mice with lung cancer. Proc. Natl. Acad. Sci. 115, E743–E752. https://doi.org/10.1073/pnas.1714703115

Hamel, S., Fantini, J., Schweisguth, F., 2010. Notch ligand activity is modulated by glycosphingolipid membrane composition in Drosophila melanogaster. J. Cell Biol. 188, 581–594. https://doi.org/10.1083/jcb.200907116

Hannun, Y.A., Obeid, L.M., 2018. Sphingolipids and their metabolism in physiology and disease. Nat. Rev. Mol. Cell Biol. 19, 175–191. https://doi.org/10.1038/nrm.2017.107

Harayama, T., Riezman, H., 2018. Understanding the diversity of membrane lipid composition. Nat. Rev. Mol. Cell Biol. 19, 281–296. https://doi.org/10.1038/nrm.2017.138

Hoadley, K.A., Yau, C., Hinoue, T., Wolf, D.M., Lazar, A.J., Drill, E., Shen, R., Taylor, A.M., Cherniack, A.D., Thorsson, Vésteinn, Akbani, R., Bowlby, R., Wong, C.K., Wiznerowicz, M., Sanchez-Vega, F., Robertson, A.G., Schneider, B.G., Lawrence, M.S., Noushmehr, H., Malta, T.M., Caesar-Johnson, S.J., Demchok, J.A., Felau, I., Kasapi, M., Ferguson, M.L., Hutter, C.M., Sofia, H.J., Tarnuzzer, R., Wang, Z., Yang, L., Zenklusen, J.C., Zhang, J. (Julia), Chudamani, S., Liu, J., Lolla, L., Naresh, R., Pihl, T.,

Sun, Q., Wan, Y., Wu, Y., Cho, J., DeFreitas, T., Frazer, S., Gehlenborg, N., Getz, G., Heiman, D.I., Kim, J., Lawrence, M.S., Lin, P., Meier, S., Noble, M.S., Saksena, G., Voet, D., Zhang, Hailei, Bernard, B., Chambwe, N., Dhankani, V., Knijnenburg, T., Kramer, R., Leinonen, K., Liu, Y., Miller, M., Reynolds, S., Shmulevich, I., Thorsson, Vesteinn, Zhang, W., Akbani, R., Broom, B.M., Hegde, A.M., Ju, Z., Kanchi, R.S., Korkut, A., Li, J., Liang, H., Ling, S., Liu, W., Lu, Y., Mills, G.B., Ng, K.-S., Rao, A., Ryan, M., Wang, Jing, Weinstein, J.N., Zhang, J., Abeshouse, A., Armenia, J., Chakravarty, D., Chatila, W.K., Bruijn, I. de, Gao, J., Gross, B.E., Heins, Z.J., Kundra, R., La, K., Ladanyi, M., Luna, A., Nissan, M.G., Ochoa, A., Phillips, S.M., Reznik, E., Sanchez-Vega, F., Sander, C., Schultz, N., Sheridan, R., Sumer, S.O., Sun, Y., Taylor, B.S., Wang, Jioajiao, Zhang, Hongxin, Anur, P., Peto, M., Spellman, P., Benz, C., Stuart, J.M., Wong, C.K., Yau, C., Hayes, D.N., Parker, J.S., Wilkerson, M.D., Ally, A., Balasundaram, M., Bowlby, R., Brooks, D., Carlsen, R., Chuah, E., Dhalla, N., Holt, R., Jones, S.J.M., Kasaian, K., Lee, D., Ma, Y., Marra, M.A., Mayo, M., Moore, R.A., Mungall, A.J., Mungall, K., Robertson, A.G., Sadeghi, S., Schein, J.E., Sipahimalani, P., Tam, A., Thiessen, N., Tse, K., Wong, T., Berger, A.C., Beroukhim, R., Cherniack, A.D., Cibulskis, C., Gabriel, S.B., Gao, G.F., Ha, G., Meyerson, M., Schumacher, S.E., Shih, J., Kucherlapati, M.H., Kucherlapati, R.S., Baylin, S., Cope, L., Danilova, L., Bootwalla, M.S., Lai, P.H., Maglinte, D.T., Berg, D.J.V.D., Weisenberger, D.J., Auman, J.T., Balu, S., Bodenheimer, T., Fan, C., Hoadley, K.A., Hoyle, A.P., Jefferys, S.R., Jones, C.D., Meng, S., Mieczkowski, P.A., Mose, L.E., Perou, A.H., Perou, C.M., Roach, J., Shi, Y., Simons, J.V., Skelly, T., Soloway, M.G., Tan, D., Veluvolu, U., Fan, H., Hinoue, T., Laird, P.W., Shen, H., Zhou, W., Bellair, M., Chang, K., Covington, K., Creighton, C.J., Dinh, H., Doddapaneni, H., Donehower, L.A., Drummond, J., Gibbs, R.A., Glenn, R., Hale, W., Han, Y., Hu, J., Korchina, V., Lee, S., Lewis, L., Li, W., Liu, X., Morgan, M., Morton, D., Muzny, D., Santibanez, J., Sheth, M., Shinbrot, E., Wang, L., Wang, M., Wheeler, D.A., Xi, L., Zhao, F., Hess, J., Appelbaum, E.L., Bailey, M., Cordes, M.G., Ding, L., Fronick, C.C., Fulton, L.A., Fulton, R.S., Kandoth, C., Mardis, E.R., McLellan, M.D., Miller, C.A., Schmidt, H.K., Wilson, R.K., Crain, D., Curley, E., Gardner, J., Lau, K., Mallery, D., Morris, S., Paulauskis, J., Penny, R., Shelton, C., Shelton, T., Sherman, M., Thompson, E., Yena, P., Bowen, J., Gastier-Foster, J.M., Gerken, M., Leraas, K.M., Lichtenberg, T.M., Ramirez, N.C., Wise, L., Zmuda, E., Corcoran, N., Costello, T., Hovens, C., Carvalho, A.L., Carvalho, A.C. de, Fregnani, J.H., Longatto-Filho, A., Reis, R.M., Scapulatempo-Neto, C., Silveira, H.C.S., Vidal, D.O., Burnette, A., Eschbacher, J., Hermes, B., Noss, A., Singh, R., Anderson, M.L., Castro, P.D., Ittmann, M., Huntsman, D., Kohl, B., Le, X., Thorp, R., Andry, C., Duffy, E.R., Lyadov, V., Paklina, O., Setdikova, G., Shabunin, A., Tavobilov, M., McPherson, C., Warnick, R., Berkowitz, R., Cramer, D., Feltmate, C., Horowitz, N., Kibel, A., Muto, M., Raut, C.P., Malykh, A., Barnholtz-Sloan, J.S., Barrett, W., Devine, K., Fulop, J., Ostrom, Q.T., Shimmel, K., Wolinsky, Y., Sloan, A.E., Rose, A.D., Giuliante, F., Goodman, M., Karlan, B.Y., Hagedorn, C.H., Eckman, J., Harr, J., Myers, J., Tucker, K., Zach, L.A., Deyarmin, B., Hu, H., Kvecher, L., Larson, C., Mural, R.J., Somiari, S., Vicha, A., Zelinka, T., Bennett, J., Iacocca, M., Rabeno, B., Swanson, P., Latour, M., Lacombe, L., Têtu, B., Bergeron, A., McGraw, M., Staugaitis, S.M., Chabot, J.,

Hibshoosh, H., Sepulveda, A., Su, T., Wang, T., Potapova, O., Voronina, O., Desjardins, L., Mariani, O., Roman-Roman, S., Sastre, X., Stern, M.-H., Cheng, F., Signoretti, S., Berchuck, A., Bigner, D., Lipp, E., Marks, J., McCall, S., McLendon, R., Secord, A., Sharp, A., Behera, M., Brat, D.J., Chen, A., Delman, K., Force, S., Khuri, F., Magliocca, K., Maithel, S., Olson, J.J., Owonikoko, T., Pickens, A., Ramalingam, S., Shin, D.M., Sica, G., Meir, E.G.V., Zhang, Hongzheng, Eijckenboom, W., Gillis, A., Korpershoek, E., Looijenga, L., Oosterhuis, W., Stoop, H., Kessel, K.E. van, Zwarthoff, E.C., Calatozzolo, C., Cuppini, L., Cuzzubbo, S., DiMeco, F., Finocchiaro, G., Mattei, L., Perin, A., Pollo, B., Chen, C., Houck, J., Lohavanichbutr, P., Hartmann, A., Stoehr, C., Stoehr, R., Taubert, H., Wach, S., Wullich, B., Kycler, W., Murawa, D., Wiznerowicz, M., Chung, K., Edenfield, W.J., Martin, J., Baudin, E., Bubley, G., Bueno, R., Rienzo, A.D., Richards, W.G., Kalkanis, S., Mikkelsen, T., Noushmehr, H., Scarpace, L., Girard, N., Aymerich, M., Campo, E., Giné, E., Guillermo, A.L., Bang, N.V., Hanh, P.T., Phu, B.D., Tang, Y., Colman, H., Evason, K., Dottino, P.R., Martignetti, J.A., Gabra, H., Juhl, H., Akeredolu, T., Stepa, S., Hoon, D., Ahn, K., Kang, K.J., Beuschlein, F., Breggia, A., Birrer, M., Bell, D., Borad, M., Bryce, A.H., Castle, E., Chandan, V., Cheville, J., Copland, J.A., Farnell, M., Flotte, T., Giama, N., Ho, T., Kendrick, M., Kocher, J.-P., Kopp, K., Moser, C., Nagorney, D., O'Brien, D., O'Neill, B.P., Patel, T., Petersen, G., Que, F., Rivera, M., Roberts, L., Smallridge, R., Smyrk, T., Stanton, M., Thompson, R.H., Torbenson, M., Yang, J.D., Zhang, L., Brimo, F., Ajani, J.A., Gonzalez, A.M.A., Behrens, C., Bondaruk, O., Broaddus, R., Czerniak, B., Esmaeli, B., Fujimoto, J., Gershenwald, J., Guo, C., Lazar, A.J., Logothetis, C., Meric-Bernstam, F., Moran, C., Ramondetta, L., Rice, D., Sood, A., Tamboli, P., Thompson, T., Troncoso, P., Tsao, A., Wistuba, I., Carter, C., Haydu, L., Hersey, P., Jakrot, V., Kakavand, H., Kefford, R., Lee, K., Long, G., Mann, G., Quinn, M., Saw, R., Scolyer, R., Shannon, K., Spillane, A., Stretch, J., Synott, M., Thompson, J., Wilmott, J., Al-Ahmadie, H., Chan, T.A., Ghossein, R., Gopalan, A., Levine, D.A., Reuter, V., Singer, S., Singh, B., Tien, N.V., Broudy, T., Mirsaidi, C., Nair, P., Drwiega, P., Miller, J., Smith, J., Zaren, H., Park, J.-W., Hung, N.P., Kebebew, E., Linehan, W.M., Metwalli, A.R., Pacak, K., Pinto, P.A., Schiffman, M., Schmidt, L.S., Vocke, C.D., Wentzensen, N., Worrell, R., Yang, H., Moncrieff, M., Goparaju, C., Melamed, J., Pass, H., Botnariuc, N., Caraman, I., Cernat, M., Chemencedji, I., Clipca, A., Doruc, S., Gorincioi, G., Mura, S., Pirtac, M., Stancul, I., Tcaciuc, D., Albert, M., Alexopoulou, I., Arnaout, A., Bartlett, J., Engel, J., Gilbert, S., Parfitt, J., Sekhon, H., Thomas, G., Rassl, D.M., Rintoul, R.C., Bifulco, C., Tamakawa, R., Urba, W., Hayward, N., Timmers, H., Antenucci, A., Facciolo, F., Grazi, G., Marino, M., Merola, R., Krijger, R. de, Gimenez-Roqueplo, A.-P., Piché, A., Chevalier, S., McKercher, G., Birsoy, K., Barnett, G., Brewer, C., Farver, C., Naska, T., Pennell, N.A., Raymond, D., Schilero, C., Smolenski, K., Williams, F., Morrison, C., Borgia, J.A., Liptay, M.J., Pool, M., Seder, C.W., Junker, K., Omberg, L., Dinkin, M., Manikhas, G., Alvaro, D., Bragazzi, M.C., Cardinale, V., Carpino, G., Gaudio, E., Chesla, D., Cottingham, S., Dubina, M., Moiseenko, F., Dhanasekaran, R., Becker, K.-F., Janssen, K.-P., Slotta-Huspenina, J., Abdel-Rahman, M.H., Aziz, D., Bell, S., Cebulla, C.M., Davis, A., Duell, R., Elder, J.B., Hilty, J., Kumar, B., Lang, J., Lehman, N.L., Mandt, R., Nguyen, P., Pilarski, R., Rai, K.,

Schoenfield, L., Senecal, K., Wakely, P., Hansen, P., Lechan, R., Powers, J., Tischler, A., Grizzle, W.E., Sexton, K.C., Kastl, A., Henderson, J., Porten, S., Waldmann, J., Fassnacht, M., Asa, S.L., Schadendorf, D., Couce, M., Graefen, M., Huland, H., Sauter, G., Schlomm, T., Simon, R., Tennstedt, P., Olabode, O., Nelson, M., Bathe, O., Carroll, P.R., Chan, J.M., Disaia, P., Glenn, P., Kelley, R.K., Landen, C.N., Phillips, J., Prados, M., Simko, J., Smith-McCune, K., VandenBerg, S., Roggin, K., Fehrenbach, A., Kendler, A., Sifri, S., Steele, R., Jimeno, A., Carey, F., Forgie, I., Mannelli, M., Carney, M., Hernandez, B., Campos, B., Herold-Mende, C., Jungk, C., Unterberg, A., Deimling, A. von, Bossler, A., Galbraith, J., Jacobus, L., Knudson, M., Knutson, T., Ma, D., Milhem, M., Sigmund, R., Godwin, A.K., Madan, R., Rosenthal, H.G., Adebamowo, C., Adebamowo, S.N., Boussioutas, A., Beer, D., Giordano, T., Mes-Masson, A.-M., Saad, F., Bocklage, T., Landrum, L., Mannel, R., Moore, K., Moxley, K., Postier, R., Walker, J., Zuna, R., Feldman, M., Valdivieso, F., Dhir, R., Luketich, J., Pinero, E.M.M., Quintero-Aguilo, M., Carlotti, C.G., Santos, J.S.D., Kemp, R., Sankarankuty, A., Tirapelli, D., Catto, J., Agnew, K., Swisher, E., Creaney, J., Robinson, B., Shelley, C.S., Godwin, E.M., Kendall, S., Shipman, C., Bradford, C., Carey, T., Haddad, A., Moyer, J., Peterson, L., Prince, M., Rozek, L., Wolf, G., Bowman, R., Fong, K.M., Yang, I., Korst, R., Rathmell, W.K., Fantacone-Campbell, J.L., Hooke, J.A., Kovatich, A.J., Shriver, C.D., DiPersio, J., Drake, B., Govindan, R., Heath, S., Ley, T., Tine, B.V., Westervelt, P., Rubin, M.A., Lee, J.I., Aredes, N.D., Mariamidze, A., Stuart, J.M., Benz, C.C., Laird, P.W., 2018. Cell-of-Origin Patterns Dominate the Molecular Classification of 10,000 Tumors from 33 Types of Cancer. Cell 173, 291-304.e6. https://doi.org/10.1016/j.cell.2018.03.022

Houten, S.M., Wanders, R.J.A., 2010. A general introduction to the biochemistry of mitochondrial fatty acid β-oxidation. J. Inherit. Metab. Dis. 33, 469–477. https://doi.org/10.1007/s10545-010-9061-2

Ji, H., Ramsey, M.R., Hayes, D.N., Fan, C., McNamara, K., Kozlowski, P., Torrice, C., Wu, M.C., Shimamura, T., Perera, S.A., Liang, M.-C., Cai, D., Naumov, G.N., Bao, L., Contreras, C.M., Li, D., Chen, L., Krishnamurthy, J., Koivunen, J., Chirieac, L.R., Padera, R.F., Bronson, R.T., Lindeman, N.I., Christiani, D.C., Lin, X., Shapiro, G.I., Jänne, P.A., Johnson, B.E., Meyerson, M., Kwiatkowski, D.J., Castrillon, D.H., Bardeesy, N., Sharpless, N.E., Wong, K.-K., 2007. LKB1 modulates lung cancer differentiation and metastasis. Nature 448, 807–810. https://doi.org/10.1038/nature06030

Johnson, D.E., O'Keefe, R.A., Grandis, J.R., 2018. Targeting the IL-6/JAK/STAT3 signalling axis in cancer. Nat. Rev. Clin. Oncol. 15, 234–248. https://doi.org/10.1038/nrclinonc.2018.8

Kerner, J., Parland, W.K., Minkler, P.E., Hoppel, C.L., 2008. Rat liver mitochondrial carnitine palmitoyltransferase-I, hepatic carnitine, and malonyl-CoA: effect of starvation. Arch. Physiol. Biochem. 114, 161–170. https://doi.org/10.1080/13813450802181062

Kim, A.-R., Hu, Y., Comjean, A., Rodiger, J., Mohr, S.E., Perrimon, N., n.d. Enhanced Protein-Protein Interaction Discovery via AlphaFold-Multimer. bioRxiv 2024. https://doi.org/10.1101/2024.02.19.580970.

Kinoshita, E., Kinoshita-Kikuta, E., Takiyama, K., Koike, T., 2006. Phosphate-binding tag, a new tool to visualize phosphorylated proteins. Mol. Cell. Proteomics MCP 5, 749–757. https://doi.org/10.1074/mcp.T500024-MCP200

Kinoshita, T., 2020. Biosynthesis and biology of mammalian GPI-anchored proteins. Open Biol. 10, 190290. https://doi.org/10.1098/rsob.190290

Klionsky, D.J., Abdel-Aziz, A.K., Abdelfatah, S., Abdellatif, M., Abdoli, A., Abel, S., Abeliovich, H., Abildgaard, M.H., Abudu, Y.P., Acevedo-Arozena, A., Adamopoulos, I.E., Adeli, K., Adolph, T.E., Adornetto, A., Aflaki, E., Agam, G., Agarwal, A., Aggarwal, B.B., Agnello, M., Agostinis, P., Agrewala, J.N., Agrotis, A., Aguilar, P.V., Ahmad, S.T., Ahmed, Z.M., Ahumada-Castro, U., Aits, S., Aizawa, S., Akkoc, Y., Akoumianaki, T., Akpinar, H.A., Al-Abd, A.M., Al-Akra, L., Al-Gharaibeh, A., Alaoui-Jamali, M.A., Alberti, S., Alcocer-Gómez, E., Alessandri, C., Ali, M., Alim Al-Bari, M.A., Aliwaini, S., Alizadeh, J., Almacellas, E., Almasan, A., Alonso, A., Alonso, G.D., Altan-Bonnet, N., Altieri, D.C., Álvarez, É.M.C., Alves, S., Alves da Costa, C., Alzaharna, M.M., Amadio, M., Amantini, C., Amaral, C., Ambrosio, S., Amer, A.O., Ammanathan, V., An, Z., Andersen, S.U., Andrabi, S.A., Andrade-Silva, M., Andres, A.M., Angelini, S., Ann, D., Anozie, U.C., Ansari, M.Y., Antas, P., Antebi, A., Antón, Z., Anwar, T., Apetoh, L., Apostolova, N., Araki, T., Araki, Y., Arasaki, K., Araújo, W.L., Araya, J., Arden, C., Arévalo, M.-A., Arguelles, S., Arias, E., Arikkath, J., Arimoto, H., Ariosa, A.R., Armstrong-James, D., Arnauné-Pelloquin, L., Aroca, A., Arroyo, D.S., Arsov, I., Artero, R., Asaro, D.M.L., Aschner, M., Ashrafizadeh, M., Ashur-Fabian, O., Atanasov, A.G., Au, A.K., Auberger, P., Auner, H.W., Aurelian, L., Autelli, R., Avagliano, L., Ávalos, Y., Aveic, S., Aveleira, C.A., Avin-Wittenberg, T., Aydin, Y., Ayton, S., Ayyadevara, S., Azzopardi, M., Baba, M., Backer, J.M., Backues, S.K., Bae, D.-H., Bae, O.-N., Bae, S.H., Baehrecke, E.H., Baek, A., Baek, S.-H., Baek, S.H., Bagetta, G., Bagniewska-Zadworna, A., Bai, H., Bai, J., Bai, X., Bai, Y., Bairagi, N., Baksi, S., Balbi, T., Baldari, C.T., Balduini, W., Ballabio, A., Ballester, M., Balazadeh, S., Balzan, R., Bandopadhyay, R., Banerjee, Sreeparna, Banerjee, Sulagna, Bánréti, Á., Bao, Y., Baptista, M.S., Baracca, A., Barbati, C., Bargiela, A., Barilà, D., Barlow, P.G., Barmada, S.J., Barreiro, E., Barreto, G.E., Bartek, J., Bartel, B., Bartolome, A., Barve, G.R., Basagoudanavar, S.H., Bassham, D.C., Bast, R.C., Basu, A., Batoko, H., Batten, I., Baulieu, E.E., Baumgarner, B.L., Bayry, J., Beale, R., Beau, I., Beaumatin, F., Bechara, L.R.G., Beck, G.R., Beers, M.F., Begun, J., Behrends, C., Behrens, G.M.N., Bei, R., Bejarano, E., Bel, S., Behl, C., Belaid, A., Belgareh-Touzé, N., Bellarosa, C., Belleudi, F., Belló Pérez, M., Bello-Morales, R., Beltran, J.S. de O., Beltran, S., Benbrook, D.M., Bendorius, M., Benitez, B.A., Benito-Cuesta, I., Bensalem, J., Berchtold, M.W., Berezowska, S., Bergamaschi, D., Bergami, M., Bergmann, A., Berliocchi, L., Berlioz-Torrent, C., Bernard, A., Berthoux, L., Besirli, C.G., Besteiro, S., Betin, V.M., Beyaert, R., Bezbradica, J.S., Bhaskar, K., Bhatia-Kissova, I., Bhattacharya, R., Bhattacharya, S., Bhattacharyya, S., Bhuiyan, M.S., Bhutia, S.K., Bi, L., Bi, X., Biden, T.J., Bijian, K., Billes, V.A., Binart, N., Bincoletto, C., Birgisdottir, A.B., Bjorkoy, G., Blanco, G., Blas-Garcia, A., Blasiak, J., Blomgran, R., Blomgren, K., Blum, J.S., Boada-Romero, E., Boban, M., Boesze-Battaglia, K., Boeuf, P., Boland, B., Bomont, P., Bonaldo, P., Bonam, S.R., Bonfili, L., Bonifacino, J.S., Boone, B.A.,

Bootman, M.D., Bordi, M., Borner, C., Bornhauser, B.C., Borthakur, G., Bosch, J., Bose, S., Botana, L.M., Botas, J., Boulanger, C.M., Boulton, M.E., Bourdenx, M., Bourgeois, B., Bourke, N.M., Bousquet, G., Boya, P., Bozhkov, P.V., Bozi, L.H.M., Bozkurt, T.O., Brackney, D.E., Brandts, C.H., Braun, R.J., Braus, G.H., Bravo-Sagua, R., Bravo-San Pedro, J.M., Brest, P., Bringer, M.-A., Briones-Herrera, A., Broaddus, V.C., Brodersen, P., Brodsky, J.L., Brody, S.L., Bronson, P.G., Bronstein, J.M., Brown, C.N., Brown, R.E., Brum, P.C., Brumell, J.H., Brunetti-Pierri, N., Bruno, D., Bryson-Richardson, R.J., Bucci, C., Buchrieser, C., Bueno, M., Buitrago-Molina, L.E., Buraschi, S., Buch, S., Buchan, J.R., Buckingham, E.M., Budak, H., Budini, M., Bultynck, G., Burada, F., Burgoyne, J.R., Burón, M.I., Bustos, V., Büttner, S., Butturini, E., Byrd, A., Cabas, I., Cabrera-Benitez, S., Cadwell, K., Cai, J., Cai, L., Cai, Q., Cairó, M., Calbet, J.A., Caldwell, G.A., Caldwell, K.A., Call, J.A., Calvani, R., Calvo, A.C., Calvo-Rubio Barrera, M., Camara, N.O., Camonis, J.H., Camougrand, N., Campanella, M., Campbell, E.M., Campbell-Valois, F.-X., Campello, S., Campesi, I., Campos, J.C., Camuzard, O., Cancino, J., Candido de Almeida, D., Canesi, L., Caniggia, I., Canonico, B., Cantí, C., Cao, B., Caraglia, M., Caramés, B., Carchman, E.H., Cardenal-Muñoz, E., Cardenas, C., Cardenas, L., Cardoso, S.M., Carew, J.S., Carle, G.F., Carleton, G., Carloni, S., Carmona-Gutierrez, D., Carneiro, L.A., Carnevali, O., Carosi, J.M., Carra, S., Carrier, A., Carrier, L., Carroll, B., Carter, A.B., Carvalho, A.N., Casanova, M., Casas, C., Casas, J., Cassioli, C., Castillo, E.F., Castillo, K., Castillo-Lluva, S., Castoldi, F., Castori, M., Castro, A.F., Castro-Caldas, M., Castro-Hernandez, J., Castro-Obregon, S., Catz, S.D., Cavadas, C., Cavaliere, F., Cavallini, G., Cavinato, M., Cayuela, M.L., Cebollada Rica, P., Cecarini, V., Cecconi, F., Cechowska-Pasko, M., Cenci, S., Ceperuelo-Mallafré, V., Cerqueira, J.J., Cerutti, J.M., Cervia, D., Cetintas, V.B., Cetrullo, S., Chae, H.-J., Chagin, A.S., Chai, C.-Y., Chakrabarti, G., Chakrabarti, O., Chakraborty, Tapas, Chakraborty, Trinad, Chami, M., Chamilos, G., Chan, D.W., Chan, E.Y.W., Chan, E.D., Chan, H.Y.E., Chan, H.H., Chan, H., Chan, M.T.V., Chan, Y.S., Chandra, P.K., Chang, C.-P., Chang, C., Chang, H.-C., Chang, K., Chao, J., Chapman, T., Charlet-Berguerand, N., Chatterjee, S., Chaube, S.K., Chaudhary, A., Chauhan, S., Chaum, E., Checler, F., Cheetham, M.E., Chen, C.-S., Chen, G.-C., Chen, J.-F., Chen, L.L., Chen, Leilei, Chen, Lin, Chen, M., Chen, M.-K., Chen, N., Chen, Q., Chen, R.-H., Chen, S., Chen, Wei, Chen, Weiqiang, Chen, X.-M., Chen, X.-W., Chen, X., Chen, Yan, Chen, Y.-G., Chen, Yingyu, Chen, Yongqiang, Chen, Y.-J., Chen, Y.-Q., Chen, Z.S., Chen, Zhi, Chen, Z.-H., Chen, Z.J., Chen, Zhixiang, Cheng, H., Cheng, J., Cheng, S.-Y., Cheng, W., Cheng, X., Cheng, X.-T., Cheng, Y., Cheng, Z., Chen, Zhong, Cheong, H., Cheong, J.K., Chernyak, B.V., Cherry, S., Cheung, C.F.R., Cheung, C.H.A., Cheung, K.-H., Chevet, E., Chi, R.J., Chiang, A.K.S., Chiaradonna, F., Chiarelli, R., Chiariello, M., Chica, N., Chiocca, S., Chiong, M., Chiou, S.-H., Chiramel, A.I., Chiurchiù, V., Cho, D.-H., Choe, S.-K., Choi, A.M.K., Choi, M.E., Choudhury, K.R., Chow, N.S., Chu, C.T., Chua, J.P., Chua, J.J.E., Chung, H., Chung, K.P., Chung, S., Chung, S.-H., Chung, Y.-L., Cianfanelli, V., Ciechomska, I.A., Cifuentes, M., Cinque, L., Cirak, S., Cirone, M., Clague, M.J., Clarke, R., Clementi, E., Coccia, E.M., Codogno, P., Cohen, E., Cohen, M.M., Colasanti, T., Colasuonno, F., Colbert, R.A., Colell, A., Čolić, M., Coll, N.S., Collins,

M.O., Colombo, M.I., Colón-Ramos, D.A., Combaret, L., Comincini, S., Cominetti, M.R., Consiglio, A., Conte, A., Conti, F., Contu, V.R., Cookson, M.R., Coombs, K.M., Coppens, I., Corasaniti, M.T., Corkery, D.P., Cordes, N., Cortese, K., Costa, M. do C., Costantino, S., Costelli, P., Coto-Montes, A., Crack, P.J., Crespo, J.L., Criollo, A., Crippa, V., Cristofani, R., Csizmadia, T., Cuadrado, A., Cui, B., Cui, J., Cui, Yixian, Cui, Yong, Culetto, E., Cumino, A.C., Cybulsky, A.V., Czaja, M.J., Czuczwar, S.J., D'Adamo, S., D'Amelio, M., D'Arcangelo, D., D'Lugos, A.C., D'Orazi, G., da Silva, J.A., Dafsari, H.S., Dagda, R.K., Dagdas, Y., Daglia, M., Dai, X., Dai, Yun, Dai, Yuyuan, Dal Col, J., Dalhaimer, P., Dalla Valle, L., Dallenga, T., Dalmasso, G., Damme, M., Dando, I., Dantuma, N.P., Darling, A.L., Das, H., Dasarathy, S., Dasari, S.K., Dash, S., Daumke, O., Dauphinee, A.N., Davies, J.S., Dávila, V.A., Davis, R.J., Davis, T., Dayalan Naidu, S., De Amicis, F., De Bosscher, K., De Felice, F., De Franceschi, L., De Leonibus, C., de Mattos Barbosa, M.G., De Meyer, G.R.Y., De Milito, A., De Nunzio, C., De Palma, C., De Santi, M., De Virgilio, C., De Zio, D., Debnath, J., DeBosch, B.J., Decuypere, J.-P., Deehan, M.A., Deflorian, G., DeGregori, J., Dehay, B., Del Rio, G., Delaney, J.R., Delbridge, L.M.D., Delorme-Axford, E., Delpino, M.V., Demarchi, F., Dembitz, V., Demers, N.D., Deng, H., Deng, Z., Dengjel, J., Dent, P., Denton, D., DePamphilis, M.L., Der, C.J., Deretic, V., Descoteaux, A., Devis, L., Devkota, S., Devuyst, O., Dewson, G., Dharmasivam, M., Dhiman, R., di Bernardo, D., Di Cristina, M., Di Domenico, F., Di Fazio, P., Di Fonzo, A., Di Guardo, G., Di Guglielmo, G.M., Di Leo, L., Di Malta, C., Di Nardo, A., Di Rienzo, M., Di Sano, F., Diallinas, G., Diao, J., Diaz-Araya, G., Díaz-Laviada, I., Dickinson, J.M., Diederich, M., Dieudé, M., Dikic, I., Ding, S., Ding, W.-X., Dini, L., Dinić, J., Dinic, M., Dinkova-Kostova, A.T., Dionne, M.S., Distler, J.H.W., Diwan, A., Dixon, I.M.C., Djavaheri-Mergny, M., Dobrinski, I., Dobrovinskaya, O., Dobrowolski, R., Dobson, R.C.J., Đokić, J., Dokmeci Emre, S., Donadelli, M., Dong, B., Dong, X., Dong, Z., Dorn Ii, G.W., Dotsch, V., Dou, H., Dou, J., Dowaidar, M., Dridi, S., Drucker, L., Du, A., Du, C., Du, G., Du, H.-N., Du, L.-L., du Toit, A., Duan, S.-B., Duan, X., Duarte, S.P., Dubrovska, A., Dunlop, E.A., Dupont, N., Durán, R.V., Dwarakanath, B.S., Dyshlovoy, S.A., Ebrahimi-Fakhari, D., Eckhart, L., Edelstein, C.L., Efferth, T., Eftekharpour, E., Eichinger, L., Eid, N., Eisenberg, T., Eissa, N.T., Eissa, S., Ejarque, M., El Andaloussi, A., El-Hage, N., El-Naggar, S., Eleuteri, A.M., El-Shafey, E.S., Elgendy, M., Eliopoulos, A.G., Elizalde, M.M., Elks, P.M., Elsasser, H.-P., Elsherbiny, E.S., Emerling, B.M., Emre, N.C.T., Eng, C.H., Engedal, N., Engelbrecht, A.-M., Engelsen, A.S.T., Enserink, J.M., Escalante, R., Esclatine, A., Escobar-Henriques, M., Eskelinen, E.-L., Espert, L., Eusebio, M.-O., Fabrias, G., Fabrizi, C., Facchiano, A., Facchiano, F., Fadeel, B., Fader, C., Faesen, A.C., Fairlie, W.D., Falcó, A., Falkenburger, B.H., Fan, D., Fan, J., Fan, Y., Fang, E.F., Fang, Yanshan, Fang, Yognqi, Fanto, M., Farfel-Becker, T., Faure, M., Fazeli, G., Fedele, A.O., Feldman, A.M., Feng, D., Feng, J., Feng, L., Feng, Yibin, Feng, Yuchen, Feng, W., Fenz Araujo, T., Ferguson, T.A., Fernández, Á.F., Fernandez-Checa, J.C., Fernández-Veledo, S., Fernie, A.R., Ferrante, A.W., Ferraresi, A., Ferrari, M.F., Ferreira, J.C.B., Ferro-Novick, S., Figueras, A., Filadi, R., Filigheddu, N., Filippi-Chiela, E., Filomeni, G., Fimia, G.M., Fineschi, V., Finetti, F., Finkbeiner, S., Fisher, E.A., Fisher, P.B., Flamigni, F., Fliesler, S.J., Flo, T.H., Florance, I., Florey, O., Florio, T.,

Fodor, E., Follo, C., Fon, E.A., Forlino, A., Fornai, F., Fortini, P., Fracassi, A., Fraldi, A., Franco, B., Franco, R., Franconi, F., Frankel, L.B., Friedman, S.L., Fröhlich, L.F., Frühbeck, G., Fuentes, J.M., Fujiki, Y., Fujita, N., Fujiwara, Y., Fukuda, M., Fulda, S., Furic, L., Furuya, N., Fusco, C., Gack, M.U., Gaffke, L., Galadari, S., Galasso, A., Galindo, M.F., Gallolu Kankanamalage, S., Galluzzi, L., Galy, V., Gammoh, N., Gan, B., Ganley, I.G., Gao, F., Gao, H., Gao, M., Gao, P., Gao, S.-J., Gao, W., Gao, X., Garcera, A., Garcia, M.N., Garcia, V.E., García-Del Portillo, F., Garcia-Escudero, V., Garcia-Garcia, A., Garcia-Macia, M., García-Moreno, D., Garcia-Ruiz, C., García-Sanz, P., Garg, A.D., Gargini, R., Garofalo, T., Garry, R.F., Gassen, N.C., Gatica, D., Ge, L., Ge, W., Geiss-Friedlander, R., Gelfi, C., Genschik, P., Gentle, I.E., Gerbino, V., Gerhardt, C., Germain, K., Germain, M., Gewirtz, D.A., Ghasemipour Afshar, E., Ghavami, S., Ghigo, A., Ghosh, M., Giamas, G., Giampietri, C., Giatromanolaki, A., Gibson, G.E., Gibson, S.B., Ginet, V., Giniger, E., Giorgi, C., Girao, H., Girardin, S.E., Giridharan, M., Giuliano, S., Giulivi, C., Giuriato, S., Giustiniani, J., Gluschko, A., Goder, V., Goginashvili, A., Golab, J., Goldstone, D.C., Golebiewska, A., Gomes, L.R., Gomez, R., Gómez-Sánchez, R., Gomez-Puerto, M.C., Gomez-Sintes, R., Gong, Q., Goni, F.M., González-Gallego, J., Gonzalez-Hernandez, T., Gonzalez-Polo, R.A., Gonzalez-Reyes, J.A., González-Rodríguez, P., Goping, I.S., Gorbatyuk, M.S., Gorbunov, N.V., Görgülü, K., Gorojod, R.M., Gorski, S.M., Goruppi, S., Gotor, C., Gottlieb, R.A., Gozes, I., Gozuacik, D., Graef, M., Gräler, M.H., Granatiero, V., Grasso, D., Gray, J.P., Green, D.R., Greenhough, A., Gregory, S.L., Griffin, E.F., Grinstaff, M.W., Gros, F., Grose, C., Gross, A.S., Gruber, F., Grumati, P., Grune, T., Gu, X., Guan, J.-L., Guardia, C.M., Guda, K., Guerra, F., Guerri, C., Guha, P., Guillén, C., Gujar, S., Gukovskaya, A., Gukovsky, I., Gunst, J., Günther, A., Guntur, A.R., Guo, Chuanyong, Guo, Chun, Guo, H., Guo, L.-W., Guo, M., Gupta, P., Gupta, S.K., Gupta, S., Gupta, V.B., Gupta, V., Gustafsson, A.B., Gutterman, D.D., H B, R., Haapasalo, A., Haber, J.E., Hać, A., Hadano, S., Hafrén, A.J., Haidar, M., Hall, B.S., Halldén, G., Hamacher-Brady, A., Hamann, A., Hamasaki, M., Han, W., Hansen, M., Hanson, P.I., Hao, Z., Harada, M., Harhaji-Trajkovic, L., Hariharan, N., Haroon, N., Harris, J., Hasegawa, T., Hasima Nagoor, N., Haspel, J.A., Haucke, V., Hawkins, W.D., Hay, B.A., Haynes, C.M., Hayrabedyan, S.B., Hays, T.S., He, C., He, Q., He, R.-R., He, Y.-W., He, Y.-Y., Heakal, Y., Heberle, A.M., Hejtmancik, J.F., Helgason, G.V., Henkel, V., Herb, M., Hergovich, A., Herman-Antosiewicz, A., Hernández, A., Hernandez, C., Hernandez-Diaz, S., Hernandez-Gea, V., Herpin, A., Herreros, J., Hervás, J.H., Hesselson, D., Hetz, C., Heussler, V.T., Higuchi, Y., Hilfiker, S., Hill, J.A., Hlavacek, W.S., Ho, E.A., Ho, I.H.T., Ho, P.W.-L., Ho, S.-L., Ho, W.Y., Hobbs, G.A., Hochstrasser, M., Hoet, P.H.M., Hofius, D., Hofman, P., Höhn, A., Holmberg, C.I., Hombrebueno, J.R., Yi-Ren Hong, C.-W.H., Hooper, L.V., Hoppe, T., Horos, R., Hoshida, Y., Hsin, I.-L., Hsu, H.-Y., Hu, B., Hu, D., Hu, L.-F., Hu, M.C., Hu, R., Hu, W., Hu, Y.-C., Hu, Z.-W., Hua, F., Hua, J., Hua, Y., Huan, C., Huang, Canhua, Huang, Chuanshu, Huang, Chuanxin, Huang, Chunling, Huang, H., Huang, K., Huang, M.L.H., Huang, R., Huang, S., Huang, T., Huang, X., Huang, Y.J., Huber, T.B., Hubert, V., Hubner, C.A., Hughes, S.M., Hughes, W.E., Humbert, M., Hummer, G., Hurley, J.H., Hussain, Sabah, Hussain, Salik, Hussey, P.J., Hutabarat, M., Hwang, H.-Y., Hwang, S., Ieni, A., Ikeda, F., Imagawa, Y.,

Imai, Y., Imbriano, C., Imoto, M., Inman, D.M., Inoki, K., Iovanna, J., Iozzo, R.V., Ippolito, G., Irazoqui, J.E., Iribarren, P., Ishaq, M., Ishikawa, M., Ishimwe, N., Isidoro, C., Ismail, N., Issazadeh-Navikas, S., Itakura, E., Ito, D., Ivankovic, D., Ivanova, S., Iyer, A.K.V., Izquierdo, J.M., Izumi, M., Jäättelä, M., Jabir, M.S., Jackson, W.T., Jacobo-Herrera, N., Jacomin, A.-C., Jacquin, E., Jadiya, P., Jaeschke, H., Jagannath, C., Jakobi, A.J., Jakobsson, J., Janji, B., Jansen-Dürr, P., Jansson, P.J., Jantsch, J., Januszewski, S., Jassey, A., Jean, S., Jeltsch-David, H., Jendelova, P., Jenny, A., Jensen, T.E., Jessen, N., Jewell, J.L., Ji, J., Jia, L., Jia, R., Jiang, L., Jiang, Q., Jiang, R., Jiang, T., Jiang, X., Jiang, Y., Jimenez-Sanchez, M., Jin, E.-J., Jin, F., Jin, H., Jin, Li, Jin, Luqi, Jin, M., Jin, S., Jo, E.-K., Joffre, C., Johansen, T., Johnson, G.V.W., Johnston, S.A., Jokitalo, E., Jolly, M.K., Joosten, L.A.B., Jordan, J., Joseph, B., Ju, D., Ju, J.-S., Ju, J., Juárez, E., Judith, D., Juhász, G., Jun, Y., Jung, C.H., Jung, S.-C., Jung, Y.K., Jungbluth, H., Jungverdorben, J., Just, S., Kaarniranta, K., Kaasik, A., Kabuta, T., Kaganovich, D., Kahana, A., Kain, R., Kajimura, S., Kalamvoki, M., Kalia, M., Kalinowski, D.S., Kaludercic, N., Kalvari, I., Kaminska, J., Kaminskyy, V.O., Kanamori, H., Kanasaki, K., Kang, C., Kang, R., Kang, S.S., Kaniyappan, S., Kanki, T., Kanneganti, T.-D., Kanthasamy, A.G., Kanthasamy, A., Kantorow, M., Kapuy, O., Karamouzis, M.V., Karim, M.R., Karmakar, P., Katare, R.G., Kato, M., Kaufmann, S.H.E., Kauppinen, A., Kaushal, G.P., Kaushik, S., Kawasaki, K., Kazan, K., Ke, P.-Y., Keating, D.J., Keber, U., Kehrl, J.H., Keller, K.E., Keller, C.W., Kemper, J.K., Kenific, C.M., Kepp, O., Kermorgant, S., Kern, A., Ketteler, R., Keulers, T.G., Khalfin, B., Khalil, H., Khambu, B., Khan, S.Y., Khandelwal, V.K.M., Khandia, R., Kho, W., Khobrekar, N.V., Khuansuwan, S., Khundadze, M., Killackey, S.A., Kim, D., Kim, D.R., Kim, D.-H., Kim, D.-E., Kim, E.Y., Kim, E.-K., Kim, H.-R., Kim, H.-S., Hyung-Ryong Kim, null, Kim, Jeong Hun, Kim, J.K., Kim, J.-H., Kim, J., Kim, Ju Hwan, Kim, K.I., Kim, P.K., Kim, S.-J., Kimball, S.R., Kimchi, A., Kimmelman, A.C., Kimura, T., King, M.A., Kinghorn, K.J., Kinsey, C.G., Kirkin, V., Kirshenbaum, L.A., Kiselev, S.L., Kishi, S., Kitamoto, K., Kitaoka, Y., Kitazato, K., Kitsis, R.N., Kittler, J.T., Kjaerulff, O., Klein, P.S., Klopstock, T., Klucken, J., Knævelsrud, H., Knorr, R.L., Ko, B.C.B., Ko, F., Ko, J.-L., Kobayashi, H., Kobayashi, S., Koch, I., Koch, J.C., Koenig, U., Kögel, D., Koh, Y.H., Koike, M., Kohlwein, S.D., Kocaturk, N.M., Komatsu, M., König, J., Kono, T., Kopp, B.T., Korcsmaros, T., Korkmaz, G., Korolchuk, V.I., Korsnes, M.S., Koskela, A., Kota, J., Kotake, Y., Kotler, M.L., Kou, Y., Koukourakis, M.I., Koustas, E., Kovacs, A.L., Kovács, T., Koya, D., Kozako, T., Kraft, C., Krainc, D., Krämer, H., Krasnodembskaya, A.D., Kretz-Remy, C., Kroemer, G., Ktistakis, N.T., Kuchitsu, K., Kuenen, S., Kuerschner, L., Kukar, T., Kumar, Ajay, Kumar, Ashok, Kumar, Deepak, Kumar, Dhiraj, Kumar, S., Kume, S., Kumsta, C., Kundu, C.N., Kundu, M., Kunnumakkara, A.B., Kurgan, L., Kutateladze, T.G., Kutlu, O., Kwak, S., Kwon, H.J., Kwon, T.K., Kwon, Y.T., Kyrmizi, I., La Spada, A., Labonté, P., Ladoire, S., Laface, I., Lafont, F., Lagace, D.C., Lahiri, V., Lai, Z., Laird, A.S., Lakkaraju, A., Lamark, T., Lan, S.-H., Landajuela, A., Lane, D.J.R., Lane, J.D., Lang, C.H., Lange, C., Langel, Ü., Langer, R., Lapaquette, P., Laporte, J., LaRusso, N.F., Lastres-Becker, I., Lau, W.C.Y., Laurie, G.W., Lavandero, S., Law, B.Y.K., Law, H.K.-W., Layfield, R., Le, W., Le Stunff, H., Leary, A.Y., Lebrun, J.-J., Leck, L.Y.W., Leduc-Gaudet, J.-P., Lee, C., Lee, C.-P., Lee, D.-H., Lee, E.B., Lee, E.F., Lee,

G.M., Lee, H.-J., Lee, H.K., Lee, J.M., Lee, J.S., Lee, J.-A., Lee, J.-Y., Lee, J.H., Lee, M., Lee, M.G., Lee, M.J., Lee, M.-S., Lee, Sang Yoon, Lee, S.-J., Lee, Stella Y., Lee, S.B., Lee, W.H., Lee, Y.-R., Lee, Y.-H., Lee, Y., Lefebvre, C., Legouis, R., Lei, Y.L., Lei, Y., Leikin, S., Leitinger, G., Lemus, L., Leng, S., Lenoir, O., Lenz, G., Lenz, H.J., Lenzi, P., León, Y., Leopoldino, A.M., Leschczyk, C., Leskelä, S., Letellier, E., Leung, C.-T., Leung, P.S., Leventhal, J.S., Levine, B., Lewis, P.A., Ley, K., Li, B., Li, D.-Q., Li, Jianming, Li, Jing, Li, Jiong, Li, K., Li, L., Li, Mei, Li, Min, Li, Min, Li, Ming, Li, Mingchuan, Li, P.-L., Li, M.-Q., Li, Q., Li, S., Li, T., Li, Wei, Li, Wenming, Li, X., Li, Y.-P., Li, Y., Li, Zhiqiang, Li, Zhiyong, Li, Zhiyuan, Lian, J., Liang, C., Liang, Q., Liang, W., Liang, Yongheng, Liang, YongTian, Liao, G., Liao, L., Liao, M., Liao, Y.-F., Librizzi, M., Lie, P.P.Y., Lilly, M.A., Lim, H.J., Lima, T.R.R., Limana, F., Lin, C., Lin, C.-W., Lin, D.-S., Lin, F.-C., Lin, J.D., Lin, K.M., Lin, K.-H., Lin, L.-T., Lin, P.-H., Lin, Q., Lin, S., Lin, S.-J., Lin, W., Lin, X., Lin, Y.-X., Lin, Y.-S., Linden, R., Lindner, P., Ling, S.-C., Lingor, P., Linnemann, A.K., Liou, Y.-C., Lipinski, M.M., Lipovšek, S., Lira, V.A., Lisiak, N., Liton, P.B., Liu, C., Liu, C.-H., Liu, C.-F., Liu, C.H., Liu, F., Liu, Hao, Liu, H.-S., Liu, H.-F., Liu, Huifang, Liu, Jia, Liu, Jing, Liu, Julia, Liu, Leyuan, Liu, Longhua, Liu, M., Liu, Q., Liu, Wei, Liu, Wende, Liu, X.-H., Liu, Xiaodong, Liu, Xingguo, Liu, Xu, Liu, Xuedong, Liu, Yanfen, Liu, Yang, Liu, Yang, Liu, Yueyang, Liu, Yule, Livingston, J.A., Lizard, G., Lizcano, J.M., Ljubojevic-Holzer, S., LLeonart, M.E., Llobet-Navàs, D., Llorente, A., Lo, C.H., Lobato-Márquez, D., Long, Q., Long, Y.C., Loos, B., Loos, J.A., López, M.G., López-Doménech, G., López-Guerrero, J.A., López-Jiménez, A.T., López-Pérez, Ó., López-Valero, I., Lorenowicz, M.J., Lorente, M., Lorincz, P., Lossi, L., Lotersztajn, S., Lovat, P.E., Lovell, J.F., Lovy, A., Lőw, P., Lu, G., Lu, H., Lu, J.-H., Lu, J.-J., Lu, M., Lu, S., Luciani, A., Lucocq, J.M., Ludovico, P., Luftig, M.A., Luhr, M., Luis-Ravelo, D., Lum, J.J., Luna-Dulcey, L., Lund, A.H., Lund, V.K., Lünemann, J.D., Lüningschrör, P., Luo, H., Luo, R., Luo, S., Luo, Z., Luparello, C., Lüscher, B., Luu, L., Lyakhovich, A., Lyamzaev, K.G., Lystad, A.H., Lytvynchuk, L., Ma, A.C., Ma, C., Ma, M., Ma, N.-F., Ma, Q.-H., Ma, X., Ma, Y., Ma, Z., MacDougald, O.A., Macian, F., MacIntosh, G.C., MacKeigan, J.P., Macleod, K.F., Maday, S., Madeo, F., Madesh, M., Madl, T., Madrigal-Matute, J., Maeda, A., Maejima, Y., Magarinos, M., Mahavadi, P., Maiani, E., Maiese, K., Maiti, P., Maiuri, M.C., Majello, B., Major, M.B., Makareeva, E., Malik, F., Mallilankaraman, K., Malorni, W., Maloyan, A., Mammadova, N., Man, G.C.W., Manai, F., Mancias, J.D., Mandelkow, E.-M., Mandell, M.A., Manfredi, A.A., Manjili, M.H., Manjithaya, R., Manque, P., Manshian, B.B., Manzano, R., Manzoni, C., Mao, K., Marchese, C., Marchetti, S., Marconi, A.M., Marcucci, F., Mardente, S., Mareninova, O.A., Margeta, M., Mari, M., Marinelli, S., Marinelli, O., Mariño, G., Mariotto, S., Marshall, R.S., Marten, M.R., Martens, S., Martin, A.P.J., Martin, K.R., Martin, Sara, Martin, Shaun, Martín-Segura, A., Martín-Acebes, M.A., Martin-Burriel, I., Martin-Rincon, M., Martin-Sanz, P., Martina, J.A., Martinet, W., Martinez, Aitor, Martinez, Ana, Martinez, J., Martinez Velazquez, M., Martinez-Lopez, N., Martinez-Vicente, M., Martins, D.O., Martins, J.O., Martins, W.K., Martins-Marques, T., Marzetti, E., Masaldan, S., Masclaux-Daubresse, C., Mashek, D.G., Massa, V., Massieu, L., Masson, G.R., Masuelli, L., Masyuk, A.I., Masyuk, T.V., Matarrese, P., Matheu, A., Matoba, S., Matsuzaki, S., Mattar, P., Matte, A., Mattoscio, D., Mauriz,

J.L., Mauthe, M., Mauvezin, C., Maverakis, E., Maycotte, P., Mayer, J., Mazzoccoli, G., Mazzoni, C., Mazzulli, J.R., McCarty, N., McDonald, C., McGill, M.R., McKenna, S.L., McLaughlin, B., McLoughlin, F., McNiven, M.A., McWilliams, T.G., Mechta-Grigoriou, F., Medeiros, T.C., Medina, D.L., Megeney, L.A., Megyeri, K., Mehrpour, M., Mehta, J.L., Meijer, A.J., Meijer, A.H., Mejlvang, J., Meléndez, A., Melk, A., Memisoglu, G., Mendes, A.F., Meng, D., Meng, F., Meng, T., Menna-Barreto, R., Menon, M.B., Mercer, C., Mercier, A.E., Mergny, J.-L., Merighi, A., Merkley, S.D., Merla, G., Meske, V., Mestre, A.C., Metur, S.P., Meyer, C., Meyer, H., Mi, W., Mialet-Perez, J., Miao, J., Micale, L., Miki, Y., Milan, E., Milczarek, M., Miller, D.L., Miller, S.I., Miller, S., Millward, S.W., Milosevic, I., Minina, E.A., Mirzaei, H., Mirzaei, H.R., Mirzaei, M., Mishra, A., Mishra, N., Mishra, P.K., Misirkic Marjanovic, M., Misasi, R., Misra, A., Misso, G., Mitchell, C., Mitou, G., Miura, T., Miyamoto, S., Miyazaki, Makoto, Miyazaki, Mitsunori, Miyazaki, T., Miyazawa, K., Mizushima, N., Mogensen, T.H., Mograbi, B., Mohammadinejad, R., Mohamud, Y., Mohanty, A., Mohapatra, S., Möhlmann, T., Mohmmed, A., Moles, A., Moley, K.H., Molinari, M., Mollace, V., Møller, A.B., Mollereau, B., Mollinedo, F., Montagna, C., Monteiro, M.J., Montella, A., Montes, L.R., Montico, B., Mony, V.K., Monzio Compagnoni, G., Moore, M.N., Moosavi, M.A., Mora, A.L., Mora, M., Morales-Alamo, D., Moratalla, R., Moreira, P.I., Morelli, E., Moreno, S., Moreno-Blas, D., Moresi, V., Morga, B., Morgan, A.H., Morin, F., Morishita, H., Moritz, O.L., Moriyama, M., Moriyasu, Y., Morleo, M., Morselli, E., Moruno-Manchon, J.F., Moscat, J., Mostowy, S., Motori, E., Moura, A.F., Moustaid-Moussa, N., Mrakovcic, M., Muciño-Hernández, G., Mukherjee, A., Mukhopadhyay, S., Mulcahy Levy, J.M., Mulero, V., Muller, S., Münch, C., Munjal, A., Munoz-Canoves, P., Muñoz-Galdeano, T., Münz, C., Murakawa, T., Muratori, C., Murphy, B.M., Murphy, J.P., Murthy, A., Myöhänen, T.T., Mysorekar, I.U., Mytych, J., Nabavi, S.M., Nabissi, M., Nagy, P., Nah, J., Nahimana, A., Nakagawa, I., Nakamura, K., Nakatogawa, H., Nandi, S.S., Nanjundan, M., Nanni, M., Napolitano, G., Nardacci, R., Narita, M., Nassif, M., Nathan, I., Natsumeda, M., Naude, R.J., Naumann, C., Naveiras, O., Navid, F., Nawrocki, S.T., Nazarko, T.Y., Nazio, F., Negoita, F., Neill, T., Neisch, A.L., Neri, L.M., Netea, M.G., Neubert, P., Neufeld, T.P., Neumann, D., Neutzner, A., Newton, P.T., Ney, P.A., Nezis, I.P., Ng, C.C.W., Ng, T.B., Nguyen, H.T.T., Nguyen, L.T., Ni, H.-M., Ní Cheallaigh, C., Ni, Z., Nicolao, M.C., Nicoli, F., Nieto-Diaz, M., Nilsson, P., Ning, S., Niranjan, R., Nishimune, H., Niso-Santano, M., Nixon, R.A., Nobili, A., Nobrega, C., Noda, T., Nogueira-Recalde, U., Nolan, T.M., Nombela, I., Novak, I., Novoa, B., Nozawa, T., Nukina, N., Nussbaum-Krammer, C., Nylandsted, J., O'Donovan, T.R., O'Leary, S.M., O'Rourke, E.J., O'Sullivan, M.P., O'Sullivan, T.E., Oddo, S., Oehme, I., Ogawa, M., Ogier-Denis, E., Ogmundsdottir, M.H., Ogretmen, B., Oh, G.T., Oh, S.-H., Oh, Y.J., Ohama, T., Ohashi, Y., Ohmuraya, M., Oikonomou, V., Ojha, R., Okamoto, K., Okazawa, H., Oku, M., Oliván, S., Oliveira, J.M.A., Ollmann, M., Olzmann, J.A., Omari, S., Omary, M.B., Önal, G., Ondrej, M., Ong, S.-B., Ong, S.-G., Onnis, A., Orellana, J.A., Orellana-Muñoz, S., Ortega-Villaizan, M.D.M., Ortiz-Gonzalez, X.R., Ortona, E., Osiewacz, H.D., Osman, A.-H.K., Osta, R., Otegui, M.S., Otsu, K., Ott, C., Ottobrini, L., Ou, J.-H.J., Outeiro, T.F., Oynebraten, I., Ozturk, M., Pagès, G., Pahari, S., Pajares, M., Pajvani, U.B., Pal, R., Paladino, S., Pallet, N.,

Palmieri, M., Palmisano, G., Palumbo, C., Pampaloni, F., Pan, L., Pan, Q., Pan, W., Pan, X., Panasyuk, G., Pandey, R., Pandey, U.B., Pandya, V., Paneni, F., Pang, S.Y., Panzarini, E., Papademetrio, D.L., Papaleo, E., Papinski, D., Papp, D., Park, E.C., Park, H.T., Park, J.-M., Park, J.-I., Park, J.T., Park, J., Park, S.C., Park, S.-Y., Parola, A.H., Parys, J.B., Pasquier, A., Pasquier, B., Passos, J.F., Pastore, N., Patel, H.H., Patschan, D., Pattingre, S., Pedraza-Alva, G., Pedraza-Chaverri, J., Pedrozo, Z., Pei, G., Pei, J., Peled-Zehavi, H., Pellegrini, J.M., Pelletier, J., Peñalva, M.A., Peng, D., Peng, Y., Penna, F., Pennuto, M., Pentimalli, F., Pereira, C.M., Pereira, G.J.S., Pereira, L.C., Pereira de Almeida, L., Perera, N.D., Pérez-Lara, Á., Perez-Oliva, A.B., Pérez-Pérez, M.E., Periyasamy, P., Perl, A., Perrotta, C., Perrotta, I., Pestell, R.G., Petersen, M., Petrache, I., Petrovski, G., Pfirrmann, T., Pfister, A.S., Philips, J.A., Pi, H., Picca, A., Pickrell, A.M., Picot, S., Pierantoni, G.M., Pierdominici, M., Pierre, P., Pierrefite-Carle, V., Pierzynowska, K., Pietrocola, F., Pietruczuk, M., Pignata, C., Pimentel-Muiños, F.X., Pinar, M., Pinheiro, R.O., Pinkas-Kramarski, R., Pinton, P., Pircs, K., Piya, S., Pizzo, P., Plantinga, T.S., Platta, H.W., Plaza-Zabala, A., Plomann, M., Plotnikov, E.Y., Plun-Favreau, H., Pluta, R., Pocock, R., Pöggeler, S., Pohl, C., Poirot, M., Poletti, A., Ponpuak, M., Popelka, H., Popova, B., Porta, H., Porte Alcon, S., Portilla-Fernandez, E., Post, M., Potts, M.B., Poulton, J., Powers, T., Prahlad, V., Prajsnar, T.K., Praticò, D., Prencipe, R., Priault, M., Proikas-Cezanne, T., Promponas, V.J., Proud, C.G., Puertollano, R., Puglielli, L., Pulinilkunnil, T., Puri, D., Puri, R., Puyal, J., Qi, X., Qi, Y., Qian, W., Qiang, L., Qiu, Y., Quadrilatero, J., Quarleri, J., Raben, N., Rabinowich, H., Ragona, D., Ragusa, M.J., Rahimi, N., Rahmati, M., Raia, V., Raimundo, N., Rajasekaran, N.-S., Ramachandra Rao, S., Rami, A., Ramírez-Pardo, I., Ramsden, D.B., Randow, F., Rangarajan, P.N., Ranieri, D., Rao, H., Rao, L., Rao, R., Rathore, S., Ratnayaka, J.A., Ratovitski, E.A., Ravanan, P., Ravegnini, G., Ray, S.K., Razani, B., Rebecca, V., Reggiori, F., Régnier-Vigouroux, A., Reichert, A.S., Reigada, D., Reiling, J.H., Rein, T., Reipert, S., Rekha, R.S., Ren, H., Ren, J., Ren, W., Renault, T., Renga, G., Reue, K., Rewitz, K., Ribeiro de Andrade Ramos, B., Riazuddin, S.A., Ribeiro-Rodrigues, T.M., Ricci, J.-E., Ricci, R., Riccio, V., Richardson, D.R., Rikihisa, Y., Risbud, M.V., Risueño, R.M., Ritis, K., Rizza, S., Rizzuto, R., Roberts, H.C., Roberts, L.D., Robinson, K.J., Roccheri, M.C., Rocchi, S., Rodney, G.G., Rodrigues, T., Rodrigues Silva, V.R., Rodriguez, A., Rodriguez-Barrueco, R., Rodriguez-Henche, N., Rodriguez-Rocha, H., Roelofs, J., Rogers, R.S., Rogov, V.V., Rojo, A.I., Rolka, K., Romanello, V., Romani, L., Romano, A., Romano, P.S., Romeo-Guitart, D., Romero, L.C., Romero, M., Roney, J.C., Rongo, C., Roperto, S., Rosenfeldt, M.T., Rosenstiel, P., Rosenwald, A.G., Roth, K.A., Roth, L., Roth, S., Rouschop, K.M.A., Roussel, B.D., Roux, S., Rovere-Querini, P., Roy, A., Rozieres, A., Ruano, D., Rubinsztein, D.C., Rubtsova, M.P., Ruckdeschel, K., Ruckenstuhl, C., Rudolf, E., Rudolf, R., Ruggieri, A., Ruparelia, A.A., Rusmini, P., Russell, R.R., Russo, G.L., Russo, M., Russo, R., Ryabaya, O.O., Ryan, K.M., Ryu, K.-Y., Sabater-Arcis, M., Sachdev, U., Sacher, M., Sachse, C., Sadhu, A., Sadoshima, J., Safren, N., Saftig, P., Sagona, A.P., Sahay, G., Sahebkar, A., Sahin, M., Sahin, O., Sahni, S., Saito, N., Saito, S., Saito, T., Sakai, R., Sakai, Y., Sakamaki, J.-I., Saksela, K., Salazar, G., Salazar-Degracia, A., Salekdeh, G.H., Saluja, A.K., Sampaio-Marques, B., Sanchez, M.C., Sanchez-Alcazar, J.A.,

Sanchez-Vera, V., Sancho-Shimizu, V., Sanderson, J.T., Sandri, M., Santaguida, S., Santambrogio, L., Santana, M.M., Santoni, G., Sanz, A., Sanz, P., Saran, S., Sardiello, M., Sargeant, T.J., Sarin, A., Sarkar, C., Sarkar, Sovan, Sarrias, M.-R., Sarkar, Surajit, Sarmah, D.T., Sarparanta, J., Sathyanarayan, A., Sathyanarayanan, R., Scaglione, K.M., Scatozza, F., Schaefer, L., Schafer, Z.T., Schaible, U.E., Schapira, A.H.V., Scharl, M., Schatzl, H.M., Schein, C.H., Scheper, W., Scheuring, D., Schiaffino, M.V., Schiappacassi, M., Schindl, R., Schlattner, U., Schmidt, O., Schmitt, R., Schmidt, S.D., Schmitz, I., Schmukler, E., Schneider, A., Schneider, B.E., Schober, R., Schoijet, A.C., Schott, M.B., Schramm, M., Schröder, B., Schuh, K., Schüller, C., Schulze, R.J., Schürmanns, L., Schwamborn, J.C., Schwarten, M., Scialo, F., Sciarretta, S., Scott, M.J., Scotto, K.W., Scovassi, A.I., Scrima, A., Scrivo, A., Sebastian, D., Sebti, S., Sedej, S., Segatori, L., Segev, N., Seglen, P.O., Seiliez, I., Seki, E., Selleck, S.B., Sellke, F.W., Selsby, J.T., Sendtner, M., Senturk, S., Seranova, E., Sergi, C., Serra-Moreno, R., Sesaki, H., Settembre, C., Setty, S.R.G., Sgarbi, G., Sha, O., Shacka, J.J., Shah, J.A., Shang, D., Shao, C., Shao, F., Sharbati, S., Sharkey, L.M., Sharma, D., Sharma, G., Sharma, K., Sharma, P., Sharma, S., Shen, H.-M., Shen, H., Shen, J., Shen, M., Shen, W., Shen, Z., Sheng, R., Sheng, Z., Sheng, Z.-H., Shi, J., Shi, X., Shi, Y.-H., Shiba-Fukushima, K., Shieh, J.-J., Shimada, Y., Shimizu, S., Shimozawa, M., Shintani, T., Shoemaker, C.J., Shojaei, S., Shoji, I., Shravage, B.V., Shridhar, V., Shu, C.-W., Shu, H.-B., Shui, K., Shukla, A.K., Shutt, T.E., Sica, V., Siddiqui, A., Sierra, A., Sierra-Torre, V., Signorelli, S., Sil, P., Silva, B.J. de A., Silva, J.D., Silva-Pavez, E., Silvente-Poirot, S., Simmonds, R.E., Simon, A.K., Simon, H.-U., Simons, M., Singh, A., Singh, L.P., Singh, R., Singh, S.V., Singh, S.K., Singh, S.B., Singh, S., Singh, S.P., Sinha, D., Sinha, R.A., Sinha, S., Sirko, A., Sirohi, K., Sivridis, E.L., Skendros, P., Skirycz, A., Slaninová, I., Smaili, S.S., Smertenko, A., Smith, M.D., Soenen, S.J., Sohn, E.J., Sok, S.P.M., Solaini, G., Soldati, T., Soleimanpour, S.A., Soler, R.M., Solovchenko, A., Somarelli, J.A., Sonawane, A., Song, F., Song, H.K., Song, J.-X., Song, K., Song, Z., Soria, L.R., Sorice, M., Soukas, A.A., Soukup, S.-F., Sousa, D., Sousa, N., Spagnuolo, P.A., Spector, S.A., Srinivas Bharath, M.M., St Clair, D., Stagni, V., Staiano, L., Stalnecker, C.A., Stankov, M.V., Stathopulos, P.B., Stefan, K., Stefan, S.M., Stefanis, L., Steffan, J.S., Steinkasserer, A., Stenmark, H., Sterneckert, J., Stevens, C., Stoka, V., Storch, S., Stork, B., Strappazzon, F., Strohecker, A.M., Stupack, D.G., Su, H., Su, L.-Y., Su, L., Suarez-Fontes, A.M., Subauste, C.S., Subbian, S., Subirada, P.V., Sudhandiran, G., Sue, C.M., Sui, X., Summers, C., Sun, G., Sun, J., Sun, K., Sun, M.-X., Sun, Q., Sun, Y., Sun, Z., Sunahara, K.K.S., Sundberg, E., Susztak, K., Sutovsky, P., Suzuki, H., Sweeney, G., Symons, J.D., Sze, S.C.W., Szewczyk, N.J., Tabęcka-Łonczynska, A., Tabolacci, C., Tacke, F., Taegtmeyer, H., Tafani, M., Tagaya, M., Tai, H., Tait, S.W.G., Takahashi, Y., Takats, S., Talwar, P., Tam, C., Tam, S.Y., Tampellini, D., Tamura, A., Tan, C.T., Tan, E.-K., Tan, Y.-Q., Tanaka, Masaki, Tanaka, Motomasa, Tang, D., Tang, J., Tang, T.-S., Tanida, I., Tao, Z., Taouis, M., Tatenhorst, L., Tavernarakis, N., Taylor, A., Taylor, G.A., Taylor, J.M., Tchetina, E., Tee, A.R., Tegeder, I., Teis, D., Teixeira, N., Teixeira-Clerc, F., Tekirdag, K.A., Tencomnao, T., Tenreiro, S., Tepikin, A.V., Testillano, P.S., Tettamanti, G., Tharaux, P.-L., Thedieck, K., Thekkinghat, A.A., Thellung, S., Thinwa, J.W.,

Thirumalaikumar, V.P., Thomas, S.M., Thomes, P.G., Thorburn, A., Thukral, L., Thum, T., Thumm, M., Tian, L., Tichy, A., Till, A., Timmerman, V., Titorenko, V.I., Todi, S.V., Todorova, K., Toivonen, J.M., Tomaipitinca, L., Tomar, D., Tomas-Zapico, C., Tomić, S., Tong, B.C.-K., Tong, C., Tong, X., Tooze, S.A., Torgersen, M.L., Torii, S., Torres-López, L., Torriglia, A., Towers, C.G., Towns, R., Toyokuni, S., Trajkovic, V., Tramontano, D., Tran, Q.-G., Travassos, L.H., Trelford, C.B., Tremel, S., Trougakos, I.P., Tsao, B.P., Tschan, M.P., Tse, H.-F., Tse, T.F., Tsugawa, H., Tsvetkov, A.S., Tumbarello, D.A., Tumtas, Y., Tuñón, M.J., Turcotte, S., Turk, B., Turk, V., Turner, B.J., Tuxworth, R.I., Tyler, J.K., Tyutereva, E.V., Uchiyama, Y., Ugun-Klusek, A., Uhlig, H.H., Ułamek-Kozioł, M., Ulasov, I.V., Umekawa, M., Ungermann, C., Unno, R., Urbe, S., Uribe-Carretero, E., Üstün, S., Uversky, V.N., Vaccari, T., Vaccaro, M.I., Vahsen, B.F., Vakifahmetoglu-Norberg, H., Valdor, R., Valente, M.J., Valko, A., Vallee, R.B., Valverde, A.M., Van den Berghe, G., van der Veen, S., Van Kaer, L., van Loosdregt, J., van Wijk, S.J.L., Vandenberghe, W., Vanhorebeek, I., Vannier-Santos, M.A., Vannini, N., Vanrell, M.C., Vantaggiato, C., Varano, G., Varela-Nieto, I., Varga, M., Vasconcelos, M.H., Vats, S., Vavvas, D.G., Vega-Naredo, I., Vega-Rubin-de-Celis, S., Velasco, G., Velázquez, A.P., Vellai, T., Vellenga, E., Velotti, F., Verdier, M., Verginis, P., Vergne, I., Verkade, P., Verma, M., Verstreken, P., Vervliet, T., Vervoorts, J., Vessoni, A.T., Victor, V.M., Vidal, M., Vidoni, C., Vieira, O.V., Vierstra, R.D., Viganó, S., Vihinen, H., Vijayan, V., Vila, M., Vilar, M., Villalba, J.M., Villalobo, A., Villarejo-Zori, B., Villarroya, F., Villarroya, J., Vincent, O., Vindis, C., Viret, C., Viscomi, M.T., Visnjic, D., Vitale, I., Vocadlo, D.J., Voitsekhovskaja, O.V., Volonté, C., Volta, M., Vomero, M., Von Haefen, C., Vooijs, M.A., Voos, W., Vucicevic, L., Wade-Martins, R., Waguri, S., Waite, K.A., Wakatsuki, S., Walker, D.W., Walker, M.J., Walker, S.A., Walter, J., Wandosell, F.G., Wang, B., Wang, Chao-Yung, Wang, Chen, Wang, Chenran, Wang, Chenwei, Wang, Cun-Yu, Wang, D., Wang, Fangyang, Wang, Feng, Wang, Fengming, Wang, G., Wang, Han, Wang, Hao, Wang, Hexiang, Wang, H.-G., Wang, Jianrong, Wang, Jigang, Wang, Jiou, Wang, Jundong, Wang, K., Wang, Lianrong, Wang, Liming, Wang, M.H., Wang, M., Wang, N., Wang, Pengwei, Wang, Peipei, Wang, Ping, Wang, Ping, Wang, Q.J., Wang, Q., Wang, Q.K., Wang, Q.A., Wang, W.-T., Wang, W., Wang, Xinnan, Wang, Xuejun, Wang, Yan, Wang, Yanchang, Wang, Yanzhuang, Wang, Y.-Y., Wang, Yihua, Wang, Yipeng, Wang, Yu, Wang, Yuqi, Wang, Zhe, Wang, Zhenyu, Wang, Zhouguang, Warnes, G., Warnsmann, V., Watada, H., Watanabe, E., Watchon, M., Wawrzyńska, A., Weaver, T.E., Wegrzyn, G., Wehman, A.M., Wei, H., Wei, L., Wei, T., Wei, Y., Weiergräber, O.H., Weihl, C.C., Weindl, G., Weiskirchen, R., Wells, A., Wen, R.H., Wen, X., Werner, A., Weykopf, B., Wheatley, S.P., Whitton, J.L., Whitworth, A.J., Wiktorska, K., Wildenberg, M.E., Wileman, T., Wilkinson, S., Willbold, D., Williams, B., Williams, R.S.B., Williams, R.L., Williamson, P.R., Wilson, R.A., Winner, B., Winsor, N.J., Witkin, S.S., Wodrich, H., Woehlbier, U., Wollert, T., Wong, E., Wong, J.H., Wong, R.W., Wong, V.K.W., Wong, W.W.-L., Wu, A.-G., Wu, C., Wu, Jian, Wu, Junfang, Wu, K.K., Wu, M., Wu, Shan-Ying, Wu, Shengzhou, Wu, Shu-Yan, Wu, Shufang, Wu, W.K.K., Wu, Xiaohong, Wu, Xiaoqing, Wu, Y.-W., Wu, Y., Xavier, R.J., Xia, H., Xia, L., Xia, Z., Xiang, G., Xiang, J., Xiang, M., Xiang, W., Xiao, B., Xiao, G., Xiao, H., Xiao, H.-T., Xiao, J., Xiao, L., Xiao, S., Xiao, Y., Xie, B., Xie, C.-M., Xie,

M., Xie, Y., Xie, Zhiping, Xie, Zhonglin, Xilouri, M., Xu, C., Xu, E., Xu, H., Xu, Jing, Xu, JinRong, Xu, L., Xu, W.W., Xu, X., Xue, Y., Yakhine-Diop, S.M.S., Yamaguchi, M., Yamaguchi, O., Yamamoto, A., Yamashina, S., Yan, S., Yan, S.-J., Yan, Z., Yanagi, Y., Yang, C., Yang, D.-S., Yang, Huan, Yang, H.-T., Yang, Hui, Yang, J.-M., Yang, Jing, Yang, Jingyu, Yang, Ling, Yang, Liu, Yang, M., Yang, P.-M., Yang, Q., Yang, Seungwon, Yang, Shu, Yang, S.-F., Yang, W., Yang, W.Y., Yang, Xiaoyong, Yang, Xuesong, Yang, Yi, Yang, Ying, Yao, H., Yao, S., Yao, X., Yao, Y.-G., Yao, Y.-M., Yasui, T., Yazdankhah, M., Yen, P.M., Yi, C., Yin, X.-M., Yin, Y., Yin, Zhangyuan, Yin, Ziyi, Ying, M., Ying, Z., Yip, C.K., Yiu, S.P.T., Yoo, Y.H., Yoshida, K., Yoshii, S.R., Yoshimori, T., Yousefi, B., Yu, B., Yu, H., Yu, J., Yu, J., Yu, L., Yu, M.-L., Yu, S.-W., Yu, V.C., Yu, W.H., Yu, Zhengping, Yu, Zhou, Yuan, J., Yuan, L.-Q., Yuan, S., Yuan, S.-S.F., Yuan, Y., Yuan, Z., Yue, J., Yue, Z., Yun, J., Yung, R.L., Zacks, D.N., Zaffagnini, G., Zambelli, V.O., Zanella, I., Zang, Q.S., Zanivan, S., Zappavigna, S., Zaragoza, P., Zarbalis, K.S., Zarebkohan, A., Zarrouk, A., Zeitlin, S.O., Zeng, J., Zeng, J.-D., Žerovnik, E., Zhan, L., Zhang, B., Zhang, D.D., Zhang, Hanlin, Zhang, Hong, Zhang, Hong, Zhang, Honghe, Zhang, Huafeng, Zhang, Huaye, Zhang, Hui, Zhang, H.-L., Zhang, Jianbin, Zhang, Jianhua, Zhang, J.-P., Zhang, K.Y.B., Zhang, L.W., Zhang, Lin, Zhang, Lisheng, Zhang, Lu, Zhang, Luoying, Zhang, M., Zhang, P., Zhang, S., Zhang, W., Zhang, Xiangnan, Zhang, X.-W., Zhang, Xiaolei, Zhang, Xiaoyan, Zhang, Xin, Zhang, Xinxin, Zhang, X.D., Zhang, Yang, Zhang, Yanjin, Zhang, Yi, Zhang, Y.-D., Zhang, Yingmei, Zhang, Y.-Y., Zhang, Yuchen, Zhang, Zhe, Zhang, Zhengguang, Zhang, Zhibing, Zhang, Zhihai, Zhang, Zhiyong, Zhang, Zili, Zhao, H., Zhao, L., Zhao, S., Zhao, T., Zhao, X.-F., Zhao, Ying, Zhao, Yongchao, Zhao, Yongliang, Zhao, Yuting, Zheng, G., Zheng, K., Zheng, L., Zheng, S., Zheng, X.-L., Zheng, Y., Zheng, Z.-G., Zhivotovsky, B., Zhong, Q., Zhou, A., Zhou, B., Zhou, C., Zhou, G., Zhou, Hao, Zhou, Hong, Zhou, Hongbo, Zhou, Jie, Zhou, Jing, Zhou, Jing, Zhou, Jiyong, Zhou, K., Zhou, R., Zhou, X.-J., Zhou, Yanshuang, Zhou, Yinghong, Zhou, Yubin, Zhou, Z.-Y., Zhou, Z., Zhu, B., Zhu, C., Zhu, G.-Q., Zhu, Haining, Zhu, Hongxin, Zhu, Hua, Zhu, W.-G., Zhu, Yanping, Zhu, Yushan, Zhuang, H., Zhuang, X., Zientara-Rytter, K., Zimmermann, C.M., Ziviani, E., Zoladek, T., Zong, W.-X., Zorov, D.B., Zorzano, A., Zou, W., Zou, Zhen, Zou, Zhengzhi, Zuryn, S., Zwerschke, W., Brand-Saberi, B., Dong, X.C., Kenchappa, C.S., Li, Zuguo, Lin, Y., Oshima, S., Rong, Y., Sluimer, J.C., Stallings, C.L., Tong, C.-K., 2021. Guidelines for the use and interpretation of assays for monitoring autophagy (4th edition)1. Autophagy 17, 1–382. https://doi.org/10.1080/15548627.2020.1797280

Komatsu, M., Waguri, S., Koike, M., Sou, Y.-S., Ueno, T., Hara, T., Mizushima, N., Iwata, J.-I., Ezaki, J., Murata, S., Hamazaki, J., Nishito, Y., Iemura, S.-I., Natsume, T., Yanagawa, T., Uwayama, J., Warabi, E., Yoshida, H., Ishii, T., Kobayashi, A., Yamamoto, M., Yue, Z., Uchiyama, Y., Kominami, E., Tanaka, K., 2007. Homeostatic levels of p62 control cytoplasmic inclusion body formation in autophagy-deficient mice. Cell 131, 1149–1163. https://doi.org/10.1016/j.cell.2007.10.035

Komatsu, M., Waguri, S., Ueno, T., Iwata, J., Murata, S., Tanida, I., Ezaki, J., Mizushima, N., Ohsumi, Y., Uchiyama, Y., Kominami, E., Tanaka, K., Chiba, T., 2005. Impairment of starvation-induced and constitutive autophagy in Atg7-deficient mice. J. Cell Biol. 169, 425–434. https://doi.org/10.1083/jcb.200412022

Kongton, K., McCall, K., Phongdara, A., 2014. Identification of gamma-interferon-inducible lysosomal thiol reductase (GILT) homologues in the fruit fly *Drosophila melanogaster*. Dev. Comp. Immunol. 44, 389–396. https://doi.org/10.1016/j.dci.2014.01.007

Kwon, Y., Song, W., Droujinine, I.A., Hu, Y., Asara, J.M., Perrimon, N., 2015. Systemic Organ Wasting Induced by Localized Expression of the Secreted Insulin/IGF Antagonist ImpL2. Dev. Cell 33, 36–46. https://doi.org/10.1016/j.devcel.2015.02.012

Laczkó-Dobos, H., Maddali, A.K., Jipa, A., Bhattacharjee, A., Végh, A.G., Juhász, G., 2021. Lipid profiles of autophagic structures isolated from wild type and Atg2 mutant *Drosophila*. Biochim. Biophys. Acta BBA - Mol. Cell Biol. Lipids 1866, 158868. https://doi.org/10.1016/j.bbalip.2020.158868

Lee, J., Ridgway, N.D., 2020. Substrate channeling in the glycerol-3-phosphate pathway regulates the synthesis, storage and secretion of glycerolipids. Biochim. Biophys. Acta BBA - Mol. Cell Biol. Lipids, Endoplasmic reticulum platforms for lipid dynamics 1865, 158438. https://doi.org/10.1016/j.bbalip.2019.03.010

Liu, F., Li, X., Lu, C., Bai, A., Bielawski, J., Bielawska, A., Marshall, B., Schoenlein, P.V., Lebedyeva, I.O., Liu, K., 2016. Ceramide activates lysosomal cathepsin B and cathepsin D to attenuate autophagy and induces ER stress to suppress myeloid-derived suppressor cells. Oncotarget 7, 83907–83925. https://doi.org/10.18632/oncotarget.13438

Liu, Jianfang, Lichtenberg, T., Hoadley, K.A., Poisson, L.M., Lazar, A.J., Cherniack, A.D., Kovatich, A.J., Benz, C.C., Levine, D.A., Lee, A.V., Omberg, L., Wolf, D.M., Shriver, C.D., Thorsson, V., Caesar-Johnson, S.J., Demchok, J.A., Felau, I., Kasapi, M., Ferguson, M.L., Hutter, C.M., Sofia, H.J., Tarnuzzer, R., Wang, Z., Yang, L., Zenklusen, J.C., Zhang, J. (Julia), Chudamani, S., Liu, Jia, Lolla, L., Naresh, R., Pihl, T., Sun, Q., Wan, Y., Wu, Y., Cho, J., DeFreitas, T., Frazer, S., Gehlenborg, N., Getz, G., Heiman, D.I., Kim, J., Lawrence, M.S., Lin, P., Meier, S., Noble, M.S., Saksena, G., Voet, D., Zhang, Hailei, Bernard, B., Chambwe, N., Dhankani, V., Knijnenburg, T., Kramer, R., Leinonen, K., Liu, Y., Miller, M., Reynolds, S., Shmulevich, I., Thorsson, V., Zhang, W., Akbani, R., Broom, B.M., Hegde, A.M., Ju, Z., Kanchi, R.S., Korkut, A., Li, J., Liang, H., Ling, S., Liu, W., Lu, Y., Mills, G.B., Ng, K.-S., Rao, A., Ryan, M., Wang, Jing, Weinstein, J.N., Zhang, J., Abeshouse, A., Armenia, J., Chakravarty, D., Chatila, W.K., Bruijn, I. de, Gao, J., Gross, B.E., Heins, Z.J., Kundra, R., La, K., Ladanyi, M., Luna, A., Nissan, M.G., Ochoa, A., Phillips, S.M., Reznik, E., Sanchez-Vega, F., Sander, C., Schultz, N., Sheridan, R., Sumer, S.O., Sun, Y., Taylor, B.S., Wang, Jioajiao, Zhang, Hongxin, Anur, P., Peto, M., Spellman, P., Benz, C., Stuart, J.M., Wong, C.K., Yau, C., Hayes, D.N., Parker, J.S., Wilkerson, M.D., Ally, A., Balasundaram, M., Bowlby, R., Brooks, D., Carlsen, R., Chuah, E., Dhalla, N., Holt, R., Jones, S.J.M., Kasaian, K., Lee, D., Ma, Y., Marra, M.A., Mayo, M., Moore, R.A., Mungall, A.J., Mungall, K., Robertson, A.G., Sadeghi, S., Schein, J.E., Sipahimalani, P., Tam, A., Thiessen, N., Tse, K., Wong, T., Berger, A.C., Beroukhim, R., Cherniack, A.D., Cibulskis, C., Gabriel, S.B., Gao, G.F., Ha, G., Meyerson, M., Schumacher, S.E., Shih, J., Kucherlapati, M.H., Kucherlapati, R.S., Baylin, S., Cope, L., Danilova, L., Bootwalla, M.S., Lai, P.H., Maglinte, D.T., Berg, D.J.V.D., Weisenberger, D.J., Auman, J.T., Balu, S., Bodenheimer,

T., Fan, C., Hoadley, K.A., Hoyle, A.P., Jefferys, S.R., Jones, C.D., Meng, S., Mieczkowski, P.A., Mose, L.E., Perou, A.H., Perou, C.M., Roach, J., Shi, Y., Simons, J.V., Skelly, T., Soloway, M.G., Tan, D., Veluvolu, U., Fan, H., Hinoue, T., Laird, P.W., Shen, H., Zhou, W., Bellair, M., Chang, K., Covington, K., Creighton, C.J., Dinh, H., Doddapaneni, H., Donehower, L.A., Drummond, J., Gibbs, R.A., Glenn, R., Hale, W., Han, Y., Hu, J., Korchina, V., Lee, S., Lewis, L., Li, W., Liu, X., Morgan, M., Morton, D., Muzny, D., Santibanez, J., Sheth, M., Shinbro, E., Wang, L., Wang, M., Wheeler, D.A., Xi, L., Zhao, F., Hess, J., Appelbaum, E.L., Bailey, M., Cordes, M.G., Ding, L., Fronick, C.C., Fulton, L.A., Fulton, R.S., Kandoth, C., Mardis, E.R., McLellan, M.D., Miller, C.A., Schmidt, H.K., Wilson, R.K., Crain, D., Curley, E., Gardner, J., Lau, K., Mallery, D., Morris, S., Paulauskis, J., Penny, R., Shelton, C., Shelton, T., Sherman, M., Thompson, E., Yena, P., Bowen, J., Gastier-Foster, J.M., Gerken, M., Leraas, K.M., Lichtenberg, T.M., Ramirez, N.C., Wise, L., Zmuda, E., Corcoran, N., Costello, T., Hovens, C., Carvalho, A.L., Carvalho, A.C. de, Fregnani, J.H., Longatto-Filho, A., Reis, R.M., Scapulatempo-Neto, C., Silveira, H.C.S., Vidal, D.O., Burnette, A., Eschbacher, J., Hermes, B., Noss, A., Singh, R., Anderson, M.L., Castro, P.D., Ittmann, M., Huntsman, D., Kohl, B., Le, X., Thorp, R., Andry, C., Duffy, E.R., Lyadov, V., Paklina, O., Setdikova, G., Shabunin, A., Tavobilov, M., McPherson, C., Warnick, R., Berkowitz, R., Cramer, D., Feltmate, C., Horowitz, N., Kibel, A., Muto, M., Raut, C.P., Malykh, A., Barnholtz-Sloan, J.S., Barrett, W., Devine, K., Fulop, J., Ostrom, Q.T., Shimmel, K., Wolinsky, Y., Sloan, A.E., Rose, A.D., Giuliante, F., Goodman, M., Karlan, B.Y., Hagedorn, C.H., Eckman, J., Harr, J., Myers, J., Tucker, K., Zach, L.A., Deyarmin, B., Hu, H., Kvecher, L., Larson, C., Mural, R.J., Somiari, S., Vicha, A., Zelinka, T., Bennett, J., Iacocca, M., Rabeno, B., Swanson, P., Latour, M., Lacombe, L., Têtu, B., Bergeron, A., McGraw, M., Staugaitis, S.M., Chabot, J., Hibshoosh, H., Sepulveda, A., Su, T., Wang, T., Potapova, O., Voronina, O., Desjardins, L., Mariani, O., Roman-Roman, S., Sastre, X., Stern, M.-H., Cheng, F., Signoretti, S., Berchuck, A., Bigner, D., Lipp, E., Marks, J., McCall, S., McLendon, R., Secord, A., Sharp, A., Behera, M., Brat, D.J., Chen, A., Delman, K., Force, S., Khuri, F., Magliocca, K., Maithel, S., Olson, J.J., Owonikoko, T., Pickens, A., Ramalingam, S., Shin, D.M., Sica, G., Meir, E.G.V., Zhang, Hongzheng, Eijckenboom, W., Gillis, A., Korpershoek, E., Looijenga, L., Oosterhuis, W., Stoop, H., Kessel, K.E. van, Zwarthoff, E.C., Calatozzolo, C., Cuppini, L., Cuzzubbo, S., DiMeco, F., Finocchiaro, G., Mattei, L., Perin, A., Pollo, B., Chen, C., Houck, J., Lohavanichbutr, P., Hartmann, A., Stoehr, C., Stoehr, R., Taubert, H., Wach, S., Wullich, B., Kycler, W., Murawa, D., Wiznerowicz, M., Chung, K., Edenfield, W.J., Martin, J., Baudin, E., Bubley, G., Bueno, R., Rienzo, A.D., Richards, W.G., Kalkanis, S., Mikkelsen, T., Noushmehr, H., Scarpace, L., Girard, N., Aymerich, M., Campo, E., Giné, E., Guillermo, A.L., Bang, N.V., Hanh, P.T., Phu, B.D., Tang, Y., Colman, H., Evason, K., Dottino, P.R., Martignetti, J.A., Gabra, H., Juhl, H., Akeredolu, T., Stepa, S., Hoon, D., Ahn, K., Kang, K.J., Beuschlein, F., Breggia, A., Birrer, M., Bell, D., Borad, M., Bryce, A.H., Castle, E., Chandan, V., Cheville, J., Copland, J.A., Farnell, M., Flotte, T., Giama, N., Ho, T., Kendrick, M., Kocher, J.-P., Kopp, K., Moser, C., Nagorney, D., O'Brien, D., O'Neill, B.P., Patel, T., Petersen, G., Que, F., Rivera, M., Roberts, L., Smallridge, R., Smyrk, T., Stanton, M.,

Thompson, R.H., Torbenson, M., Yang, J.D., Zhang, L., Brimo, F., Ajani, J.A., Gonzalez, A.M.A., Behrens, C., Bondaruk, J., Broaddus, R., Czerniak, B., Esmaeli, B., Fujimoto, J., Gershenwald, J., Guo, C., Lazar, A.J., Logothetis, C., Meric-Bernstam, F., Moran, C., Ramondetta, L., Rice, D., Sood, A., Tamboli, P., Thompson, T., Troncoso, P., Tsao, A., Wistuba, I., Carter, C., Haydu, L., Hersey, P., Jakrot, V., Kakavand, H., Kefford, R., Lee, K., Long, G., Mann, G., Quinn, M., Saw, R., Scolyer, R., Shannon, K., Spillane, A., Stretch, J., Synott, M., Thompson, J., Wilmott, J., Al-Ahmadie, H., Chan, T.A., Ghossein, R., Gopalan, A., Levine, D.A., Reuter, V., Singer, S., Singh, B., Tien, N.V., Broudy, T., Mirsaidi, C., Nair, P., Drwiega, P., Miller, J., Smith, J., Zaren, H., Park, J.-W., Hung, N.P., Kebebew, E., Linehan, W.M., Metwalli, A.R., Pacak, K., Pinto, P.A., Schiffman, M., Schmidt, L.S., Vocke, C.D., Wentzensen, N., Worrell, R., Yang, H., Moncrieff, M., Goparaju, C., Melamed, J., Pass, H., Botnariuc, N., Caraman, I., Cernat, M., Chemencedji, I., Clipca, A., Doruc, S., Gorincioi, G., Mura, S., Pirtac, M., Stancul, I., Tcaciuc, D., Albert, M., Alexopoulou, I., Arnaout, A., Bartlett, J., Engel, J., Gilbert, S., Parfitt, J., Sekhon, H., Thomas, G., Rassl, D.M., Rintoul, R.C., Bifulco, C., Tamakawa, R., Urba, W., Hayward, N., Timmers, H., Antenucci, A., Facciolo, F., Grazi, G., Marino, M., Merola, R., Krijger, R. de, Gimenez-Roqueplo, A.-P., Piché, A., Chevalier, S., McKercher, G., Birsoy, K., Barnett, G., Brewer, C., Farver, C., Naska, T., Pennell, N.A., Raymond, D., Schilero, C., Smolenski, K., Williams, F., Morrison, C., Borgia, J.A., Liptay, M.J., Pool, M., Seder, C.W., Junker, K., Omberg, L., Dinkin, M., Manikhas, G., Alvaro, D., Bragazzi, M.C., Cardinale, V., Carpino, G., Gaudio, E., Chesla, D., Cottingham, S., Dubina, M., Moiseenko, F., Dhanasekaran, R., Becker, K.-F., Janssen, K.-P., Slotta-Huspenina, J., Abdel-Rahman, M.H., Aziz, D., Bell, S., Cebulla, C.M., Davis, A., Duell, R., Elder, J.B., Hilty, J., Kumar, B., Lang, J., Lehman, N.L., Mandt, R., Nguyen, P., Pilarski, R., Rai, K., Schoenfield, L., Senecal, K., Wakely, P., Hansen, P., Lechan, R., Powers, J., Tischler, A., Grizzle, W.E., Sexton, K.C., Kastl, A., Henderson, J., Porten, S., Waldmann, J., Fassnacht, M., Asa, S.L., Schadendorf, D., Couce, M., Graefen, M., Huland, H., Sauter, G., Schlomm, T., Simon, R., Tennstedt, P., Olabode, O., Nelson, M., Bathe, O., Carroll, P.R., Chan, J.M., Disaia, P., Glenn, P., Kelley, R.K., Landen, C.N., Phillips, J., Prados, M., Simko, J., Smith-McCune, K., VandenBerg, S., Roggin, K., Fehrenbach, A., Kendler, A., Sifri, S., Steele, R., Jimeno, A., Carey, F., Forgie, I., Mannelli, M., Carney, M., Hernandez, B., Campos, B., Herold-Mende, C., Jungk, C., Unterberg, A., Deimling, A. von, Bossler, A., Galbraith, J., Jacobus, L., Knudson, M., Knutson, T., Ma, D., Milhem, M., Sigmund, R., Godwin, A.K., Madan, R., Rosenthal, H.G., Adebamowo, C., Adebamowo, S.N., Boussioutas, A., Beer, D., Giordano, T., Mes-Masson, A.-M., Saad, F., Bocklage, T., Landrum, L., Mannel, R., Moore, K., Moxley, K., Postier, R., Walker, J., Zuna, R., Feldman, M., Valdivieso, F., Dhir, R., Luketich, J., Pinero, E.M.M., Quintero-Aguilo, M., Carlos Gilberto Carlotti, J., Santos, J.S.D., Kemp, R., Sankarankuty, A., Tirapelli, D., Catto, J., Agnew, K., Swisher, E., Creaney, J., Robinson, B., Shelley, C.S., Godwin, E.M., Kendall, S., Shipman, C., Bradford, C., Carey, T., Haddad, A., Moyer, J., Peterson, L., Prince, M., Rozek, L., Wolf, G., Bowman, R., Fong, K.M., Yang, I., Korst, R., Rathmell, W.K., Fantacone-Campbell, J.L., Hooke, J.A., Kovatich, A.J., Shriver, C.D., DiPersio, J., Drake, B., Govindan, R., Heath, S., Ley, T., Tine, B.V., Westervelt, P.,

Rubin, M.A., Lee, J.I., Aredes, N.D., Mariamidze, A., Hu, H., 2018. An Integrated TCGA Pan-Cancer Clinical Data Resource to Drive High-Quality Survival Outcome Analytics. Cell 173, 400-416.e11. https://doi.org/10.1016/j.cell.2018.02.052

Liu, Y., Saavedra, P., Perrimon, N., 2022. Cancer cachexia: lessons from Drosophila. Dis. Model. Mech. 15, dmm049298. https://doi.org/10.1242/dmm.049298

Liu, Ying, Dantas, E., Ferrer, M., Miao, T., Qadiri, M., Liu, Yifang, Comjean, A., Davidson, E.E., Perrier, T., Ahmed, T., Hu, Y., Goncalves, M.D., Janowitz, T., Perrimon, N., 2025. Hepatic gluconeogenesis and PDK3 upregulation drive cancer cachexia in flies and mice. Nat. Metab. 7, 823–841. https://doi.org/10.1038/s42255-025-01265-2

Mirdita, M., Schütze, K., Moriwaki, Y., Heo, L., Ovchinnikov, S., Steinegger, M., 2022. ColabFold: making protein folding accessible to all. Nat. Methods 19, 679–682. https://doi.org/10.1038/s41592-022-01488-1

Mizutani, Y., Kihara, A., Igarashi, Y., 2005. Mammalian Lass6 and its related family members regulate synthesis of specific ceramides. Biochem. J. 390, 263–271. https://doi.org/10.1042/BJ20050291

Mulakkal, N.C., Nagy, P., Takats, S., Tusco, R., Juhász, G., Nezis, I.P., 2014. Autophagy in Drosophila: From Historical Studies to Current Knowledge. BioMed Res. Int. 2014, 273473. https://doi.org/10.1155/2014/273473

Mullen, T.D., Hannun, Y.A., Obeid, L.M., 2012. Ceramide synthases at the centre of sphingolipid metabolism and biology. Biochem. J. 441, 789–802. https://doi.org/10.1042/BJ20111626

Ni, H.-M., Woolbright, B.L., Williams, J., Copple, B., Cui, W., Luyendyk, J.P., Jaeschke, H., Ding, W.-X., 2014. Nrf2 promotes the development of fibrosis and tumorigenesis in mice with defective hepatic autophagy. J. Hepatol. 61, 617–625. https://doi.org/10.1016/j.jhep.2014.04.043

Ota, A., Morita, H., Naganuma, T., Miyamoto, M., Jojima, K., Nojiri, K., Matsuda, J., Kihara, A., 2023. Bifunctional DEGS2 has higher hydroxylase activity toward substrates with very-long-chain fatty acids in the production of phytosphingosine ceramides. J. Biol. Chem. 299. https://doi.org/10.1016/j.jbc.2023.104603

Passaro, S., Corso, G., Wohlwend, J., Reveiz, M., Thaler, S., Somnath, V.R., Getz, N., Portnoi, T., Roy, J., Stark, H., Kwabi-Addo, D., Beaini, D., Jaakkola, T., Barzilay, R., 2025. Boltz-2: Towards Accurate and Efficient Binding Affinity Prediction. BioRxiv Prepr. Serv. Biol. 2025.06.14.659707. https://doi.org/10.1101/2025.06.14.659707

Pelosof, L.C., Gerber, D.E., 2010. Paraneoplastic Syndromes: An Approach to Diagnosis and Treatment. Mayo Clin. Proc. 85, 838–854. https://doi.org/10.4065/mcp.2010.0099

Pewzner-Jung, Y., Park, H., Laviad, E.L., Silva, L.C., Lahiri, S., Stiban, J., Erez-Roman, R., Brügger, B., Sachsenheimer, T., Wieland, F., Prieto, M., Merrill, A.H., Futerman, A.H., 2010. A Critical Role for Ceramide Synthase 2 in Liver Homeostasis: I. ALTERATIONS IN LIPID METABOLIC PATHWAYS*. J. Biol. Chem. 285, 10902–10910. https://doi.org/10.1074/jbc.M109.077594

Qi, D., Song, X., Xue, C., Yao, W., Shen, P., Yu, H., Zhang, Z., 2021. AKT1/FOXP3 axis-mediated expression of CerS6 promotes p53 mutant pancreatic tumorigenesis. Cancer Lett. 522, 105–118. https://doi.org/10.1016/j.canlet.2021.06.024

Qian, H., Chao, X., Williams, J., Fulte, S., Li, T., Yang, L., Ding, W.-X., 2021. Autophagy in liver diseases: A review. Mol. Aspects Med. 82, 100973. https://doi.org/10.1016/j.mam.2021.100973

Qing, H., Desrouleaux, R., Israni-Winger, K., Mineur, Y.S., Fogelman, N., Zhang, C., Rashed, S., Palm, N.W., Sinha, R., Picciotto, M.R., Perry, R.J., Wang, A., 2020. Origin and Function of Stress-Induced IL-6 in Murine Models. Cell 182, 372-387.e14. https://doi.org/10.1016/j.cell.2020.05.054

Queiroz, A.L., Dantas, E., Ramsamooj, S., Murthy, A., Ahmed, M., Zunica, E.R.M., Liang, R.J., Murphy, J., Holman, C.D., Bare, C.J., Ghahramani, G., Wu, Z., Cohen, D.E., Kirwan, J.P., Cantley, L.C., Axelrod, C.L., Goncalves, M.D., 2022. Blocking ActRIIB and restoring appetite reverses cachexia and improves survival in mice with lung cancer. Nat. Commun. 13, 4633. https://doi.org/10.1038/s41467-022-32135-0

Raichur, S., Brunner, B., Bielohuby, M., Hansen, G., Pfenninger, A., Wang, B., Bruning, J.C., Larsen, P.J., Tennagels, N., 2019. The role of C16:0 ceramide in the development of obesity and type 2 diabetes: CerS6 inhibition as a novel therapeutic approach. Mol. Metab. 21, 36–50. https://doi.org/10.1016/j.molmet.2018.12.008

Riebeling, C., Allegood, J.C., Wang, E., Merrill, A.H., Futerman, A.H., 2003. Two Mammalian Longevity Assurance Gene (LAG1) Family Members, *trh1* and *trh4*, Regulate Dihydroceramide Synthesis Using Different Fatty Acyl-CoA Donors*. J. Biol. Chem. 278, 43452–43459. https://doi.org/10.1074/jbc.M307104200

Rowland, L.A., Guilherme, A., Henriques, F., DiMarzio, C., Munroe, S., Wetoska, N., Kelly, M., Reddig, K., Hendricks, G., Pan, M., Han, X., Ilkayeva, O.R., Newgard, C.B., Czech, M.P., 2023. De novo lipogenesis fuels adipocyte autophagosome and lysosome membrane dynamics. Nat. Commun. 14, 1362. https://doi.org/10.1038/s41467-023-37016-8

Ryter, S.W., Cloonan, S.M., Choi, A.M.K., 2013. Autophagy: A Critical Regulator of Cellular Metabolism and Homeostasis. Mol. Cells 36, 7–16. https://doi.org/10.1007/s10059-013-0140-8

Saavedra, P., Dumesic, P.A., Hu, Y., Jouandin, P., Binari, R., Wilensky, S.E., Filine, E., Rodiger, J., Wang, H., Spiegelman, B.M., Perrimon, N., 2021. REPTOR/CREBRF encode key regulators of muscle energy metabolism. https://doi.org/10.1101/2021.12.17.473012

Saftig, P., Klumperman, J., 2009. Lysosome biogenesis and lysosomal membrane proteins: trafficking meets function. Nat. Rev. Mol. Cell Biol. 10, 623–635. https://doi.org/10.1038/nrm2745

Schütter, M., Graef, M., 2020. Localized de novo phospholipid synthesis drives autophagosome biogenesis. Autophagy 16, 770–771. https://doi.org/10.1080/15548627.2020.1725379

Skotland, T., Sandvig, K., 2019. The role of PS 18:0/18:1 in membrane function. Nat. Commun. 10, 2752. https://doi.org/10.1038/s41467-019-10711-1

Song, W., Kir, S., Hong, S., Hu, Y., Wang, X., Binari, R., Tang, H.-W., Chung, V., Banks, A.S., Spiegelman, B., Perrimon, N., 2019. Tumor-Derived Ligands Trigger Tumor Growth and Host Wasting via Differential MEK Activation. Dev. Cell 48, 277-286.e6. https://doi.org/10.1016/j.devcel.2018.12.003

Song, W., Owusu-Ansah, E., Hu, Y., Cheng, D., Ni, X., Zirin, J., Perrimon, N., 2017. Activin signaling mediates muscle-to-adipose communication in a mitochondria dysfunction-associated obesity model. Proc. Natl. Acad. Sci. 114, 8596–8601. https://doi.org/10.1073/pnas.1708037114

Stone, R.L., Nick, A.M., McNeish, I.A., Balkwill, F., Han, H.D., Bottsford-Miller, J., Rupaimoole, R., Armaiz-Pena, G.N., Pecot, C.V., Coward, J., Deavers, M.T., Vasquez, H.G., Urbauer, D., Landen, C.N., Hu, W., Gershenson, H., Matsuo, K., Shahzad, M.M.K., King, E.R., Tekedereli, I., Ozpolat, B., Ahn, E.H., Bond, V.K., Wang, R., Drew, A.F., Gushiken, F., Lamkin, D., Collins, K., DeGeest, K., Lutgendorf, S.K., Chiu, W., Lopez-Berestein, G., Afshar-Kharghan, V., Sood, A.K., 2012. Paraneoplastic Thrombocytosis in Ovarian Cancer [WWW Document]. N. Engl. J. Med. https://doi.org/10.1056/NEJMoa1110352

Taniguchi, M., Kitatani, K., Kondo, T., Hashimoto-Nishimura, M., Asano, S., Hayashi, A., Mitsutake, S., Igarashi, Y., Umehara, H., Takeya, H., Kigawa, J., Okazaki, T., 2012. Regulation of Autophagy and Its Associated Cell Death by “Sphingolipid Rheostat.” J. Biol. Chem. 287, 39898–39910. https://doi.org/10.1074/jbc.M112.416552

Tiede, A., Nischan, C., Schubert, J., Schmidt, R.E., 2000. Characterisation of the enzymatic complex for the first step in glycosylphosphatidylinositol biosynthesis. Int. J. Biochem. Cell Biol. 32, 339–350. https://doi.org/10.1016/S1357-2725(99)00122-3

Turk, V., Turk, B., Turk, D., 2001. Lysosomal cysteine proteases: facts and opportunities. EMBO J. 20, 4629–4633. https://doi.org/10.1093/emboj/20.17.4629

Ueno, T., Komatsu, M., 2017. Autophagy in the liver: functions in health and disease. Nat. Rev. Gastroenterol. Hepatol. 14, 170–184. https://doi.org/10.1038/nrgastro.2016.185

Wang, B., Moya, N., Niessen, S., Hoover, H., Mihaylova, M.M., Shaw, R.J., Yates, J.R., Fischer, W.H., Thomas, J.B., Montminy, M., 2011. A hormone-dependent module regulating energy balance. Cell 145, 596–606. https://doi.org/10.1016/j.cell.2011.04.013

Wegner, M.-S., Wanger, R.A., Oertel, S., Brachtendorf, S., Hartmann, D., Schiffmann, S., Marschalek, R., Schreiber, Y., Ferreirós, N., Geisslinger, G., Grösch, S., 2014. Ceramide synthases CerS4 and CerS5 are upregulated by 17β-estradiol and GPER1 via AP-1 in human breast cancer cells. Biochem. Pharmacol. 92, 577–589. https://doi.org/10.1016/j.bcp.2014.10.007

Weidberg, H., Shvets, E., Elazar, Z., 2011. Biogenesis and Cargo Selectivity of Autophagosomes. Annu. Rev. Biochem. 80, 125–156. https://doi.org/10.1146/annurev-biochem-052709-094552

Woodcock, K.J., Kierdorf, K., Pouchelon, C.A., Vivancos, V., Dionne, M.S., Geissmann, F., 2015. Macrophage-derived upd3 cytokine causes impaired glucose homeostasis and reduced lifespan in Drosophila fed a lipid-rich diet. Immunity 42, 133–144. https://doi.org/10.1016/j.immuni.2014.12.023

Wu, X., Tao, P., Zhou, Q., Li, Jie, Yu, Z., Wang, X., Li, Jiaanfang, Li, C., Yan, M., Zhu, Z., Liu, B., Su, L., 2017. IL-6 secreted by cancer-associated fibroblasts promotes epithelial-mesenchymal transition and metastasis of gastric cancer via JAK2/STAT3 signaling pathway. Oncotarget 8, 20741–20750. https://doi.org/10.18632/oncotarget.15119

Wueest, S., Konrad, D., 2020. The controversial role of IL-6 in adipose tissue on obesity-induced dysregulation of glucose metabolism. Am. J. Physiol.-Endocrinol. Metab. 319, E607–E613. https://doi.org/10.1152/ajpendo.00306.2020

Xie, Z., Nair, U., Klionsky, D.J., 2008. Atg8 controls phagophore expansion during autophagosome formation. Mol. Biol. Cell 19, 3290–3298. https://doi.org/10.1091/mbc.e07-12-1292

Xu, J., Kim, A.-R., Cheloha, R.W., Fischer, F.A., Li, J.S.S., Feng, Y., Stoneburner, E., Binari, R., Mohr, S.E., Zirin, J., Ploegh, H.L., Perrimon, N., 2022. Protein visualization and manipulation in Drosophila through the use of epitope tags recognized by nanobodies. eLife 11, e74326. https://doi.org/10.7554/eLife.74326

Xu, J., Liu, Y., Yang, F., Cao, Y., Chen, W., Li, J.S.S., Zhang, S., Comjean, A., Hu, Y., Perrimon, N., 2024. Mechanistic characterization of a Drosophila model of paraneoplastic nephrotic syndrome. Nat. Commun. 15, 1241. https://doi.org/10.1038/s41467-024-45493-8

Yang, X., Wang, J., Chang, C.-Y., Zhou, F., Liu, J., Xu, H., Ibrahim, M., Gomez, M., Guo, G.L., Liu, H., Zong, W.-X., Wondisford, F.E., Su, X., White, E., Feng, Z., Hu, W., 2024. Leukemia inhibitory factor suppresses hepatic de novo lipogenesis and induces cachexia in mice. Nat. Commun. 15, 627. https://doi.org/10.1038/s41467-024-44924-w

Yu, H., Kortylewski, M., Pardoll, D., 2007. Crosstalk between cancer and immune cells: role of STAT3 in the tumour microenvironment. Nat. Rev. Immunol. 7, 41–51. https://doi.org/10.1038/nri1995